NTNU – Trondheim
Norwegian University of
Science and Technology

Bayesian Estimation of Non-Stationary Ship Response Spectra

Christian Møgster

Marine Technology
Submission date: June 2015
Supervisor: Asgeir Johan Sørensen, IMT
Co-supervisor: Ulrik Dam Nielsen, DTU
Astrid Brodtkorb, IMT
Svenn Are Tutturen, IMT

Norwegian University of Science and Technology
Department of Marine Technology

NTNU Trondheim
Norwegian University of Science and Technology
Department of Marine Technology

Project Description

Christian Møgster

Master Thesis NTNU

Delivery 10.06.15

Project Description: Bayesian Estimation of Non-Stationary Ship Response Spectra

Environmental data from reliable sources has been of great importance to ensure safe operations at sea. Recently, there has been a development towards using already existing sensors in most waters, which are ships by applying *the wave buoy analogy*. The wave buoy analogy uses the ship response and estimate the wave spectrum by this movement. Most methods today assume that both the short-term sea state and the ship response are stationary. Assuming that the short-term sea state is a stationary stochastic process is well established in the literature. However, by assuming that the ship response is stationary, the recreation of the spectrum is dependent on the operational conditions, such as constant course direction, and constant vessel speed. In this thesis it is desirable to investigate if there exist methods that are not dependent on the operational conditions, such that the vessel data can be used constantly.

This thesis should address the non-stationary problem, using multivariate analysis and Bayesian statistics. The aim of the project is be to obtain spectral information from a non-stationary response.

Scope of work

1. Perform a literature review to provide background and relevant references on
   - General methods for estimating wave spectra.
   - Stochastic theory related to the subject.
2. Investigate the ship response behaviour and present relevant concepts to wave theory.
3. Propose a theoretical mathematical method that can investigate non-stationary response spectrum.
4. Formulate the non-stationary ship response as an estimation problem, and relate the method to known estimation techniques in Marine Cybernetic environment, and apply the method on a simple process to verify the estimation technique. Evaluate the algorithm's performance of estimating the parameters of this process.
5. Estimate the spectrum of simulated stationary ship response processes, and evaluate the performance.

6. Estimate the spectrum of simulated non-stationary ship response processes, and evaluate the performance.

7. Identify key factors and limitations of the algorithm.

8. Implement the algorithm on model test results and evaluated the performance.

Guidelines

The scope of work may prove to be larger than initially anticipated. By the approval from the supervisor, described topics may be deleted or reduced in extent without consequences with regard to grading.

The candidate shall present his personal contribution to the resolution of problems within the scope of work. Theories and conclusions should be based on mathematical derivations and logic reasoning identifying the various steps in the deduction.

The report shall be organized in a rational manner to give a clear exposition of results, assessments, and conclusions. The text should be brief and to the point, with a clear language. The report shall be written in English (preferably US) and contain the following elements: Summary, preface, table of contents, main body, conclusions with recommendations for further work, list of symbols and acronyms, references, and optional appendices. All figures and tables shall be numerated. The original contribution of the candidate and material taken from other sources shall be clearly identified. Work from other sources shall be properly acknowledged using quotations and a Harvard citation style. The work is expected to be conducted in an honest and ethical manner, without any sort of plagiarism and misconduct. Such practice is taken very seriously by the University and will have consequences. NTNU can use the results freely in research and teaching by proper referencing, unless otherwise agreed upon.

The thesis shall be submitted with two printed and electronic copies, to 1) the main supervisor and 2) the archive. The final revised version of this thesis description must be included. The report must appear in a bound volume or a binder according to the NTNU standard template.

Supervisor: Asgeir J. Sørensen
Co-Supervisor: Roger Skjetne
Co-Supervisor: Ulrik D. Nielsen
Co-Supervisor: Astrid H. Brodtkorb
Co-Supervisor: Svenn A. Tutturen

Summary

The main topic of this master thesis is to obtain spectral information of non-stationary ship responses, with the motive of facilitating improvement of sea state estimation methods, that are using the wave buoy analogy. The wave buoy analogy is a method that uses the ship response to estimate the wave spectra. This method is restricted by constant operational conditions, such as vessel speed and direction, and is therefore limited to stationary processes. By introducing a method that can obtain spectral information from a time-varying ship response, the sea state estimation can be done without restrictions on the operational conditions. This can be achieved by the use of a parametric method, which is derived in this thesis.

The parametric method uses a time-varying auto-regressive model (TVAR) and Bayesian estimation methods to estimate the time-varying parameters, which can be transformed to the time-dependent power density spectrum of the ship response.

The algorithm is tested on stationary and non-stationary processes where key factors and limitations are identified. Simulation studies show that the performance of the algorithm is sensitive to the ratio between the co-variance of the state noise and the observation noise. The main limitation of the study is that this ratio needs to be tuned manually, and not in an adaptive way. In addition, the algorithm has a decreasing performance when the level of non-stationarity and the complexity of the spectrum increase.

The algorithm is tested on real data in a model test with Cybership III conducted in the MClab at NTNU. Unfortunately, the RAO's of Cybership were for different load conditions than those tested. Since the test study was approximately stationary, the algorithm could be compared with another using Fast Fourier Transform and smoothing functions. However, it was due to work with this thesis that the RAO's were found to be for a different load condition. Furthermore, it was found that the algorithm estimate a more narrow spectrum than the Fourier Transform method.

Sammendrag

Hovedtema for denne masteroppgaven er å estimere spektralinformation av ikke-stasjonære skipsresponser, for å legge til rette forbedringer av metoder som bruker bølgebøye analogien til å sjøtilstandsestimering. Bølgebøyeanalogien er en metode som bruker skipsresponser til å estimere bølgespektre. Denne metoden er begrenset av konstante operasjonelle betingelser, slik som fartøyets fart og kurs, og er derfor bundet til stasjonære prosesser. Ved å innføre en metode som kan estimere spektral information fra et tidsvarierende skipsresponsespectrum, så kan sjøtilstandsestimering uten begrensninger på operasjonelle forhold. Dette kan gjøres med en parametrisk metode som er utledet i denne masteroppgaven.

Den parametriske metoden bruker en tidsvarierende auto-regressiv model, og Bayesiske estimeringsmetoder til å estimere de tidsvarierende parametrene, som kan transformeres til det tidsvariande skipsresponsspekteret.

Algoritmen er testet på stasjonære og ikke-stasjonære prosesser, hvor viktige faktorer er funnet. I korte trekk, så viser simuleringsstudier at algoritmen estimerer de dominante frekvensene bedre enn den estimerer størrelsen på spekteret. I tillegg viser studiene at ytelsen er svært følsomt ovenfor forholdet mellom kovariansen til tilstandsstøyen, og kovariansen til målestøyen i den matematiske modellen. Den største begrensningen til algoritmen er at dette forholdet bestemmes manuelt, og ikke automatisk. I tillegg så viser algoritmen en avtagende ytelse når kompleksiteten og graden av ikke-stasjonæritet øker.

Algoritmen er også testet på model data av Cybership III utført i MClab på Marin Teknisk Senter NTNU. Dessverre viste det seg at transferfunksjonene til Cybership III var for en annen lastkondisjon enn den som var i modelforsøket. Siden test forsøket var implementert som en tilnærmet stasjonær prosess, så kunne algorithmen bli sammenlignet med en metode som bruker Fourier Transform og glattefunksjoner. Det var i denne masteroppgaven det ble funnet ut at transfer funksjonen var for en annen lastkondisjon. Resultatet viste at den parametriske metoden estimerer et smalere spekter enn metoden med Fourier Transformasjon.

Preface

This study is a Master thesis at the Norwegian University of Science and Technology (NTNU) at the Department of Marine Cybernetics. The work has been conducted in the period from January 2015 to June 2015.

The thesis originates from a special interest I gathered in stochastic theory and statistics during my study at NTNU. After taking the subject ME111: Factor Models in Time Series with Applications in Macroeconomics and Finance at London School of Economics (LSE) Summer School in 2014, I started to look for marine applications where time series estimation theories could be used. During the Fall 2010, I further developed my skill in estimation theories by writing my project thesis about Bayesian filtering methods. Discussions with Professor Asgeir J. Sørensen, Professor Roger Skjetne and Ulrik D. Nielsen in how to improve sea state estimation, made the idea of analyzing the ship response, which resulted in this master thesis.

I would like to thank my supervisor, Professor Asgeir Sørensen (NTNU), for feedback and limitless inspiration during the project period and throughout the study. Furthermore, I would like to give a special thanks to my co-supervisor Associate Professor Ulrik D. Nielsen, Technical University of Denmark (DTU) for discussions regarding wave spectrum estimation and the relation to the ship response. Your knowledge within this field of study is unquestionable. Furthermore, my other co-supervisors PhD Candidate Astrid H. Brodtkorb and PhD Candidate Sven A. Tutturen deserve a great thanks for their tireless work in helping me. Lastly, I would like to thank Associate Professor Edmund Brekke (NTNU), for discussions regarding estimation theories.

Trondheim, June 10, 2015.

Christian Møgster

Contents

List of Acronyms

Acronym	Description
AIC	Akaikes Information Criteria
AR	Autoregressive model
ARMA	Autoregressive Moving Average model
BIC	Bayesian Information Criteria
DP	Dynamic Positioning
EPDS	Evolutionary Power Density Spectrum
FFT	Fast Fourier transform
IID	Independent and identically distributed
LQE	Linear Quadratic Estimator
LSE	Log Square Error
LSME	Log Mean Square Error
MA	Moving Average model
PM	Pierson-Moscowitz
PSD	Power spectral density
RAO	Response amplitude operator
SNR	Signal to noise ratio
TVAR	Time varying auto regression

Symbols and Notation

Symbol	Description
ω	Frequency in radians per seconds
f	Frequency in hertz
$S_\zeta(\omega)$	Wave spectrum
$S_y(\omega)$	Ship Response spectrum
ψ	Direction of the vessel
β	Angle between the ships direction and the encountering waves
y_k	Measurement
$a_{k,j}$	Parameter at time instant k, and order index j
p	Order of mathematical model
e_k	Model residuals
σ_e^2	Variance of model residuals/variance of observation noise
v_k	State noise
σ_v^2	Variance of state noise
$\mathcal{N}$	Gaussian distribution
$\mathcal{R}$	Rayleigh distribution
$\mathcal{C}$	Cauchy distribution
σ_c	Cauchy scaling parameter
R	Co-variance matrix of observation noise
Q	Co-variance matrix of state noise
x_k	States
$h(x)$	Monte Carlo integrand
$p(x)$	Probability density function
$p(x_k\|y_{1:k})$	Posterior density function
$p(y_k\|x_k)$	Likelihood function
$p(x_{k+1}\|y_{1:k})$	Prior density function
$P_{k\|k}$	Measurement updated covariance
$\hat{P}$	Same as $P_{k\|k}$, used in the Kalman filter derivation
$\mu_{k\|k}$	Measurement updated expected value

$P_{k+1\|k}$	Time updated co-variance
$\bar{P}$	Same as $P_{k+1\|k}$, used in Kalman filter derivation
$\mu_{k+1\|k}$	Time updated expected value
$\bar{\mu}$	Same as $\mu_{k+1\|k}$, used in Kalman filter derivation
$q(x_k\|y_{1:k})$	Importance density function
N	Total number of particles
$x^i \sim p(x)$	x is sampled from the random distribution *p(x)*
$\delta(x-x^{(i)})$	Dirac delta function
w_k	Particle weights
$S_y(f,k)$	Evolutionary power density spectrum of ship response
$S_e(f)$	Spectrum of white noise
$H(f)$	Frequency transfer function
$H(f,k)$	Frequency and time-dependent transfer function
ι	Imaginary unit
N_k	Total number of time instant
$\hat{L}$	Maximum likelihood function
z	z-transform
Ω	Dimensionless frequency
f_s	Sampling frequency
Δt	Sampling time

Chapter 1

Introduction

This thesis is part of the research, carried out at the Center for Autonomous Marine Operations and Systems (AMOS), in analyzing the ship response, with the underlying motive of improving sea state estimation. The thesis has a particular focus of estimating spectral information of non-stationary ship response, with emphasis on using Bayesian methods.

1.1 Motivation

Environmental data from reliable sources has been of great importance to ensure safe marine operations at sea. The wave-rider buoy has primarily been the most important source to establish oceanographic statistics. However, recently there has been a development towards using already existing sensors that travel most waters, namely ships, inviting the "big data" revolution to the study of Marine Technology. Although the value of information from wave buoys is unquestionable, the possibility of extracting meaningful and useful information out of the large amount of data already available on vessels, could be of tremendous importance. In the future, maybe this concept can make it possible to create a common database describing and predicting the seas all around the world. Challenges related to this extend to several disciplines in the Marine Cybernetic study, and knowledge within wave theory, weather forecasting, observer technology, sensor fusion, stochastic process analysis, statistics and computer science. All these elements are required to reach the common aim in making the sea more predictable, safer and operational effective.

1.2 Background

The method of using ship response to estimate the wave spectrum is called *the wave buoy analogy*. An example of this methodology, proposed by Nielsen (2005), is shown in Figure 1.1.

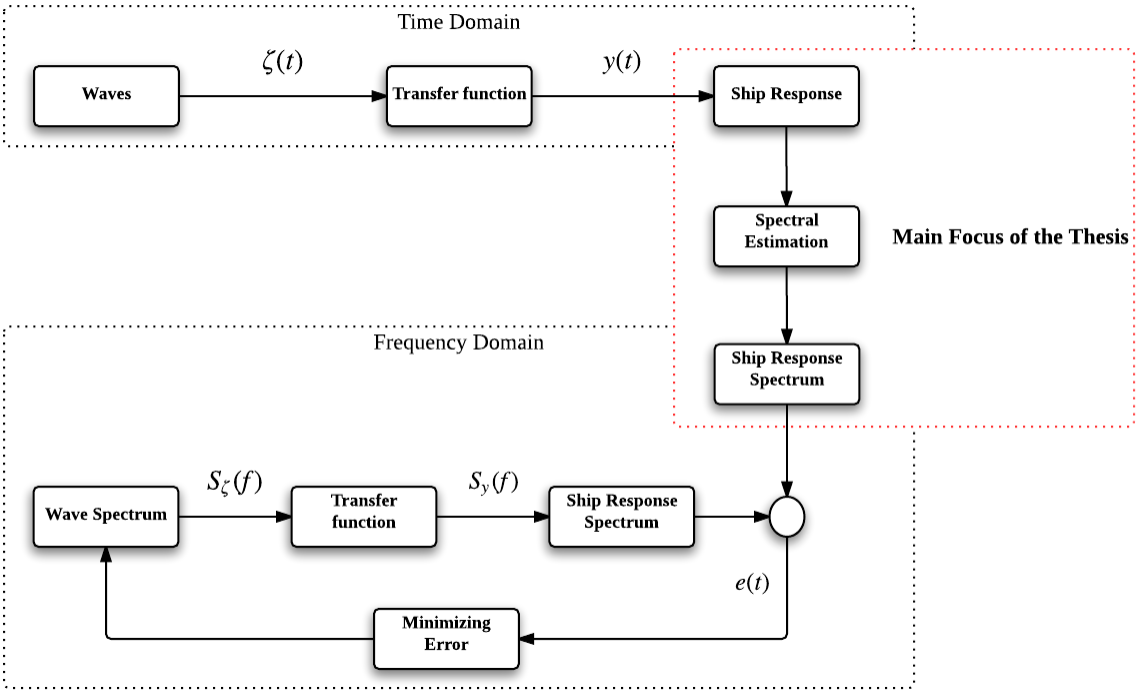

Figure 1.1: Wave spectrum estimation algorithm.

In brief, the figure shows the movement of the vessel $y(t)$ is transformed to a ship response spectrum $S_y(f)$. This is compared with a ship response spectrum generated from a wave spectrum and a transfer function. Furthermore, the correct wave spectrum is then found by minimizing the error between the two ship response spectra.

In this thesis, the main focus is to analyze the ship response transform between the time domain and the frequency domain, which is the three blocks outlined in red in the figure above. The reason for this is elaborated below.

Most methods today, are assuming that both the short term sea state, and the ship response can be considered as stationary. It is well established in the literature that the short term sea state can be considered as stationary, see Faltinsen (1990). However, the ship response can only be assumed stationary for constant operational conditions, such as constant heading and vessel speed. This is not suitable for the purpose of having a database receiving data from vessels simultaneously. For changing operational conditions,

the ship response should therefore be considered as non-stationary (Nielsen 2005).

The aim of this thesis is therefore to propose an alternative method that can recreate the non-stationary ship response, which facilitates the possibility of recreating the wave spectrum when the operational conditions vary with time. This is obtained by using a time-varying auto regressive model (TVAR), and Bayesian estimation methods.

1.3 Previous Work

Sea state estimation originates from the 1970's with use of moored wave buoys. The method is also an important contributor of oceanographic analysis today, in particular in areas close to shore. In harsher and deeper seas, wave buoys are exposed to damage, and the cost of mooring lines increases substantially as the sea depth increases. The wave buoy analogy solves this problem using motion spectra from ships to estimate the wave spectra, see Nielsen (2005) and Tannuri et al. (2003). These methods assume stationary ship response, making the estimation problem applicable for the Fast Fourier Transform.

The use of parametric spectral estimation methods, such as TVAR, was in the engineering aspect first used for earthquake modeling, see Kitagawa & Gersch (1985). Earthquakes are highly non-stationary, and therefore the non-parametric methods fail. The TVAR-estimation theory has been used on offshore structures by Yazid et al. (2012), and on ship response by Iseki & Terada (2003) and Iseki (2004).

1.4 Main Contribution

The main contributions of this thesis is the development of an algorithm that can analyze a non-stationary ship response. The algorithm exist on different applications, however to the author's knowledge, the derivation of the whole algorithm lacks important considerations in the literature. Therefore a rigorous derivation of the algorithm is presented, where the essential is presented in Chapters 4 to 7. In addition, two different mathematical state space models are proposed and tested, through a parameter study, see Section 8.1. Furthermore, identification of key factors and limitations of the algorithm are also given in Chapter 8, and Chapter 9. It is found that a low ratio between the state noise and the observation noise in the Kalman filter is decisive to obtain a proper result.

1.5 Outline

The thesis is divided into three parts: Part I: Ship Response, Part II: Spectral Estimation of Ship Response, and Part III: Case Studies.

Part I includes the following chapters:

- Chapter 2: Wave Theory, which contains background information of the relation between the wave spectrum and the ship response.
- Chapter 3: Non-stationary Ship Response , which explains the non-stationary behavior of the ship response.

Part II addresses the derivation of the algorithm that can recreate the non-stationary ship response, and is composed of

- Chapter 4: Mathematical Modeling, which contains a rigorous description of the mathematical models chosen to analyze the ship response.
- Chapter 5: Bayesian Estimation of TVAR parameters, presents derivation of the estimation techniques that are used in order to recreate the spectrum.
- Chapter 6: Model Order Selection contains a brief description of the evaluation criteria used to choose the correct model for the problem.
- Chapter 7: Estimation of Time Dependent Response Spectrum the relation between the estimated parameters and the recreated spectrum is derived.

Part III consisting in analyzing the performance of the algorithm, by different case studies, divided into

- Chapter 8: Stationary Simulation Studies consists of different stationary case studies made for identifying key factors and limitations in the method.
- Chapter 9: Non-Stationary Simulation Studies consists of non-stationary case study to test the robustness of the algorithm.
- Chapter 10: Ship Response Estimation of Cybership III the case study is implemented on real data from a model test, with the vessel Cybership III conducted in the MClab at the Department of Marine Technology, NTNU.

Part I

Ship Response

Introduction to the Ship Response

In this thesis, the ship response refers to the wave-induced response of the first order wave forces. Knowledge about the waves is therefore of particular importance when analyzing the ship response, and therefore wave theory is presented in Chapter 2.

The relation between the wave spectrum and the ship response for constant operational conditions is shown in Figure 1.2. However, for changing operational condition the transfer function also changes. This induces non-stationary behavior of the ship response. This will be discussed in Chapter 3.

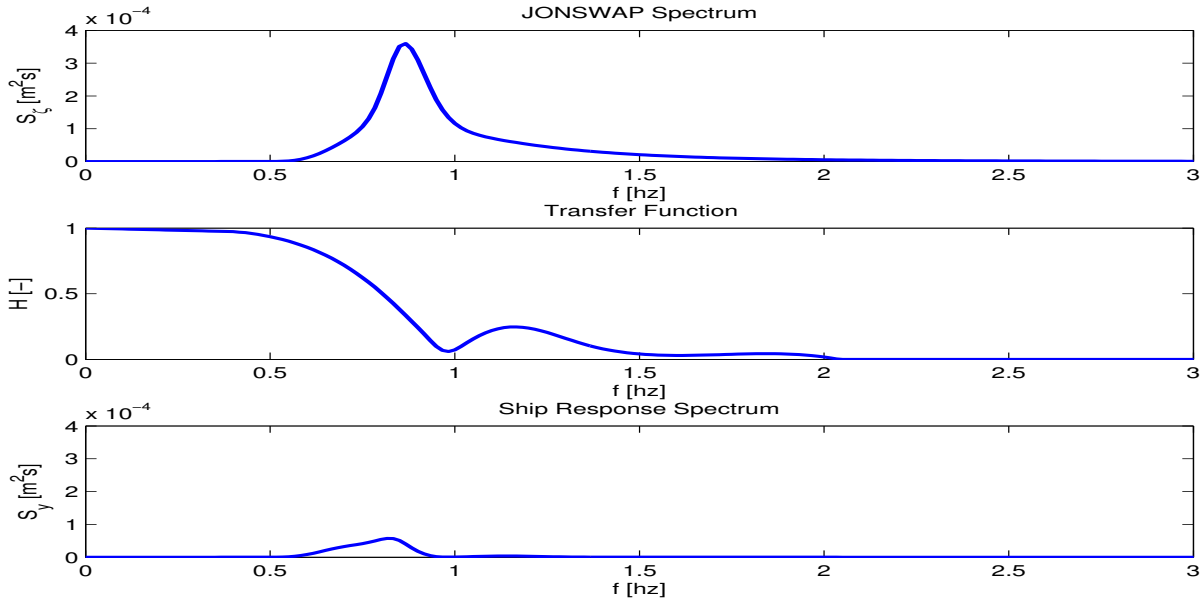

Figure 1.2: Wave spectrum, transfer function and ship response.

Chapter 2

Wave Theory

A brief description of the relevant wave theory is given is this chapter. The description is referred to Faltinsen (1990), Myrhaug (2007), Fossen (2011), and Sørensen (2012).

2.1 Sea State

The sea state is defined as the statistical representation of the wave height, distributed over the wave frequencies and the wave directions, and can be described by the significant wave height H_s, and the peak period T_p. The significant wave height is defined as the average of the $\frac{1}{3}$ highest waves Myrhaug (2007), and the peak period is defined as the dominant period in wave spectrum $S(\omega)$ which will be defined in Section 2.2.

The sea states are divided into short term sea state and long term sea state:

- Short term sea state is a statistical description of the wave heights as function of frequency and direction, for a specific duration of time in a specific area. The significant wave height, and peak period are constant. A typical duration time is around three hours.

- Long term sea state is a statistical description of which of the short term sea state that might takes place. The time length can be up to several months, and the significant wave height and the peak period vary.

The sea states are furthermore categorized in different codes, depending on the significant wave height (Price & Bishop 1974), see table Table 2.1.

Sea State Code	**Description of Sea**	**Significant Wave Height H_s**
0	Calm (Glassy)	0 m
1	Calm (Rippled)	0 - 0.1 m
2	Smooth (Wavelets)	0.1 - 0.5 m
3	Slight	0.5 - 1.25 m
4	Moderate	1.25 - 2.5 m
5	Rough	2.5 - 4 m
6	Very Rough	4 - 6 m
7	High	6 - 9 m
8	Very High	9 - 14 m
9	Phenomenal	Over 14 m

Table 2.1: Sea state codes (Price & Bishop 1974).

2.2 Wave Spectrum

A way to describe a sea state is to represent the energy as function of frequency and direction of the waves. This is called a wave spectrum, and consists of a *frequency spectrum* $S(\omega)$, and a *spreading function* $D(\psi)$,

$$S(\omega, \psi) = S(\omega)D(\psi). \tag{2.1}$$

The frequency spectrum $S(\omega)$, which is in general called a power density spectrum, describes the energy distribution of the sea state as a function of frequency ω, see Figure 2.1a, while the spreading function $D(\psi)$ gives the directional distribution of the wave energy, see Figure 2.1b.

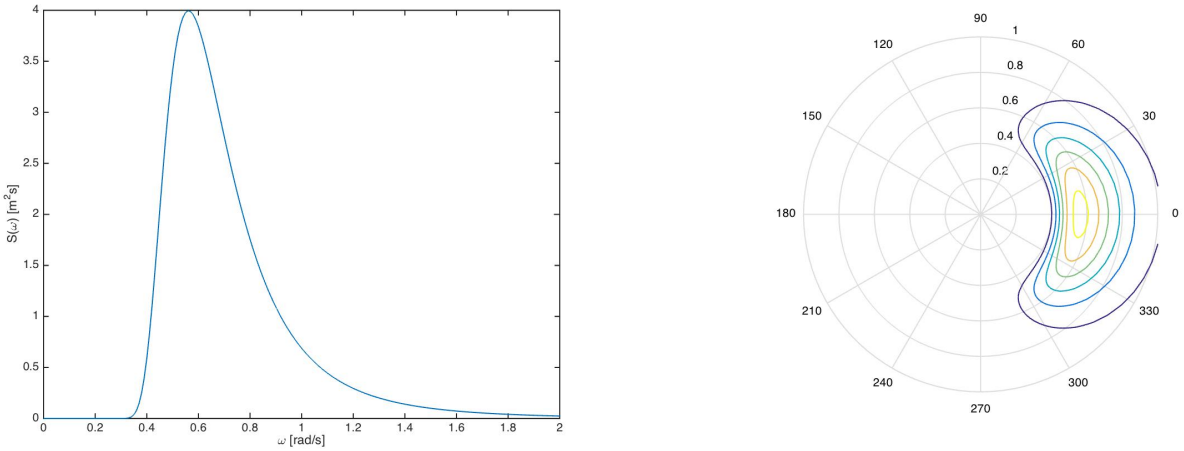

(a) Frequency spectrum of the sea state.

(b) Spreading function.

Figure 2.1: Frequency spectrum and spreading function.

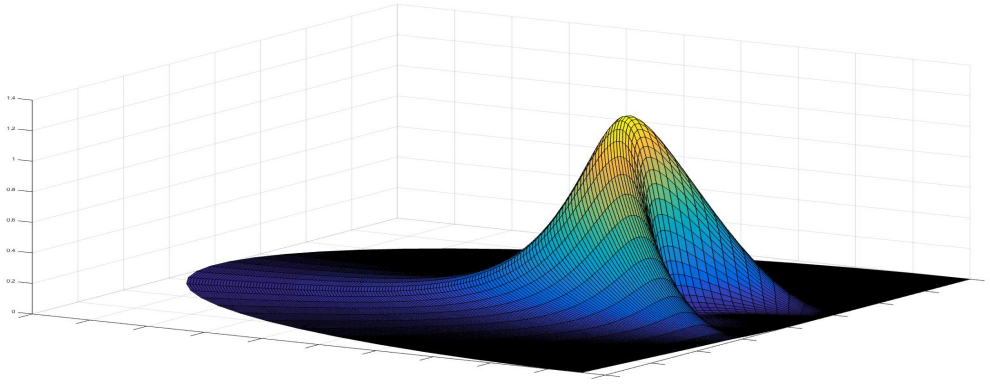

Figure 2.2: Directional wave spectrum.

In Figure 2.2 the frequency spectrum and the spreading function are combined, and is often referred to as the directional wave spectrum. In the following the emphasis will be on the frequency spectrum, and the wave spectrum will be consider only as the frequency spectrum, that is $S(\omega, \psi) = S(\omega)$.

There exist a lot of established wave spectrum, playing an important role in the design of ships and offshore structures.

The Pierson-Moskowitz spectrum (PM) is a spectrum made for representing fully developed wind-generated seas, which is an empirical made spectrum, made from samples from the North Atlantic Ocean. The formula for the spectrum is given as

$$S(\omega) = A\omega^{-5}e^{-B\omega^{-4}}, \tag{2.2}$$

where $A = 8.1 \times 10^{-3}g^2$, and $B = \frac{3.11}{H_s^2}$.

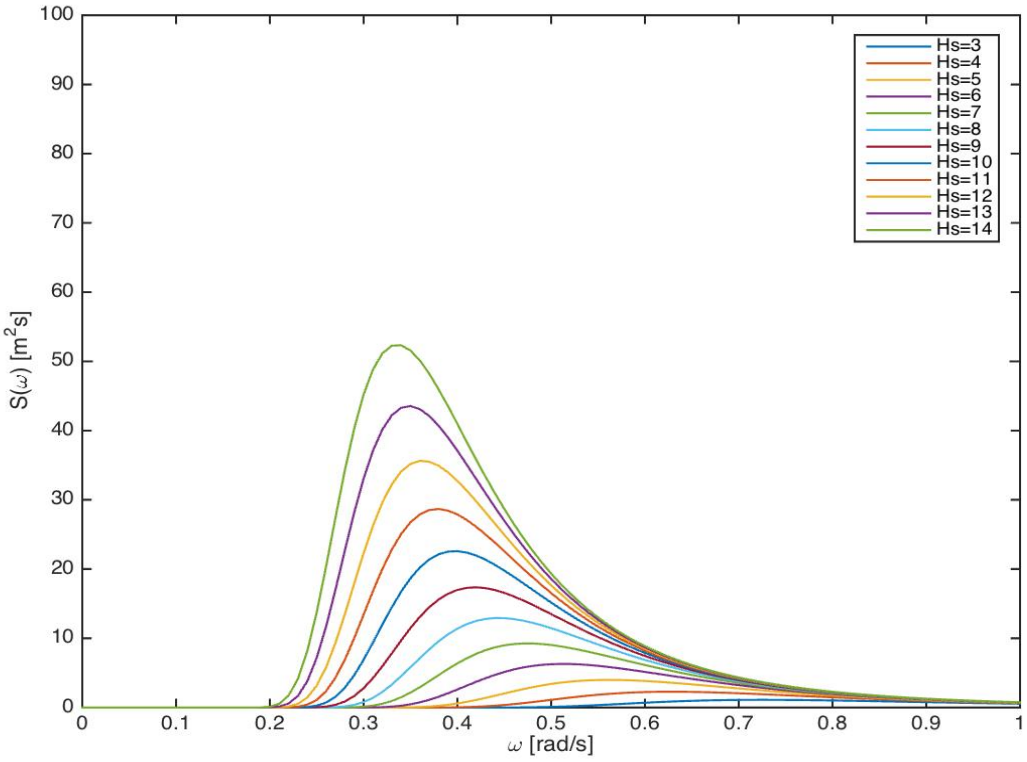

Figure 2.3: Pierson-Moscowitz spectrum for H_s = 3,4,...,14 m.

In Figure 2.3, the Pierson-Moscovitz is plotted for $H_s = 3 - 14m$. It can be seen in the figure that the spectrum is a single-peaked spectrum.

The JONSWAP spectrum is a spectrum for developing seas, and is based on measurements in the North Sea (Sørensen 2012). From Faltinsen (1990) the spectral density is given as

$$S(\omega) = 155\frac{H_s^2}{T_1^4}w^{-5}e^{-\frac{944}{T_1^{-4}}\omega^4}\gamma^Y, \tag{2.3}$$

where $\gamma = 3.3$, and Y is given as

$$Y = \exp\Big[-\Big(\frac{0.191\omega T_1}{\sqrt{2}\sigma}\Big)^2\Big], \tag{2.4}$$

where σ is given as

$$\sigma = \begin{cases} 0.07 & \text{for } \omega \leq \frac{5.24}{T_1} \\ 0.09 & \text{for } \omega > \frac{5.24}{T_1}, \end{cases} \tag{2.5}$$

where $T_1 = 0.834T_0$ (Fossen 2011), and T_0 is the peak period.

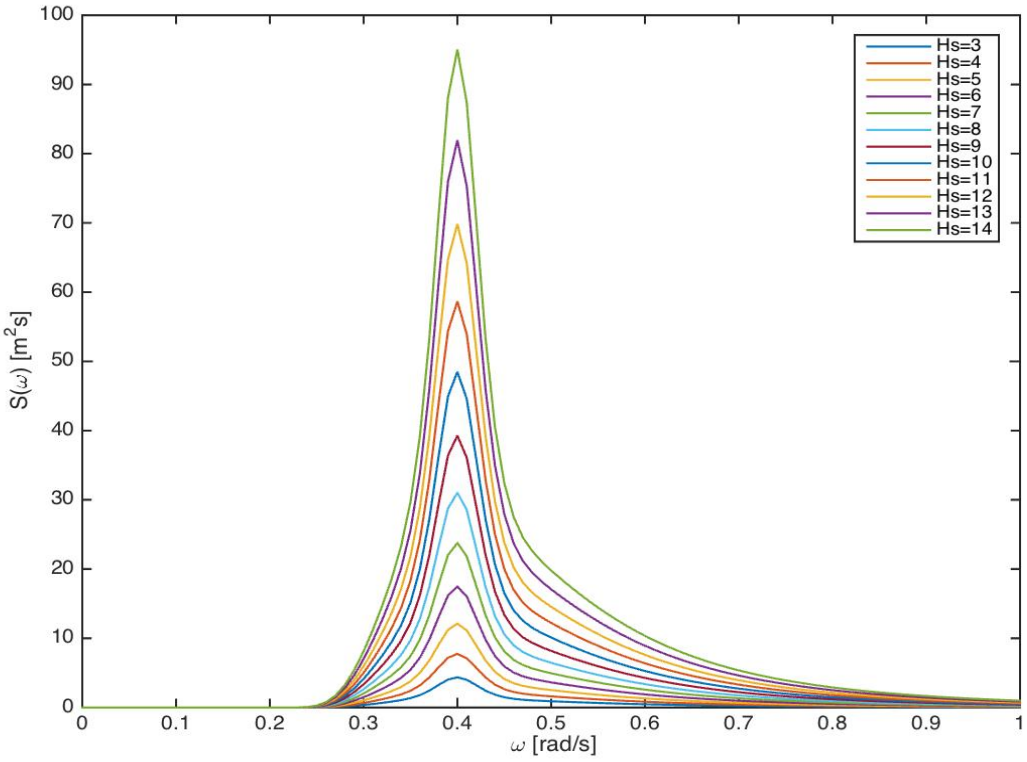

Figure 2.4: JONSWAP spectrum for H_s = 3,4,...,14 m.

In Figure 2.4, the JONSWAP spectrum is plotted for $H_s = 3 - 14m$, and $w_p = 0.4[rad/s]$. The spectrum has a sharper peak than spectrum for fully developed seas such as the PM spectrum, see Figure 2.3 and Figure 2.4.

The Torsethaugen spectrum has two spectral peaks. The first peak is due to the effect of swell, and the second is because of wind generated seas. This is an empirical spectrum which was made for Norsk Hydro in 1996 [1].

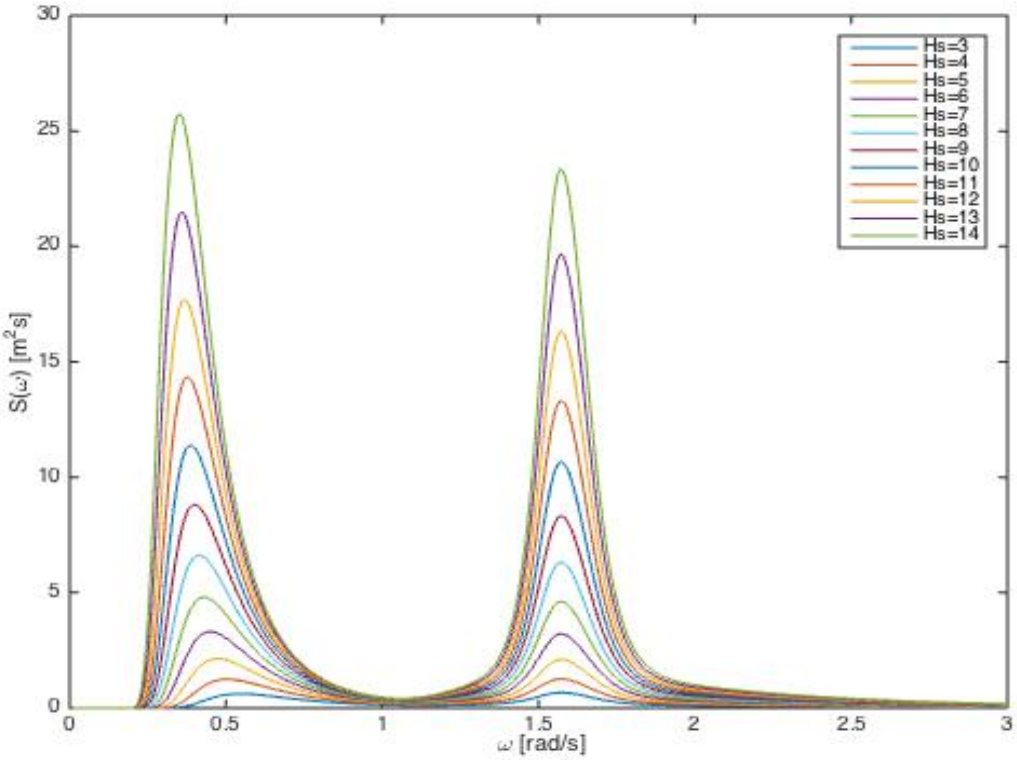

Figure 2.5: Torsethaugen spectrum for H_s = 3,4,...,14 m, and T_0=4.

In Figure 2.5 the Torsethaugen spectrum is plotted for $H_s = 3 - 14m$.

As mentioned, it is common to use time series drawn from the wave spectra in simulation studies. This is called *realizations*, and is derived in the next section.

[1] The spectrum was generated by Thor Inge Fossen's MSS toolbox in Matlab.

2.3 Realizations

The total energy in the sea state can be found by taking the integral of all frequencies and directions (Sørensen 2012), and can be written as

$$S_{tot} = \int_0^\infty \int_0^{2\pi} S(\omega, \psi) d\psi d\omega. \tag{2.6}$$

Assuming linearity, superposition of harmonic wave components extracted from the wave spectrum, can be made. Thus, a set of harmonic wave components can represent the total energy of the spectrum. The sum of these components is called irregular waves, and can be found from the wave spectrum if the chosen frequencies and direction ensure that the spectral area is covered, so that energy is conserved. This relation is given as

$$\zeta(x, y, t) = \sum_{q=1}^{N} \sum_{r=1}^{M} \sqrt{2S(\omega, \psi)\Delta\omega\Delta\psi} \sin(\omega_q t + \epsilon - k_q(x \cos(\psi_r) + y \sin(\psi_r))), \tag{2.7}$$

where k is the wave number, and ϵ is uniformly distributed between -2π to 2π, that is $\epsilon \sim \mathcal{U}(-2\pi, 2\pi)$. This is called *short-crested irregular waves*. By disregarding the directional contribution, Equation (2.7) reduces to

$$\zeta(x, y, t) = \sum_{q=1}^{N} \sqrt{2S(\omega_q)\Delta\omega} \sin(\omega_q t + \epsilon), \tag{2.8}$$

which describes *long-crested irregular waves*.

Chapter 3

Non-Stationary Ship Response

In this chapter, a few facts about stationary and non-stationary processes will be given, and the consequence related to the ship response is briefly discussed. As part of the discussion it is shown that, although a sea state itself often can be considered stationary, the induced response of a vessel operating in it, are not necessarily stationary.

3.1 Stationary Short Term Sea State

The relation between a stationary process and a power density spectrum is shown in this section.

The probability density function has time-invariant parameters for stationary processes, see Appendix A.1. For instance for Gaussian processes, the mean and the variance will be constant. According to Faltinsen (1990) the wave elevation $\zeta(t)$ can, at a specific locations for a given period of time, be assumed to be Gaussian with zero mean and variance σ_ζ^2, denoted as $\zeta(t) \sim \mathcal{N}(0, \sigma_\zeta)$. The variance is defined to be the first moment of the spectra, that is $\sigma_\zeta^2 = m_0$, where

$$m_0 = \int S(\omega) d\omega. \tag{3.1}$$

Faltinsen (1990) also states that the wave heights can be assumed to be Rayleigh distributed, denoted as $H \sim \mathcal{R}(\sigma_\zeta)$. The significant wave height and the variance can then be related by

$$\begin{aligned} H_s &= 4\sqrt{m_0} \\ &= 4\sigma_\zeta. \end{aligned} \tag{3.2}$$

Furthermore, T_p is proportional to the average wave period T_1 which is given as

$$\begin{aligned} T_1 &= 2\pi \frac{m_0}{m_1} \\ &= 2\pi \frac{\sigma_\zeta^2}{m_1}, \end{aligned} \tag{3.3}$$

and, thus, T_p depends also on the variance. Therefore, from a stationary process it follows a spectrum with constant parameters H_s and T_p, which makes the spectrum independent of time. Non-stationary processes will have time-dependent spectra because the describing parameters are time-dependent, for instance a time-dependent variance.

Although the short term sea state can be considered as stationary, it does not mean that the ship response has the same behavior, which will be discussed in the next section.

3.2 Time Dependent Response Amplitude Operator

Assuming linear theory and stationary processes, the relation between the wave spectrum and the ship response can be formulated by

$$S_y(\omega) = |H(\iota\omega)|^2 S_\zeta(\omega), \tag{3.4}$$

where $\iota = \sqrt{-1}$, $S_y(\omega)$ is the response spectrum, $S_\zeta(\omega)$ is the wave spectrum, and $H(\iota\omega)$ is the response amplitude operator (RAO), see Figure 3.1. The RAO is a transfer function relating the wave amplitude to the movement of the vessel, and is usually known for each vessel.

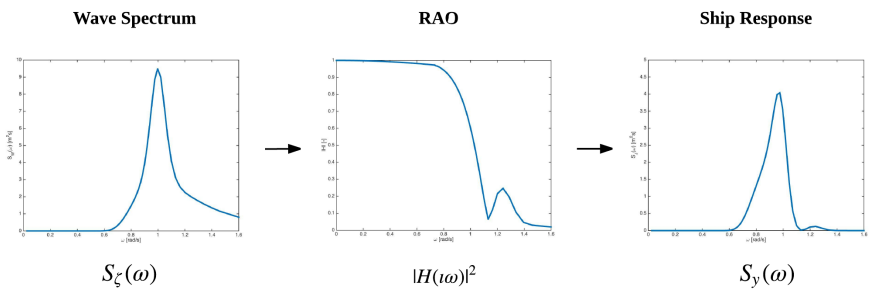

Figure 3.1: Example of a wave spectrum, RAO and the corresponding ship response.

The relation in Equation (3.4) does not hold if the operational condition changes, for instance changes in the vessel speed V, or the angle β between the vessel and the encountering waves. These two operational parameters are the ones mostly affected by decisions of the ship master, and - strictly speaking - the RAO in Equation (3.4) needs to

continuously reflect any decision made by the vessel operator. Consequently, by noting that both vessel speed and direction can be interpreted as time dependent functions, the transfer function therefore becomes time dependent, and the relation in Equation (3.4) extends to

$$S_y(\omega, t) = |H(\iota\omega), t|^2 S_\zeta(\omega). \tag{3.5}$$

This results in a time-dependent spectrum $S_y(\omega, t)$, which is non-stationary see Figure 3.2.

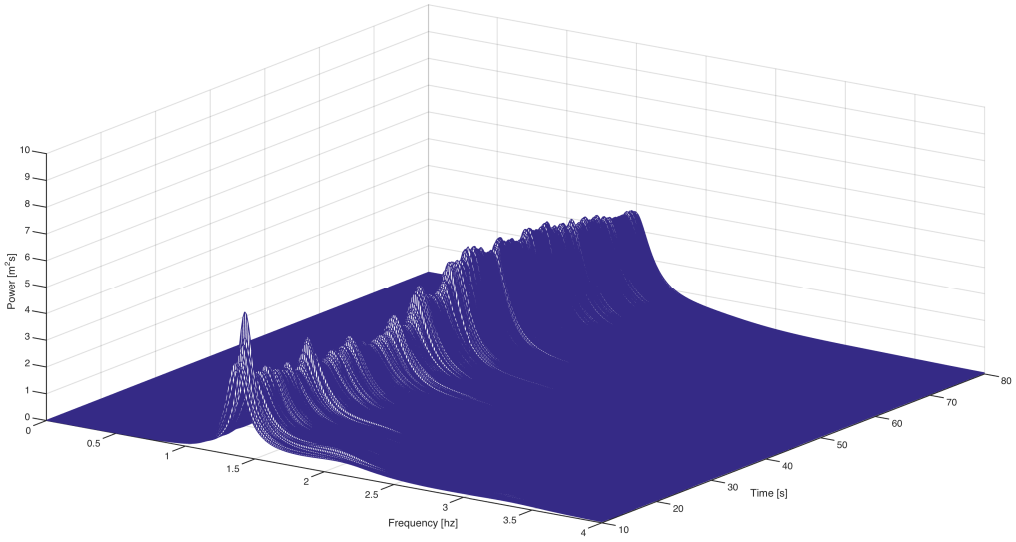

Figure 3.2: Example of evolutionary power density spectrum. The spectrum is non-stationary since it changes magnitude during the time sequence.

Part II

Spectral Estimation of Ship Response

Introduction to Spectral Estimation of Ship Response

Mainly, there exist two methods for spectral estimation: the parametric approach and the non-parametric approach, see Figure 3.3. The parametric approach assumes that the process follows a model, while in the non-parametric approach there is not any assumptions on the structure of the process.

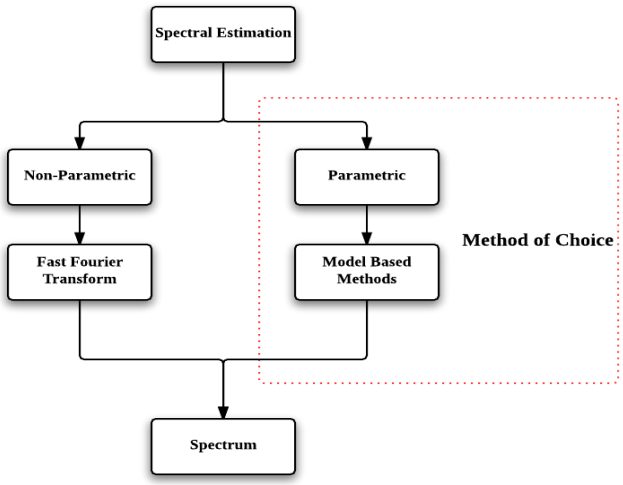

Figure 3.3: Parametric and non-parametric spectral estimation methods.

Assuming a stationary processes, the ship response spectrum can be recreated by the non-parametric method, using the Fast Fourier transform (FFT). These methods often require a long sequence of data in order to get a satisfying frequency resolution Proakis & Manolakis (2006). During this time, the ship response might have had non-stationary behavior, which makes the spectrum recreation spurious. Therefore it is more or less a trade off between frequency resolution and time resolution for the non-parametric methods in this application. In parametric methods it is assumed that the process follows a model. Therefore the method does not require such a long time time series in order to get a reasonable frequency resolution. In addition the parametric methods are able to handle

non-stationary processes which will be shown in Chapter 4. The parametric approach consists of several more steps than the non-parametric approach, see Figure 3.4. In the next chapters the different steps are derived, beginning with mathematical modeling.

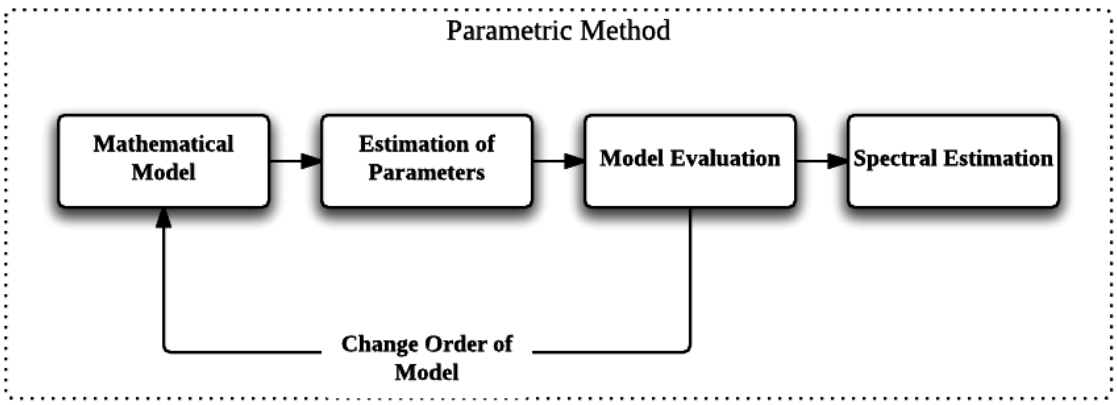

Figure 3.4: Parametric spectral estimation algorithm.

Chapter 4

Mathematical Modeling

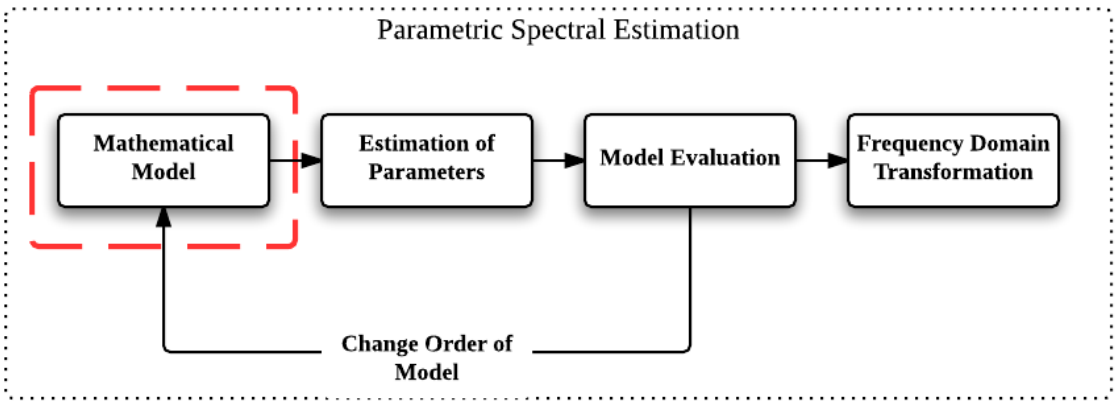

Figure 4.1: Focus area of Chapter 4 marked in red.

As mentioned in the introduction of this part, the parametric spectral method assumes that the process follows a mathematical parametric model. In this chapter, some potential models are presented, and the choice of them is justified. Furthermore, it is given indications that the particular model is able to handle non-stationary processes by introducing time-varying parameters. This action requires to formulate the model on a state space approach, and is done in the last part of this chapter. Note that two different state spaces are proposed, resulting in two mathematical models.

4.1 Parametric Mathematical Models

In this thesis the term mathematical model is used for a simplified description of a *process*, which is a comprehensive description of the real system. There exists a lot of different models of physical systems, see Figure 4.2. There also exist mathematical models which do not necessarily need to have a physical interpretation. The parametric Auto-Regressive model (AR), the Moving Average model (MA) and the Auto-Regressive Moving Average model (ARMA) are examples of such models, and are explained briefly below.

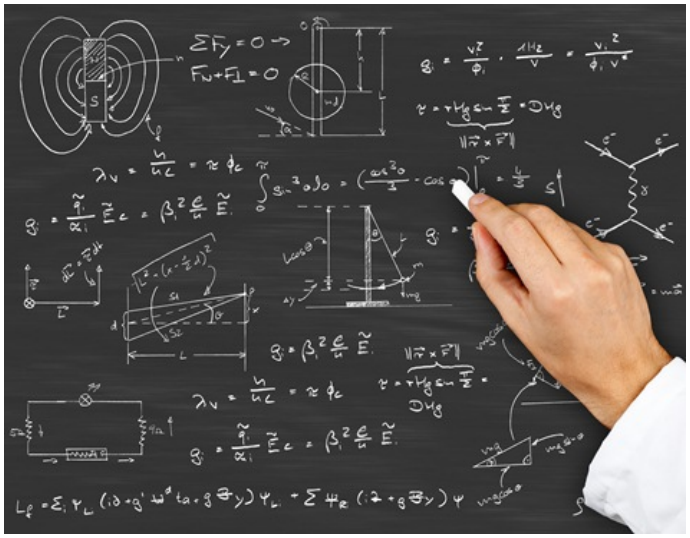

Figure 4.2: Different mathematical models. Property of Robotnor Centre for Advanced Robothics (2015).

AR, MA and ARMA models

The AR model is characterized by that the output is a linear combination of the previous outputs (Ting & Bahar 2011). The equation is given as

$$y_k = \sum_{j=1}^{p} a_j y_{k-j} + e_k, \tag{4.1}$$

where y_k is the output, p is the order of the model determining how many linear combinations of the previous data that are required, a_j are the auto regressive coefficients, and e_k is the error at time k between the data and the weighted linear combination of previous data.

The MA model is described in a slightly different way. The output is a linear combination

of the current and previous error terms

$$y_k = \mu + e_k + \sum_{j=1}^{r} b_j e_{k-j}, \tag{4.2}$$

where μ is the average of the data, r is the order of the model determining how many combinations of the error e_k that are needed.

A combination of Equation (4.1) and Equation (4.2), is called the ARMA model, and has the characteristics of both models. The ARMA model can be written as

$$y_k = \sum_{j=1}^{p} a_j y_{k-j} + \mu + e_k + \sum_{j=1}^{r} b_j e_{k-j}. \tag{4.3}$$

The models have different spectral characteristics, and the choice of them is based on initial knowledge on the spectrum which is desirable to estimate. That is which shape the ship response spectrum is most likely to take. The main differences between these model are

- the AR model has a spectrum characterized by peaks, which corresponds to having dominant frequencies (Spyers-Ashby et al. 1998),
- the MA model has a spectrum characterized by notches, which means absence of power at certain frequencies (Spyers-Ashby et al. 1998),
- and the ARMA model has a spectrum characterized by both peaks and notches (Spyers-Ashby et al. 1998).

In Section 2.2 it was shown that wave spectra can have both peaks and notches. As elaborated in Section 3.2, the ship response depends on the wave spectrum, since the ship response takes a filtrated[1] form of it. The apparent method to use seems to be the ARMA model, but according to Spyers-Ashby et al. (1998) the AR parameters are less computationally demanding than the ARMA-parameters. In a addition the ARMA model can be obtained from AR-model if the order is high enough (Marple 1986). Therefore the AR model is the model of choice.

Furthermore, in order to model a non-stationary process, the model has to be non-stationary itself. In the next paragraph, the stationary conditions of the AR model will be checked.

[1]The RAO filtrates the wave spectrum into the ship response, see Section 3.2

Stationary Analysis of AR model

Assuming that the process is Gaussian, a stationary process has a constant mean, and a co-variance that is only dependent on the time-shift, see Appendix A.1. For an AR process the mean can be calculated as

$$\begin{aligned}\mu &= E(y_k) \\ &= E(\sum_{j=1}^{p} a_j y_{k-j}) + \underbrace{E(e_k)}_{0} \\ &= \sum_{j=1}^{p} a_j \mu \\ &= \frac{0}{1-\sum_{j=1}^{p} a_j} = 0, \qquad \sum_{j=1}^{p} a_j \neq 1\end{aligned} \tag{4.4}$$

where $E(y_{k-1}) = E(y_k) = \mu$, and it is assumed that the model residuals are identically, independently distributed (IID) Gaussian white noise, that is $e_k \sim \mathcal{N}(0, \sigma_e)$. In Equation (4.4) it can be seen that the mean is constant.

Furthermore, in order to find the co-variance, the variance needs to be found and is given as

$$\begin{aligned}\sigma_y &= var(y_k) \\ &= E(y_k^2) - \underbrace{E(y_k)^2}_{0} \\ &= E((\sum_{j=1}^{p} a_j y_{k-j} + e_k)^2) \\ &= E((\sum_{j=1}^{p} a_j y_{k-j})^2) + \underbrace{2E(\sum_{j=1}^{p} a_j y_{k-j}) e_k)}_{0} + E(e_k^2) \\ &= \sum_{j=1}^{p} a_j^2 \sigma_y^2 + \sigma_e^2 \\ &= \frac{\sigma_e^2}{1-\sum_{j=1}^{p} a_j^2}, \qquad \sum_{j=1}^{p} a_j^2 \neq 1\end{aligned} \tag{4.5}$$

where $E(y_{k-1}^2) = E(y_k^2) = \sigma_y^2$. In addition it is assumed that the model residuals are

uncorrelated with the output. The co-variance of the expression can now be found by

$$\begin{aligned}\gamma_1 &= cov(y_k, y_{k+1}) = E(y_k, y_{k+1}),\\ &= E(y_k a_1 y_k + y_k a_2 y_{k-1}, ..., y_k a_p y_{k+1-p} + \underbrace{y_k e_{k+1}}_{0})),\\ &= a_1\gamma_0 + a_2\gamma_1, ..., a_p\gamma_{p-1}\\ &= \frac{a_1\gamma_0 +, ..., +a_p\gamma_{p-1}}{1 - a_2}.\end{aligned} \tag{4.6}$$

To solve Equation (4.6), the same has to be elaborated for $\gamma_i, i = 2, ..., p$, which results in p unknowns with p equation which can be solved. This is called the Yule Walker Equations, see Stoica & Moses (1997). However, the important point is to note that this expression is the same for $cov(y_{k-10}, y_{k-9})$, and therefore explicitly independent of time[2] will not be equal to for instance $cov(y_k, y_{k-10})$.

Since the mean is constant and the co-variance only depend on the time shift, this is a stationary process, and can not be applied to analyze a non-stationary ship response. Therefore a slightly modification of the AR model are needed in order to handle non-stationary processes which will be discussed in the next section.

[2]It is dependent on the time-shift since $cov(y_k, y_{k-10})$

4.2 Time Varying Auto Regression

By letting the coefficients a_j vary with time, the co-variance becomes time dependent,

$$\gamma_1(t) = \frac{a_1(t)\gamma_0(t) + , ..., + a_p(t)\gamma_{p-1}(t)}{1 - a_2(t)}, \tag{4.7}$$

and the model becomes non-stationary. Models of this type is called time-varying auto regressive models (TVAR), and is defined below. In the definition discrete time is used, indexed by k.

Definition 1 (TVAR model) *The time-varying auto-regressive model is given as*

$$y_k = \sum_{j=1}^{p} a_{k,j} y_{k-j} + e_k \tag{4.8}$$

where p is the order of the model, y_k is the output, $a_{k,j}$ are the unknown parameter coefficients, and e_k is the estimation error.

The challenge with this approach is to estimate the parameters in the TVAR model, both the static parameter p, and the time varying parameters $a_{k,j}$. The time-varying parameters will be estimated by Bayesian tools described in Chapter 5, and the static parameter will be determined by an information criteria which is presented in Chapter 6.

Due to the time-dependency of the parameters, the model needs to be formulated in a state space approach to describe how the parameters change. This is also required in order to use the Bayesian estimation techniques, and will be derived in the next section.

4.3 State Space Formulation

In order to use Bayesian prediction tools like the Kalman filter or the Particle filter, the model needs to be formulated in a *state space approach*. In this approach the mathematical model is extended to have a set of differential equations, describing the evolution of the *states*.

A state space is composed of the *observation equation* and *the transition equation*, which will be further analyzed in the upcoming sections. Note that two different state spaces will be proposed, which require different estimation filters to be solved.

4.3.1 Observation Equation

The observation equation is a compact form of Equation (4.8). This equation shows the relation between the output and the time varying parameters, which are defined as the states, $x_k = [a_{k,1}, a_{k,2}, ..., a_{k,p}]^T$. It is written as

$$y_k = C_k x_k + e_k, \tag{4.9}$$

where $C_k = [y_{k-1}, y_{k-2}, ..., y_{k-p}]$. This equation is time varying and linear. The error term e_k is assumed to be Gaussian distributed with zero mean, and with a variance of σ_e^2, denoted as $e_k \sim \mathcal{N}(0, \sigma_e)$. The reason for this assumption is that Gaussian distributions should be assumed first, unless other information is available (Brekke 2010).

Probability Density Function of Observation Equation

Since the variable is subject to white noise in Equation (4.10), the variable y_k becomes a random variable. Random variables are often described by *probability density functions*, which is defined as the probability that y_k will fall within a small interval dy. However, since that the states x_k are already known at this point, y_k is conditional random variable, and can be described by the conditional probability density function. This is defined as the probability that y_k fall into the interval dy, given the states x_k.

The equation for the conditional density function can be found by rearranging Equation (4.10), so that

$$y_k - C_k x_k = e_k. \tag{4.10}$$

Thus, the left hand side needs to have the same distribution as the right hand side. Since the e_k is Gaussian distributed, the expression $p(y_k|x_k)$ is also Gaussian distributed. This

can be written as

$$p(y_k|x_k) = p_e(y_k - C_k x_k), \tag{4.11}$$

where p_e is the probability density function of the model residuals.

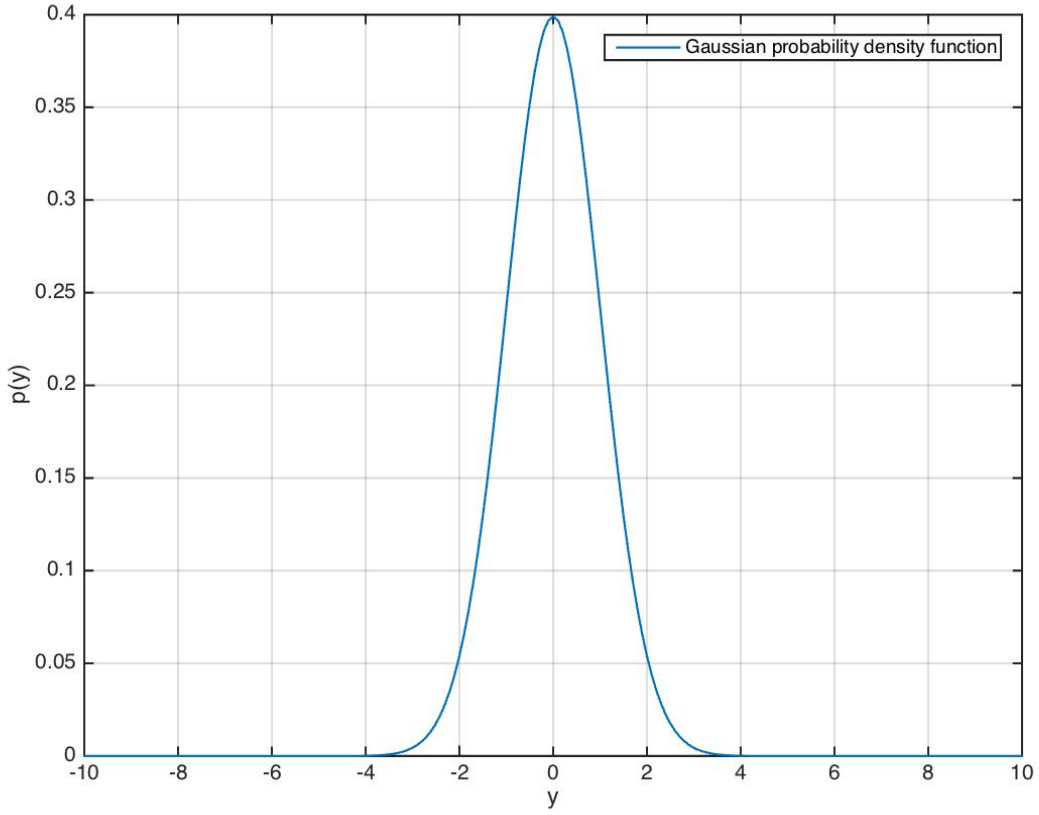

Figure 4.3: Gaussian probability density function, with zero mean and unity variance

The formula for the Gaussian probability density function is given as

$$p(y_k|x_k) = \frac{1}{\sqrt{2\pi\sigma_e^2}} e^{\frac{(y_k - C_k x_k)^2}{2\sigma_e^2}} \tag{4.12}$$

An example is shown in Figure 4.3 with zero mean and unity variance.

4.3.2 Transition Equation

The transition equation represents the differential equations in the state space. These equations show the rate of change of the variables in our system. The discrete version of these equations are called difference equations which are used here.

Because the model is based on an auto regressive model without a physical interpretation it is hard to predict how the difference equations are related and will evolve. Thus, assumptions are required, and are discussed in the next paragraphs.

Assumption 1 *The transition equation follows a first order Markov property.*

Definition 2 (Markov Property) *Given the Markov property, the probability of x_k at time k, given the sequential set $x_{1:k-1}$ is only dependent on the set x_{k-1}, given at the previous time instant, and can be mathematically stated as*

$$p(x_k|x_{1:k-1}) = p(x_k|x_{k-1}, x_{1:k-1}) = p(x_k|x_{k-1}). \tag{4.13}$$

The reason for choosing this property is that it is computational effective, and therefore will simplify the estimation calculations.

Assumption 2 *The difference equation of the states follows a random noise.*

The reason for doing this assumption is to allow the states to change. Inspired by bias estimation in the dynamical positioning (DP) equation, the transition equation is proposed to be equal to

$$x_k = \Phi x_{k-1} + \Gamma v_k, \tag{4.14}$$

where Φ is the identity matrix. In Yazid et al. (2012) this also used which support this proposition.

In the introduction of this section, it was mentioned that two state space approaches are suggested. This in terms of which probability density function the state noise v_k is assumed to follow. These two will be presented in the following paragraphs.

Gaussian distributed state noise

In the first model it is assumed that the transition equation is subject to Gaussian identical independent (IID) white noise with zero mean and variance denoted as σ_v^2, i.e. $v_k \sim \mathcal{N}(0, \sigma_v)$. Thus, the transition kernel is stochastic and can be written as

$$p(x_k|x_{k-1}) = p_v(x_k - x_{k-1}), \tag{4.15}$$

where p_v is the Gaussian probability density function of v_k. If the order p is higher than one, meaning that x_k is a vector, the distribution becomes multivariate and can be written as

$$p_v = \frac{1}{(2\pi)^{\frac{p}{2}}|Q|^{\frac{1}{2}}} e^{-\frac{1}{2}(x_k - x_{k-1})^T Q^{-1}(x_k - x_{k-1})}, \tag{4.16}$$

where $|Q|$ is the determinant of multivariate co-variance Q. Note that we use the multivariate co-variance matrix and mean, as it handles multidimensional random variables x_k. These are denoted as

$$Q = \begin{bmatrix} \sigma_{v_{1,1}} & 0 & \dots & 0 \\ 0 & \sigma_{v_{2,2}} & \dots & 0 \\ \vdots & \vdots & \ddots & \vdots \\ 0 & 0 & \dots & \sigma_{v_{p,p}} \end{bmatrix}, \qquad \mu_v = \begin{bmatrix} E[v_1] \\ E[v_2] \\ \vdots \\ E[v_p] \end{bmatrix} = \begin{bmatrix} 0 \\ 0 \\ \vdots \\ 0 \end{bmatrix}. \tag{4.17}$$

Cauchy distributed state noise

The other state noise that is proposed is noise generated from the Cauchy distribution, see (Leira 2005).

In extreme conditions, the transient response may change rapidly, making the time varying parameters to change drastically in the state space. Therefore, it might be necessary to increase the variance of the Gaussian distribution in order to capture a bigger state space. However, this could lead to a more noise in the state evolution which is not desirable.

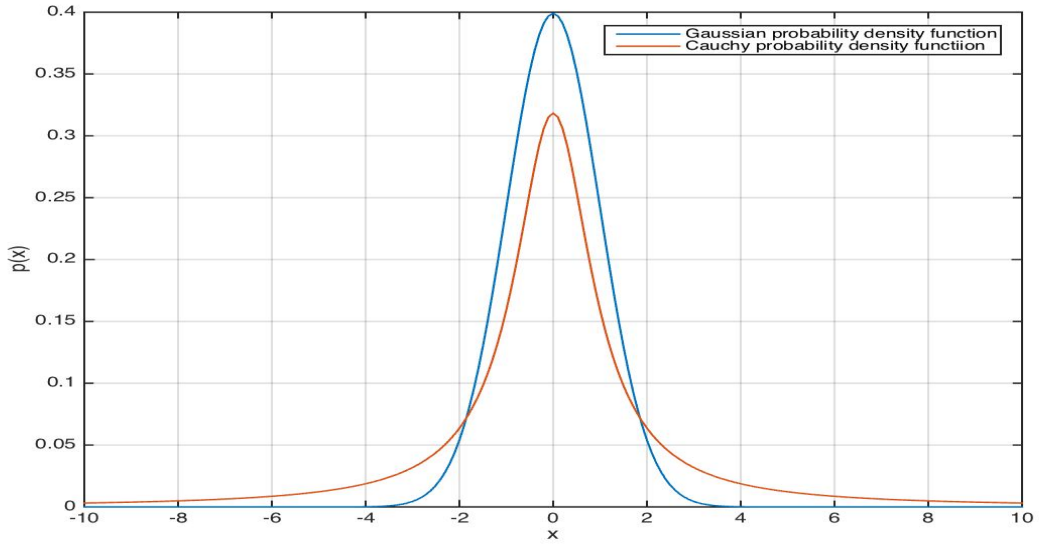

Figure 4.4: Gaussian and Cauchy Probability Density Function

The Cauchy distribution is more long tailed and more narrow in the center than the Gaussian distribution, see Figure 4.4). Therefore the Cauchy noise is maybe able to capture sudden changes without increasing the noise on the states.

Thus Cauchy distributed noise could be a more favorable choice of state noise in extreme conditions. This is discussed more in Chapter 8. The formula for the Cauchy probability

density function is given as

$$p(x_k|x_{k-1}) = \frac{1}{\pi\sigma_c[1 + (x_k - x_{k-1})^2/\sigma_c^2]} \tag{4.18}$$

where σ_c is a scaling parameter.

4.3.3 Resulting Mathematical Model

The state space can be written as

$$\begin{bmatrix} x_{k,1} \\ x_{k,2} \\ \vdots \\ x_{k,p} \end{bmatrix} = \underbrace{\begin{bmatrix} 1 & 0 & \dots & 0 \\ 0 & 1 & \dots & 0 \\ \vdots & \vdots & \ddots & \vdots \\ 0 & 0 & \dots & 1 \end{bmatrix}}_{\Phi} \begin{bmatrix} x_{k-1,1} \\ x_{k-1,2} \\ \vdots \\ x_{k-1,p} \end{bmatrix} + \underbrace{\begin{bmatrix} 1 & 0 & \dots & 0 \\ 0 & 1 & \dots & 0 \\ \vdots & \vdots & \ddots & \vdots \\ 0 & 0 & \dots & 1 \end{bmatrix}}_{\Gamma} \begin{bmatrix} v_{k,1} \\ v_{k,2} \\ \vdots \\ v_{k,p} \end{bmatrix} \tag{4.19}$$

$$y_k = \underbrace{\begin{bmatrix} y_{k-1} & y_{k-2} & \dots & y_{k-p} \end{bmatrix}}_{C_k} \begin{bmatrix} x_{k,1} \\ x_{k,2} \\ \vdots \\ x_{k,p} \end{bmatrix} + e_k \tag{4.20}$$

where the state noise $v_{k,1}, v_{k,2}, \dots, v_{k,p}$ is assumed to be Gaussian or Cauchy distributed, and e_k is assumed to be Gaussian distributed. In other words the system is either a linear time-variant Gaussian system, or a linear time-variant non-Gaussian system.

The mathematical frame has been established, and to make it applicable both static and time-varying parameters need to be determined. The static parameters to be determined:

- The order of the model p.
- The co-variance of the state noise σ_v.
- The co-variance of the observation noise σ_e.

The time-varying parameters to be estimated:

- The timevarying parameters x_k.

Observers can be constructed to estimate time varying parameters. Mainly there exists two main categories of observers, known as deterministic observers and stochastic observers. Deterministic observers are acquired for deterministic systems without uncertainty. The most famous deterministic observer is called the Luenberger observer (Luenberger 1971). Stochastic observers are most applicable to systems with uncertainties, and Bayesian observers fall into this category. Two observers that can be derived from Bayesian theory are the Kalman filter and the Particle filter. These are going to be used to estimate the time varying parameters of the two different state spaces proposed in this chapter.

Chapter 5

Bayesian Estimation of TVAR Parameters

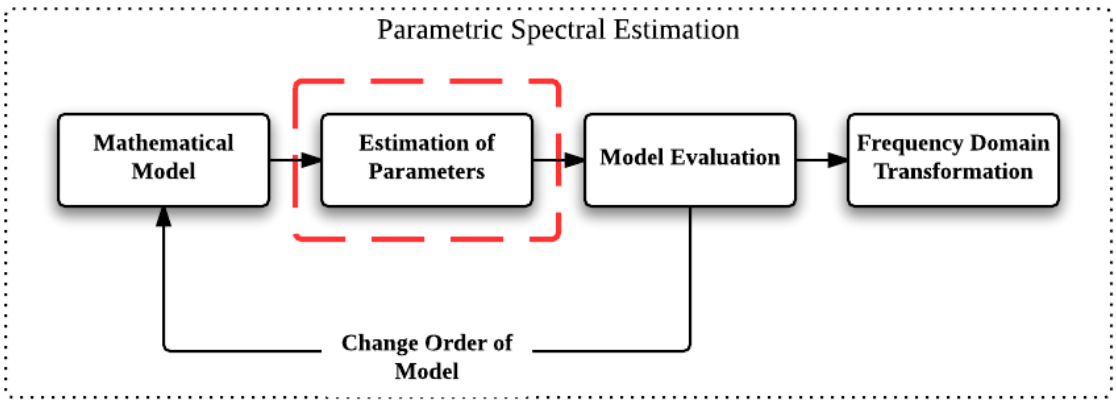

Figure 5.1: Focus area of Chapter 5 marked in red.

In Chapter 4 two state space models were proposed. The estimation techniques used to estimate the time-varying parameters on these models, will be derived from a Bayesian perspective in this chapter. Firstly, preliminaries of Bayesian estimation is presented. Based on this, both the Kalman filter and the Particle filter are derived, and will be presented in the last sections.

5.1 Preliminaries of Bayesian Estimation

First in this section the motive of Bayesian estimation is presented. Furthermore, the Bayesian update recursion is presented which is the fundamental algorithm that Bayesian estimation techniques is built upon.

5.1.1 Motive of Bayesian Estimation

In Bayesian estimation the time varying parameter vector $x_k = [a_{k,1}, a_{k,2}, ..., a_{k,p}]^T$ is considered to be a stochastic variable, instead of an unknown, and this is done in Equation (4.14), where the unknown parameter vector is transformed to a stochastic variable because of the random noise. As mentioned in Section 4.3.1 stochastic variables, given certain information, are described by the conditional distribution. Two such distributions are called *the prior distribution* and *the posterior distribution*.

- The prior distribution, denoted as $p(x_k|y_{1:k-1})$, defines the conditional probability density function of the random variable x_k, given the measurements $y_{1:k-1}$ up to the previous time step. This is a predictive term.
- The posterior density, denoted as $p(x_k|y_{1:k})$, represents the probability density function of x_k given $y_{1:k}$ current time step. This is a correcting term.

The most likely value of the time varying parameters x_k, given $y_{1:k}$ can be estimated by taking the mean of the posterior distribution. Hence finding the posterior distribution is the main motive of Bayesian estimation techniques.

The Bayesian recursion is an recursive algorithm to calculates the prior and the posterior density function, and is derived in the next section.

5.1.2 Bayesian Update Recursion

The Bayes update recursion is fundamental for all Bayesian filtering, and consists of two steps:

- *The Measurement Update*: Correction from measurements (posterior).
- *Time Update*: Prediction in time (prior).

The derivation of the of the Bayesian update recursion is given in Appendix A.3, and is summarized below.

Algorithm 1 Bayes Update Recursion

- Measurement update

$$p(x_k|y_{1:k}) = \frac{p(y_k|x_k)p(x_k|y_{1:k-1})}{p(y_k|y_{1:k-1})} \tag{5.1}$$

- Marginalization

$$p(y_k|y_{1:k-1}) = \int p(y_k|x_k)p(x_k|y_{1:k-1})dx_k \tag{5.2}$$

- Time Update

$$p(x_{k+1}|y_{1:k}) = \int p(x_{k+1}|x_k)p(x_k|y_{1:k})dx_k \tag{5.3}$$

5.2 Kalman Filter

The Kalman filter by Kalman (1960) is a recursive algorithm to find expected value, and the co-variance of the posterior distribution. In particular in navigation and guidance for vehicles such as aircraft, spacecraft or marine vessels this estimation theory has been pioneering, but is today used in every aspect of estimation.

5.2.1 Gaussian Simplification

For Gaussian systems, only the expected value and the covariance are needed to represent the posterior $p(x_k|y_{1:k})$ (Simon (2006)), that is

$$p(x_k|y_{1:k}) = \mathcal{N}(x_k, \mu_{k|k}, P_{k|k}). \tag{5.4}$$

For linear Gaussian system, the posterior is calculated analytically and it is this simplification that makes this possible. This will be shown in the next sections.

5.2.2 Kalman Filter Equations

The Kalman equations can be derived in several different ways, for instance as the linear quadratic estimator (LQE) or by the Bayesian update recursion. In this thesis it will be done by the latter.

Measurement update

The measurement update starts with Bayes law given in Equation (5.1), where the normalization Equation (5.2) is omitted. This is allowed since this term only serve to normalize the posterior density distribution, meaning that

$$\int p(x_k|y_{1:k})dx_k = 1. \tag{5.5}$$

However, this means that the posterior density function given in Equation (5.1), is proportional to

$$p(x_k|y_{1:k}) \propto p(y_k|x_k)p(x_k|y_{1:k-1}). \tag{5.6}$$

Both the prior $p(x_k|y_{1:k-1})$ and the likelihood function, denoted $p(y_k|x_k)$ are Gaussian, therefore the posterior can be written as

$$\begin{aligned} p(x_k|y_{1:k}) &\propto \mathcal{N}(y_k, C_k x_k, R)\mathcal{N}(x_k, \mu_{k|k-1}, P_{k|k-1}), \\ &= \mathcal{N}(x_k, \mu_{k|k}, P_{k|k}). \end{aligned} \tag{5.7}$$

Therefore, the posterior can be found by finding $\mu_{k|k}$, and $P_{k|k}$. The derivation of the measurement update for these two are given in Appendix A.4, and the final result is written as

$$\begin{aligned} P_{k|k} &= \Big(I - K_k C_k\Big) P_{k|k-1}, \\ \mu_{k|k} &= \mu_{k|k-1} + K_k(y - C_k \mu_{k|k-1}), \end{aligned} \tag{5.8}$$

where the kalman gain is given as

$$K_k = P_{k|k-1} C_k^T (R + C_k P_{k|k-1} C_k^T)^{-1}. \tag{5.9}$$

Time update

The time update for the expected value and the covariance, is given in Appendix A.4.

$$\begin{aligned} P_{k+1|k} &= \Phi P_{k|k} \Phi^T + \Gamma Q \Gamma^T \\ \mu_{k+1|k} &= \Phi \mu_{k|k} \end{aligned} \tag{5.10}$$

The total algorithm is summarized below. Note that the following notation $\bar{x}_k = \mu_{k+1|k}$, $\hat{x}_k = \mu_{k|k}$, $\bar{P}_k = P_{k+1|k}$, and $\hat{P}_k = P_{k|k}$ is used.

Algorithm 2 Kalman filter (Fossen 2011)

Initialization

- Design matrices:

$$Q_k = Q_k^T, \quad R_k = R_k^T \tag{5.11}$$

- Initial conditions:

$$\bar{x}(0) = x_0, \quad \bar{P}(0) = P_0 \tag{5.12}$$

Measurement update

- Kalman gain matrix:

$$K_k = \bar{P}_k H_k^T [H_k \bar{P}_k H_k^T + R_k]^{-1} \tag{5.13}$$

- Expected value correction update

$$\hat{x}_k = \bar{x}_k + K_k[y_k - H_k \bar{x}_k] \tag{5.14}$$

- Covariance correction update

$$\begin{aligned} \hat{P}_k = [I - K_k H_k]\bar{P}_k[I - K_k H_k]^T \\ + K_k R_k K_k^T \end{aligned} \tag{5.15}$$

Time update

- Expected value prediction update

$$\bar{x} = \Phi_k \hat{x}_k \tag{5.16}$$

- Co-variance prediction update

$$\bar{P} = \Phi_k \hat{P}_k \Phi_k^T + \Gamma_k Q_k \Gamma_k^T \tag{5.17}$$

Remark 1 *Note that the Q and R values, have contradictory functions, and it is the ratio between them that decides how much state noise and observation noise that is accepted in the estimate. The ratio can be described by the signal to noise ratio (SNR) (Gustafsson 2010*b*).*

$$SNR \propto \sqrt{det(Q)/det(R)} \tag{5.18}$$

5.3 Particle filter

To solve the non-Gaussian model proposed in Chapter 4, the Particle filter is used. The Particle filter theory can be traced back to Hammersley & Morton (1954), but was first discussed as a complete algorithm in Gordon et al. (1993). Then, the method was further developed by Kitagawa (1996), Isard & Blake (1998), and Doucet et al. (2001).

The Particle filter approximates the posterior density function, and is able to handle non-linear and non-Gaussian processes.

5.3.1 Introduction to Monte Carlo Simulation

In the Bayesian update recursion given in Section 5.1.2, problems might arise when evaluating the integrals. The distributions may have high dimensions, making it hard to solve Equation (5.3) numerically. In addition, the distribution can be unknown. These problems can be addressed by *Monte Carlo integration*. The Monte Carlo integration is given as

$$\begin{aligned} I &= \int h(x)p(x)dx \\ &\approx \frac{1}{N}\sum_{i=1}^{N} h(x^i), \qquad x^i \sim p(x), \end{aligned} \tag{5.19}$$

where $h(x)$ and $p(x)$ are Monte Carlo factors, and x^i means that x is sampled from a distribution $p(x)$, denoted $x^i \sim p(x)$. Noting that if $h(x) = x_k$, and $p(x) = p(x_k|y_{1:k})$, this integral evaluates the expected value of the posterior density function.

However, since the posterior density function is not Gaussian, it is unknown, and therefore sampling from it is not possible. This problem can be solved by *importance sampling*.

Importance sampling is a technique in Monte Carlo simulation of finding the expected value of a distribution by sampling from another distribution. This density function is called the importance sampling function $q(x_k|y_{1:k})$. By multiplying and dividing the importance sampling with Equation (5.19), the expression for the expected value can be

written as,

$$\begin{aligned} E(x_k) &= \int x_k p(x_k|y_{1:k}) dx_k, \\ &= \int \underbrace{x_k \frac{p(x_k|y_{1:k})}{q(x_k|y_{1:k})}}_{h(x)} \underbrace{q(x_k|y_{1:k})}_{p(x)} dx_k, \\ &\approx \frac{1}{N} \sum_{i=1}^{N} x_k^i \frac{p(x_k^i|y_{1:k})}{q(x_k^i|y_{1:k})}, \\ &= \frac{1}{N} \sum_{i=1}^{N} x_k^i w_k^i, \qquad x_k^i \sim q(x_k^i|y_{1:k}), \end{aligned} \tag{5.20}$$

where

$$w_k = \frac{p(x_k^i|y_{1:k})}{q(x_k^i|y_{1:k})} \tag{5.21}$$

are called the importance weights. Here, it is assumed that it is possible to evaluate w_k, at the points x^i. However, usually this can be evaluated up to a normalization constant, which is unknown in this case. Below, the Monte Carlo integral is evaluated when the normalization constant is unknown.

The normalized distributions are given as

$$\tilde{p}(x_k|y_{1:k}) = \frac{p(x_k|y_{1:k})}{c_p}, \qquad \tilde{q}(x_k|y_{1:k}) = \frac{q(x_k|y_{1:k})}{c_q}, \tag{5.22}$$

where the $\tilde{p}(x_k|y_{1:k})$, and $\tilde{q}(x_k|y_{1:k})$ are the normalized distribution with the respective normalization constants given as

$$c_p = \int p(x|y_{1:k}) dx > 0, \qquad c_q = \int q(x|y_{1:k}) dx > 0. \tag{5.23}$$

By inserting Equation (5.22) into Equation (5.20), the expected value can be written as

$$\begin{aligned} E(x_k) &= \int x_k \tilde{p}(x_k|y_{1:k}) dx_k \\ &= \int x_k \frac{\tilde{p}(x_k|y_{1:k})}{\tilde{q}(x_k|y_{1:k})} q(x_k|y_{1:k}) dx_k \\ &= \int \underbrace{x \frac{p(x_k|y_{1:k})}{q(x_k|y_{1:k})} \frac{c_q}{c_p}}_{h(x)} \underbrace{q(x_k|y_{1:k})}_{p(x)} dx_k \\ &\approx \frac{c_q}{c_p} \frac{1}{N} \sum_{i=1}^{N} x_k^i w_k^i, \qquad x_k^i \sim q(x_k|y_{1:k}) \end{aligned} \tag{5.24}$$

where $w_k = \frac{p(x_k|y_{1:k})}{q(x_k|y_{1:k})}$ are the unnormalized importance weights. The ratio[1] between the normalization constant, can be computed by

$$\begin{aligned}\frac{c_p}{c_q} &= \frac{1}{c_q}\int \tilde{p}(x_k|y_{1:k})dx_k \\ &= \int \underbrace{\frac{p(x_k|y_{1:k})}{q(x_k|y_{1:k})}}_{h(x)} \underbrace{\tilde{q}(x_k|y_{1:k})}_{p(x)} dx_k \\ &\approx \frac{1}{N}\sum_{i=1}^{N} w_k, \qquad x_i \sim q(x_k|y_{1:k}).\end{aligned} \tag{5.25}$$

Putting Equation (5.25) into Equation (5.24), the following relationship is obtained,

$$\begin{aligned}E(x) &\approx \frac{\frac{1}{N}\sum_{i=1}^{N} x_k^i \tilde{w}(x_k^i)}{\frac{1}{N}\sum_{i=1}^{N} \tilde{w}(x_k^i)}, \\ &= \sum_{i=1}^{N} \frac{x_k^i \tilde{w}(x_k^i)}{\sum_{i=1}^{N} \tilde{w}(x_k^i)} \\ &= \sum_{i=1}^{N} x_k^i \hat{w}_k, \qquad x_k^i \sim q(x_k),\end{aligned} \tag{5.26}$$

where $\hat{w}_k = \frac{w_k}{\sum_{i=1}^{N} w_k}$ are the normalized importance weights. This is the estimate of the expected value of the posterior. The normalized importance weights are still unknown, and these are found by the Particle filter derived in the next section.

5.3.2 Derivation of the Particle Filter

According to Arulampalam et al. (2002) the posterior distribution can be estimated by

$$p(x_k|y_{1:k}) = \sum_{i=1}^{N_p} \hat{w}_k \delta(x_k - x_k^i), \qquad x^i \sim q(x_k|y_{1:k}) \tag{5.27}$$

where $\delta(x_k - x_k^i)$ is the dirac delta function[2], meaning that a weighted sum of impulse functions is an estimate of the posterior. Note that in this expression the posterior density function is parameterized by the importance weights w_k, and the samples x_k^i from the sampling distribution $q(x_k|y_{1:k})$. The importance weights are called particle weights and the samples are called particles, and therefore it is called the Particle filter. In the following the update laws of these parameters are derived.

[1] Note that the ratio have been flipped for simplicity.

[2] Note that this is only for the mathematical derivation, and is not implemented.

The unnormalized particle weights can written as

$$w_k \propto \frac{p(x^i_{0:k}|y_{1:k})}{q(x^i_{0:k}|y_{1:k})} \tag{5.28}$$

Here it can be seen that the particle weights are dependent on the information from the whole trajectory, that is $\{x_j\}_{k=0}^{N_k}$, and $\{y_j\}_{k=0}^{N_k}$. This is computationally inefficient. Therefore the particle weights should be calculated recursively, meaning that the weights are dependent on the previous weights w_{k-1} instead of the information from the whole trajectory. This is derived in Appendix A.6, and gives the following result

$$w^i_k \propto w^i_{k-1}\frac{p(y_k|x^i_k)p(x^i_k|x^i_{k-1})}{q(x^i_k|x_{k-1}i, y_{1:k})}, \qquad x^i \sim q(x_k|x_{k-1}, y_k), \tag{5.29}$$

where $p(y_k|x^i_k)$ is derived in Equation (4.12), and $p(x^i_k|x^i_{k-1})$ is given in Equation (4.18).

By choosing $q(x_k|x_{k-1}, y_k) = p(x_{k+1}|x_k)$, the weight update law in Equation (5.29) reduces to

$$w^i_k \propto w^i_{k-1}p(y_k|x^i_k). \tag{5.30}$$

Then by normalizing the weights by

$$\hat{w}^i_k = \frac{w^i_k}{\sum_{i=1}^N w^i_k}, \tag{5.31}$$

the algorithm is complete. To sum up, N_p particles x^i are sampled from $p(x_k|x_{k-1})$, and $p(y_k|x^i_k)$ is evaluated. Furthermore, the weights w^i_k for each particle are updated and normalized. The posterior density function can therefore be found by Equation (5.27), see Figure 5.2. Furthermore, the expected value can be found by Equation (5.26).

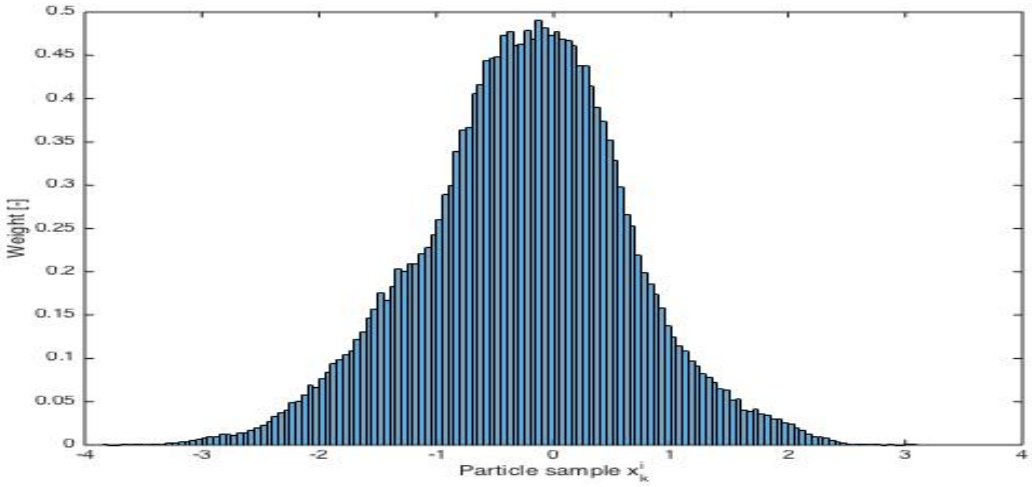

Figure 5.2: Particles with their normalized weights as an estimate of the posterior density function.

5.3.3 Resampling

A common problem with this algorithm is that after a few iterations, only a few particles have considerable weights, while the others have weights equal to zero, see Figure 5.3.

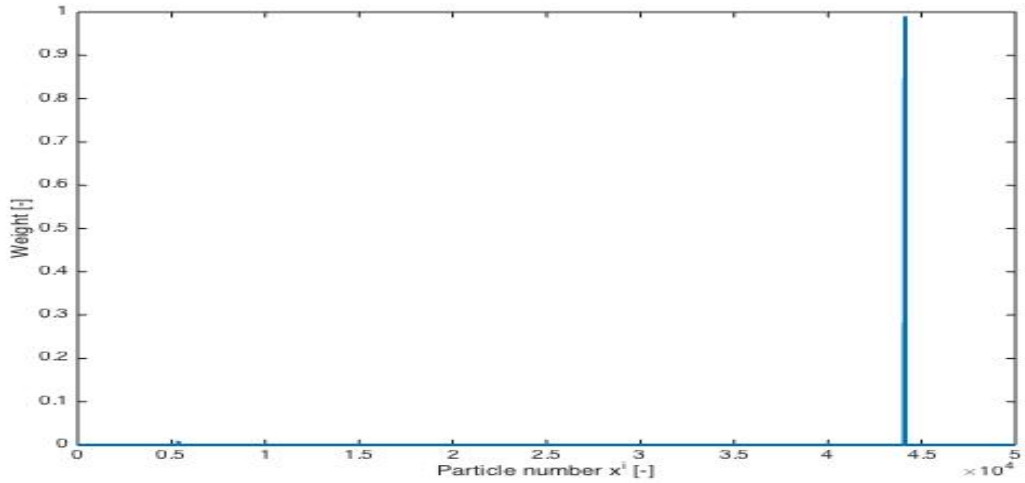

Figure 5.3: Degeneration problem, where only a few particles have considerable weights.

This is called degeneracy or depletion, and is computationally inefficient (Arulampalam et al. 2002). In Equation (5.26), it can be seen that this also reduces the quality of the estimate of the expected value.

Means to avoid this, is by using a resampling strategy. The purpose of this strategy is to neglect the particles with negligible weights and duplicate those with bigger weights.

By doing this, the only particles with high relative probability of being close to the real trajectory are being used (Gustafsson 2010*a*).

A proper measure of depletion is the estimate of the effective sample size $\hat{N}_{eff}$ and is according to Arulampalam et al. (2002) defined as

$$\hat{N}_{eff} = \frac{1}{\sum_{i=1}^{N}(w_k^i)^2}. \tag{5.32}$$

When $N_{eff} < N_{th}$ with $N_{th} = \frac{2}{3}N$, resampling should be initialized (Gustafsson 2010*a*).

There exists a lot of different resampling techniques. In the implementation done in this project, Ripley's method are used. See Gustafsson (2010*a*) for details. A summary of the Particle filter is given below.

Algorithm 3 Particle filter (Gustafsson 2010*a*)

Initialization

- Choose the proposal distribution $q(x_{k+1}|x_{1:k}, y_{k+1}) = p(x_{k+1}|x_k)$, a resampling strategy and the number of particles N.
- Generate $x_1^i \sim p_{x_0}, i = 1, ..., N$ and let $w_{1|0}^i = \frac{1}{N}$

Measurement update

- For $i = 1, ..., N$

$$w_{k|k}^i = \frac{1}{c_k} w_{k|k-1}^i p(y_k|x_k^i) \tag{5.33}$$

  where

$$c_k = \sum_i^N w_{k|k}^i p(y_k|x_k^i) \tag{5.34}$$

- Resampling: Take N samples with replacement from the set $x_{1:k i=1}^{i\ N}$, where the probability of the sample i is $w_{k|k}^i$. Then assign equal weights $w_{k|k}^i = \frac{1}{N}$.
- Estimation: The mean is approximated by

$$\hat{x}_k = \sum_{i=1}^{N} w_{k|k}^i \; x_k^i \tag{5.35}$$

Time update

- Sample N particles from state transition probability density function

$$x_{k+1}^i \sim p(x_{k+1}|x_k) \tag{5.36}$$

Chapter 6

Model Order Selection

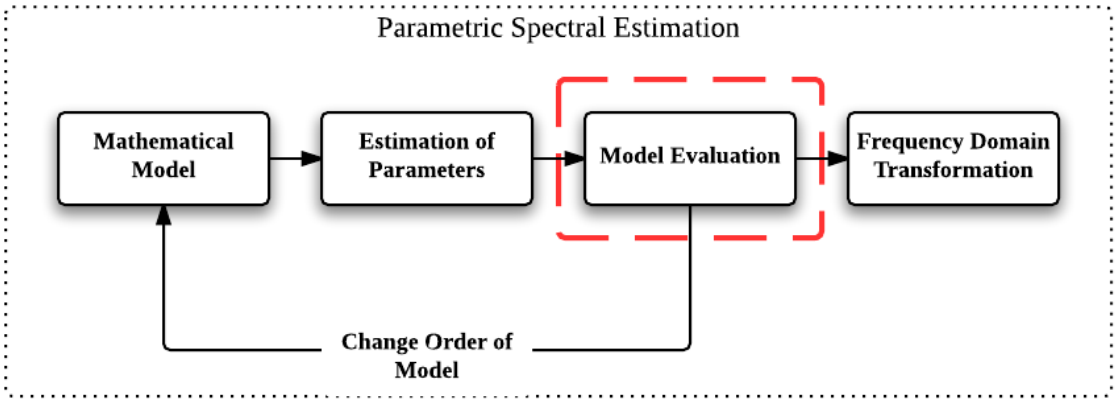

Figure 6.1: Focus area of Chapter 6 marked in red.

The model evaluation problem, is the evaluation and determination of the model order p. There exist many different ways of doing this, for instance Akaikes Information Criteria (AIC) (Akaike 1974), and the Bayesian Information Criteria (BIC) Schwarz et al. (1978). In this chapter, the latter method is presented.

6.1 Bayesian Information Criteria

The Bayesian information criteria, is a value that describes how accurate the model is, and penalize the fact of having too many time-varying parameters. The number is relative, meaning that it is only informative if several models are tested. The model giving the least BIC number is the optimal model, from the BIC criteria. The general equation of the BIC number is given as

$$BIC = -2\ln(\hat{L}) + p\ln(N_k) \tag{6.1}$$

where $\hat{L}$ is maximum likelihood function, and N is the number of observations. If the errors e_k in Equation (4.8) are Gaussian distributed, the BIC number can be written as

$$BIC = N_k\ln(RSS/N_k) + p\ln(N_k) \tag{6.2}$$

where $RSS = \sum_{i=1}^{N_k}(y_i - \hat{y}_i)^2$. As previously discussed in Section 4.3.1, the error is assumed to be Gaussian distributed, and this simplified method can be used (Priestley 1965).

6.2 Decision Support

Having a too low model order, will result in inaccurate modeling of the ship response. This leads to poor recreation of the response spectrum, for instance by the lack of important peak frequencies. If the model order is too high, could also lead to false result, and peaks which do not exist might appear (Reddy & Rao 2014). However, the information criteria does not contain any information about having model order which is leading to false recreation of the spectrum. Therefore, the model order should serve as an indicator, and not as law.

The final evaluation should be based on our initial knowledge of the spectrum. For instance, by suddenly having a spectral peak at 10 hertz in the ship response spectrum for a large crude carrier, the model order should be reduced, even though this is the optimal order seen from the BIC point of view.

Chapter 7

Estimation of Time Dependent Response Spectrum

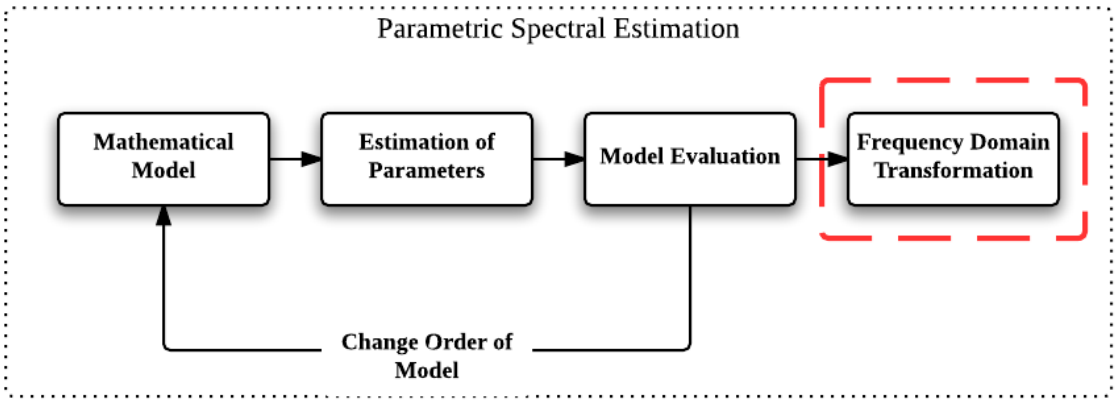

Figure 7.1: Focus area of Chapter 7 marked in red.

The relation between the estimated time varying parameters and the spectrum of the ship response is derived in this chapter. As indicated in Chapter 3, the power spectrum of a non-stationary process is a time and frequency dependent spectrum called the evolutionary power density spectrum (EPDS). The derivation of this spectrum is given in the next sections.

7.1 Derivation of Evolutionary Power Density Spectrum

The EPDS spectrum of the discrete time ship response process y_k is denoted $S_y(f,k)$, and is based on the spectra relation, the spectrum of white noise, and the transfer function between the model residuals and the output.

7.1.1 Spectra Relation

The relation between two spectra describing different processes, is the squared of the transfer function between the two processes, and is given as

$$S_y(f,k) = |H(f,k)|^2 S_e(f), \tag{7.1}$$

where $S_e(f)$ is the spectrum of the model residuals $e_{1:k}$ in Equation (4.8), and $H(f,k)$ is the discrete time dependent transfer function between y_k and e_k (Gardner 1990). Before deriving the transfer function, the spectrum of the model residuals will be presented.

7.1.2 Spectrum of White Noise

The model residuals are assumed to be Gaussian white noise, see Section 4.3.1. Gaussian white noise processes have a constant power spectral density, $S_e(f) = N_0$. In addition, the variance of the spectrum is given as

$$\begin{aligned} \sigma_e^2 &= \int_{-\frac{f_s}{2}}^{\frac{f_s}{2}} S(f) df \\ &= N_0 \int_{-\frac{f_s}{2}}^{\frac{f_s}{2}} df \\ &= N_0 f_s, \end{aligned} \tag{7.2}$$

where f_s is the sampling frequency.

Remark 2 *The sampling theorem states, that it is only possible to capture the frequencies which are less than the half of the sample frequency f_s (Balchen et al. 2003). Therefore the integral limits in Equation* (7.2)*, becomes $f = [-\frac{f_s}{2}, \frac{f_s}{2}]$.*

By inverting this formula, the expression for the PSD for white noise is found as

$$N_0 = \frac{\sigma_e^2}{f_s} \tag{7.3}$$

The variance σ_e of the residual can be estimated by taking the sample variance of

$$\begin{aligned} var(e_k) &= var(y_k - \sum_{j=1}^{p} a_{k,j} y_{k-j}) \\ \sigma_e^2 &= \frac{1}{N-p} \sum_{k=p+1}^{N-1} \left| y_k - \sum_{j=1}^{p} a_{k,j} y_{k-j} \right|^2 . \end{aligned} \tag{7.4}$$

7.1.3 Transfer Function

The transfer function is the relation between the input and output of a linear system. In the particular process of interest, the driving input of the system is the model residuals e_k, and the output is the measurements y_k, see Figure 7.2.

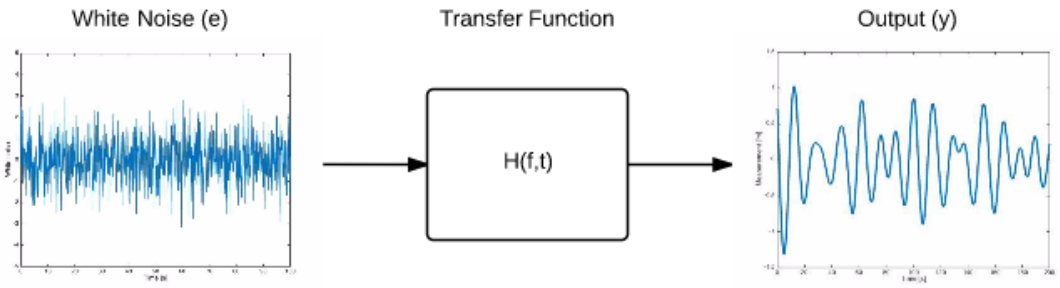

Figure 7.2: Transfer function.

The transfer function can be found by using the time-step property of the z-transform (Balchen et al. 2003). Recall Equation (4.8), and note that since this is a linear system it can be written on the *z-domain form*, $Y(z,k) = H(z,k)E(z)$. The z-transform converts a discrete time signal to the frequency domain, and can be seen as an equivalent of the Laplace domain for continuous systems.

Taking the z-transform of Equation (4.8), the transfer function can be obtained and is given as

$$\begin{aligned} Y(z,k) &= \sum_{j=1}^{p} a_{k,j} Y(z,k) z^{-j} + E(z) \\ Y(z,k)(1 - \sum_{j=1}^{p} a_{k,j} z^{-j}) &= E(z) \\ H(z,k) &= \frac{Y(z,k)}{E(z)} = \frac{1}{1 - \sum_{j=1}^{p} a_{k,j} z^{-j}}, \end{aligned} \tag{7.5}$$

where $Y(z,k)$, and $E(z)$ is the z-transformations of respectively the measurements y_k and the model residuals e_k at time instant k, and z is the complex z-domain variable.

To obtain the frequency domain, z can be substituted with $z^j = e^{\iota Omega j}$, where Ω is a dimensionless frequency. By substituting $\Omega = 2\pi f \Delta t$, the transfer function is a function of f in hertz (Balchen et al. 2003). The transfer function can therefore be written as

$$H(f,k) = \frac{1}{|1 - \sum_{j=1}^{p} a_{k,j} e^{-j2\pi\iota f}|^2}. \tag{7.6}$$

By combining Equation (7.1), Equation (7.3) and Equation (7.6), the spectrum $S_y(f,k)$ can be written as

$$S_y(f,k) = \frac{\sigma_e^2 \Delta t}{|1 - \sum_{j=1}^{p} a_{k,j} e^{-j2\pi\iota f \Delta t}|^2}, \tag{7.7}$$

where $\Delta t = \frac{1}{f_s}$.

7.1.4 Spectrum Scaling

Recall that in Section 2.2 the spectra were presented as functions of $\omega(\frac{rad}{s})$. The estimated spectrum in this chapter, was given as a function of frequency f in [hz]. Because of the conservation of energy, the spectra is scaled differently for different function variables, and it is therefore desirable to have both the wave spectra and the estimated spectra scaled correctly. Therefore it is chosen to scale both spectra after frequency in hertz, and the wave spectra need to be scaled.

In order to present the spectrum as a function of frequency f in hertz, a change of variables is required. To do a change of variables, the energy of the spectrum must be conserved, and the spectrum needs to be scaled.

The total energy of a spectrum is given as

$$E_{tot} = \int_{-\infty}^{\infty} S(\omega) d\omega. \tag{7.8}$$

The same has to hold, if using frequency f in herz instead of frequency ω, that is

$$E_{tot} = \int_{-\infty}^{\infty} S'(f)df. \tag{7.9}$$

By doing a change of variable in Equation (7.8) from ω to f, and comparing with Equation (7.9), it follows that

$$\begin{aligned} E_{tot} &= \int_{-\infty}^{\infty} S(\omega)d\omega \\ &= \int_{-\infty}^{\infty} S(\omega(f))\frac{d\omega}{df}df \\ &= \int_{-\infty}^{\infty} \underbrace{S(2\pi f)2\pi}_{S'(f)}\, df, \end{aligned} \tag{7.10}$$

where $\omega(f) = 2\pi f$, and $\frac{d\omega}{df} = 2\pi$.

In Equation (7.2), the spectrum was defined in $f \in [-\frac{f_s}{2}, \frac{f_s}{2}]$, which is a double sided spectrum. Physical systems operate in $f \in [0, \infty]$, and are therefore the preferred interval to use. Assuming that the spectrum is symmetric around the y-axis, the single sided spectrum can be found by

$$E_{tot} = \int_{-\infty}^{\infty} S(f)df = \int_{0}^{\infty} \underbrace{2 \cdot S(f)}_{S^+(f)}\, df. \tag{7.11}$$

The single sided spectrum scaled with frequency f in hertz is given as

$$S_y^+(f,k) = 2 \cdot \frac{\sigma_e^2 \Delta t}{|1 - \sum_{j=1}^{p} a_{k,j} e^{-j2\pi\iota f \Delta t}|^2}, \tag{7.12}$$

which is the formula the evolutionary power density spectrum of the ship response.

Part III

Case Studies

Introduction to Case Studies

Three sets of case studies are presented in this part. The main motivation of considering these, is to identify the key factors and limitations which is decisive for the algorithm's performance in estimating the non-stationary ship response spectrum. The case studies are presented in three different chapters namely,

- Chapter 8: Stationary Simulation Studies,
- Chapter 9: Non-Stationary Simulation Studies,
- Chapter 10: Estimating Ship Response of Cybership III.

Chapter 8

Stationary Simulation Studies

In this chapter, the robustness of the algorithm will be tested through stationary case studies.

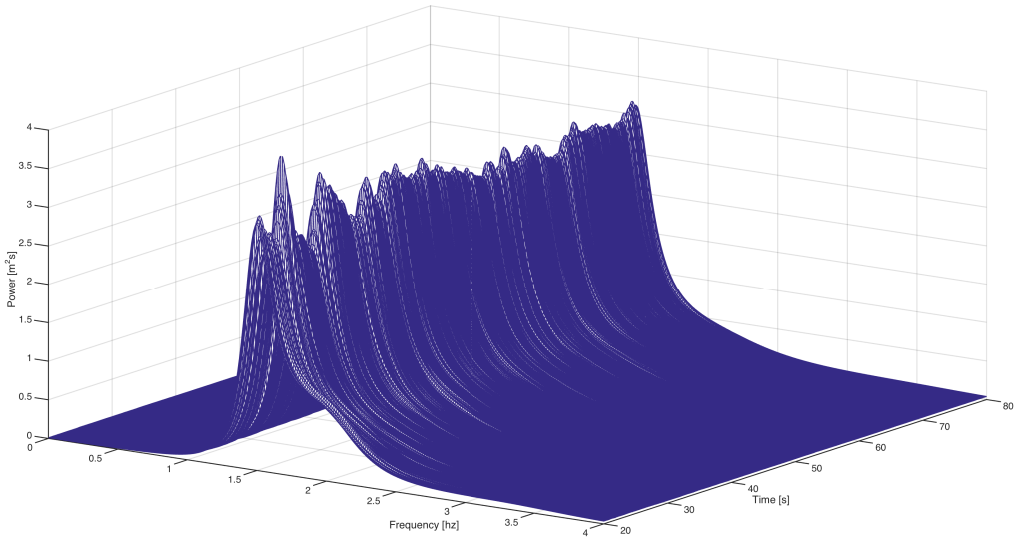

Figure 8.1: Example of an EPDS of a stationary process.

8.1 Case Study 1: Parameter Estimation Study

In this case study, estimation of the parameters of an AR(2) process is provided. Both the Gaussian model and the Cauchy model, proposed in Chapter 4, are tested. To estimate the parameters of the Gaussian model the Kalman filter is used, and the Particle filter is used on the Cauchy model. Furthermore, an analysis of the results are made with the use of logarithmic squared error and variance analysis.

The purpose of this case study is to validate whether the algorithm is able to detect the unknown parameters from a simple simulated process. In addition, a comparison of the performance of the Kalman and Particle filter is made. The model order evaluation, and the estimation of the spectrum are not looked into in this case study, see Figure 8.2.

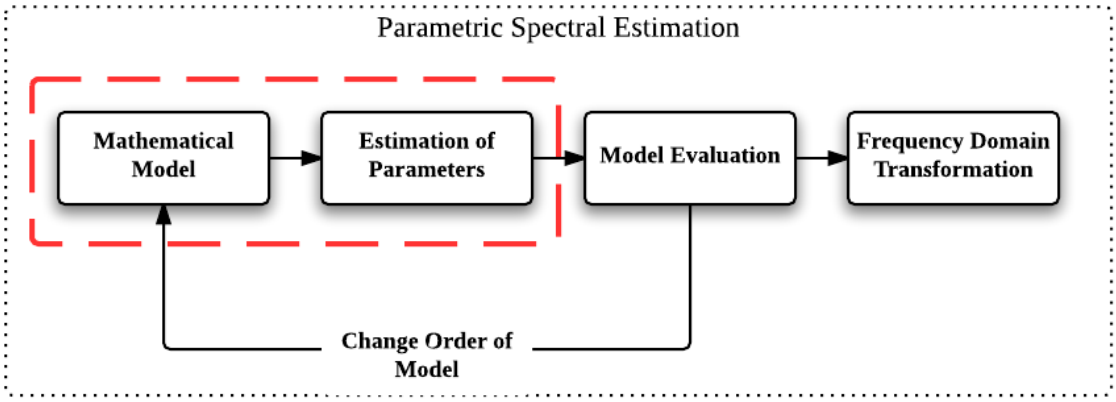

Figure 8.2: Focus area of Case 1 marked in red.

8.1.1 Process Plant

The AR(2) process implemented in this section is a process with two unknown constant parameters subject to Gaussian white noise. The process is

$$y_k = -0.7y_{k-1} - 0.9y_{k-2} + e_k, \tag{8.1}$$

where $e_k \sim \mathcal{N}(0, 1)$. The process is simulated in Figure 8.3, with a simulation time of $t = 50s$ and time step of $\Delta t = 0.1s$.

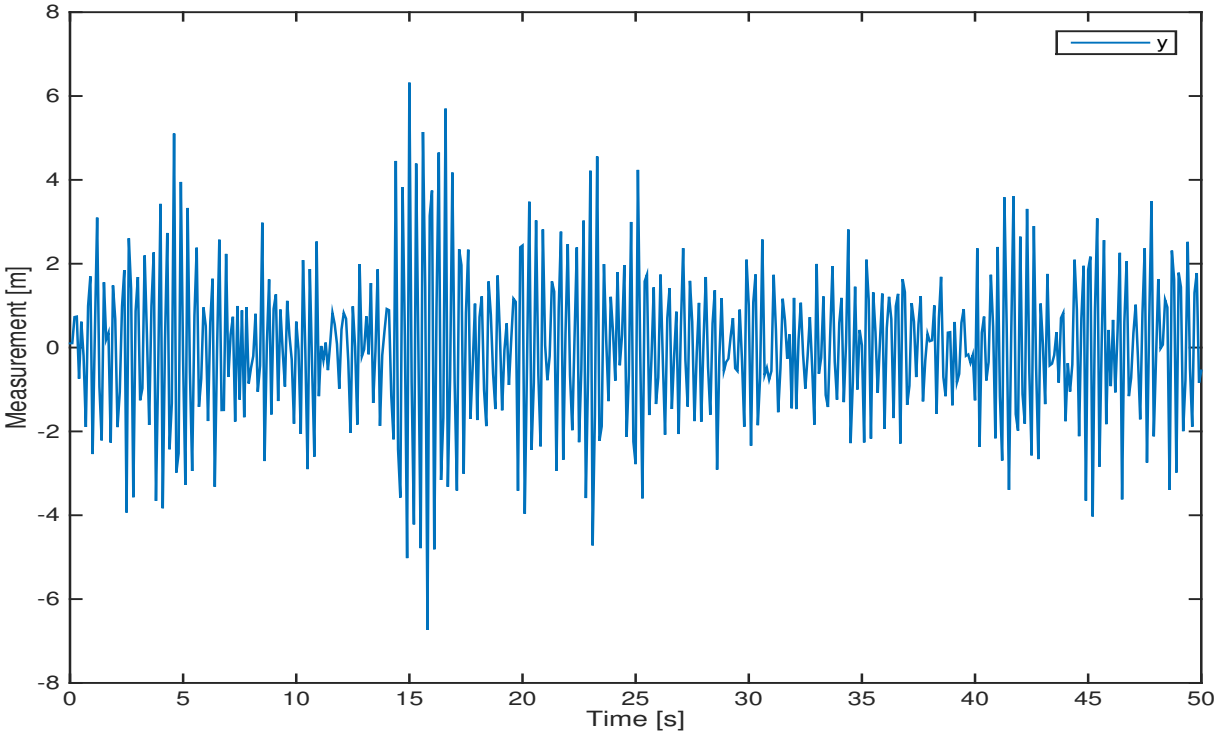

Figure 8.3: AR(2) process simulated in this case study.

8.1.2 Mathematical Model

As discussed in Section 4.3, the observation equation can be written in compact form of Equation (8.1) as

$$y_k = \underbrace{\begin{bmatrix} y_{k-1} & y_{k-2} \end{bmatrix}}_{C_k} \begin{bmatrix} x_{k,1} \\ x_{k,2} \end{bmatrix} + e_k, \tag{8.2}$$

where $x_{k,1} = a_{k,1}$, $x_{k,2} = a_{k,2}$, and $\hat{e}_k \sim \mathcal{N}(0, \hat{\sigma})$. Furthermore, the transition equation is according to Equation (4.14) written as

$$\begin{bmatrix} x_{k,1} \\ x_{k,2} \end{bmatrix} = \begin{bmatrix} 1 & 0 \\ 0 & 1 \end{bmatrix} \begin{bmatrix} x_{1,k} \\ x_{2,k} \end{bmatrix} + \begin{bmatrix} 1 & 0 \\ 0 & 1 \end{bmatrix} \begin{bmatrix} v_{k,1} \\ v_{k,2} \end{bmatrix}, \tag{8.3}$$

where $v_{k,1} \sim \mathcal{N}$, and $v_{k,2} \sim \mathcal{N}$ for the Gaussian model, and $v_{k,1} \sim \mathcal{C}$, and $v_{k,2} \sim \mathcal{C}$ for the Cauchy model. The model order is here $p = 2$, and assumed known.

8.1.3 Initial Conditions on Estimation Filters

The Kalman filter, and the Particle filter which were discussed in Chapter 5, are implemented with the following initial conditions.

KF Conditions	**Value**	**PF Conditions**	**Value**
Initial state $a_{1,1}$	-10	Initial state $a_{1,1}$	-10
Initial state $a_{1,2}$	-10	Initial state $a_{1,2}$	-10
Initial covariance $P_{k\|k}$	I	Number of particles	100000
State noise Q	$10^{-12} \cdot I$	Scaling Cauchy parameter σ_c	0.1
Observation noise R	1	Observation noise R	1

Table 8.1: Filter initial conditions.

The initial state is chosen far away from the real parameters. The reason for this is to check the algorithms detection abilities.

8.1.4 Estimation Results

In this section the estimation results are provided. Both the results from the Kalman filter and the Particle filter are presented, each containing an error and variance analysis.

Kalman Filter Performance

The following plots show how the Kalman filter estimates the unknown parameters, $a_{k,1}$ and $a_{k,2}$. The red line indicates the true value of the process, and the blue represents the estimated result.

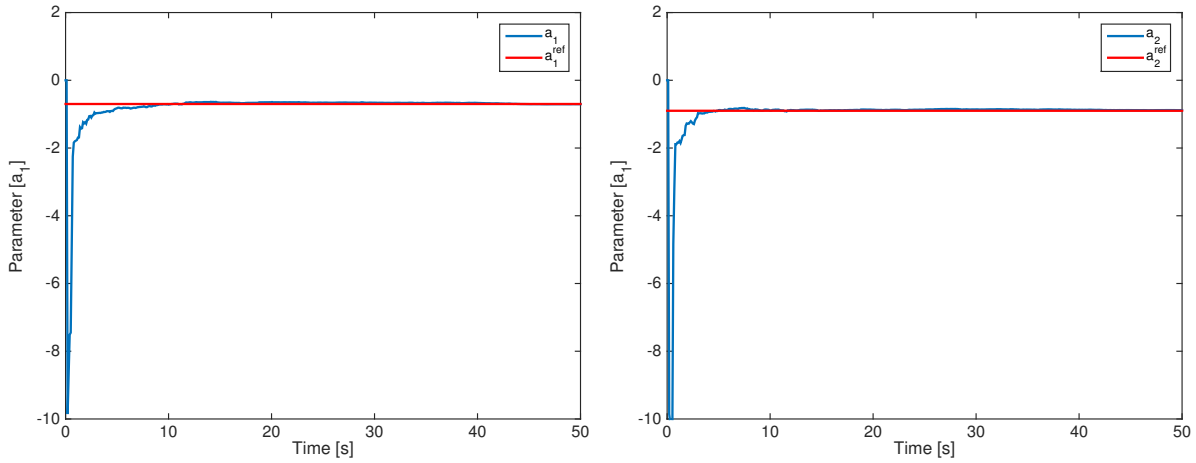

(a) Parameter estimates $a_{k,1}$.

(b) Parameter estimates $a_{k,2}$.

Figure 8.4: Kalman filter parameter estimates.

In Figure 8.4, it can be seen that the Kalman filter is able to estimate the correct values, and therefore able to meet the motive of this case study.

Error Analysis: Since the error is close to zero, the LSE quantity gives a detailed view of how close to zero the error is. The LSE for the $a_{k,1}$ is given as

$$LSE = \log[(a_{k,1} - a_{k,1}^{\text{ref}})^2], \tag{8.4}$$

and is plotted for both parameters in Figure 8.5. In addition the mean of these two quantities, which is known as the Logarithmic Mean Squared Error (LSME), is plotted in Figure 8.6 to evaluate the total performance.

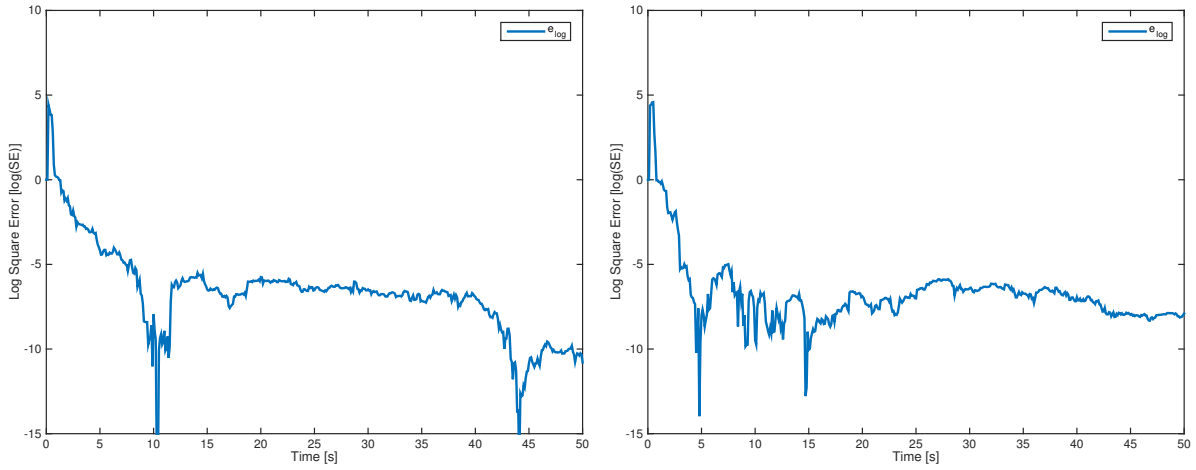

(a) LSE of $a_{k,1}$. (b) LSE of $a_{k,2}$.

Figure 8.5: Logarithmic squared error of parameter estimates from Kalman filter.

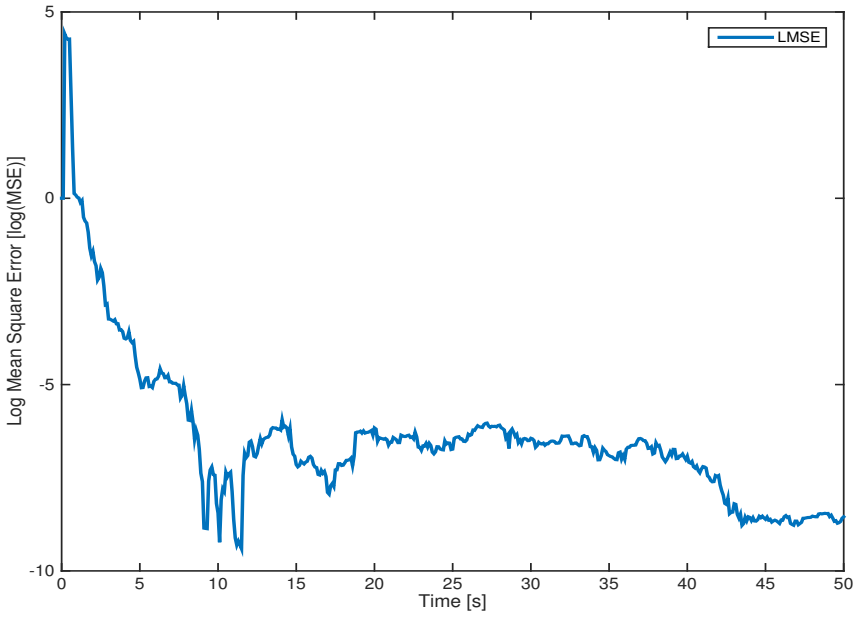

Figure 8.6: Logarithmic mean squared error of parameter estimates from Kalman filter.

It can be observed in Figure 8.5a, and Figure 8.5b that both parameters are estimated with approximately the same performance. In Figure 8.6, it can be seen that the parameters

are being estimated with a LSME error of magnitude of 10^{-8} after $t = 45s$. It can be observed that a transient behavior exists, which is due to the Kalman filter's initialization process.

Variance Analysis: As mentioned in Section 5.1.2, the expected value of the posterior distribution is in this thesis considered as the best estimate. However, this could lead to misleading result, when not considering the variance. A small variance correspond to a narrow posterior density function. This implies that the mean is a good representative of the obtained posterior.

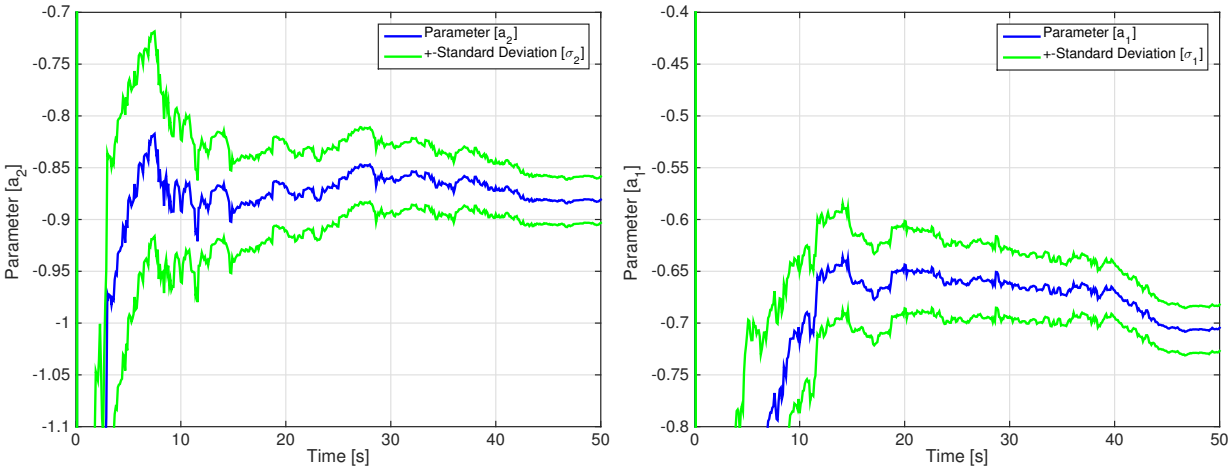

(a) Standard deviation for $a_{k,1}$.

(b) Standard deviation for $a_{k,2}$.

Figure 8.7: Kalman filter standard deviation.

Figure 8.7, it can be seen that the standard deviations are approximately equal to 0.025, and remain constant after the transient period.

Particle Filter Performance

The same simulations as in the previous section, are also repeated for the Particle filter.

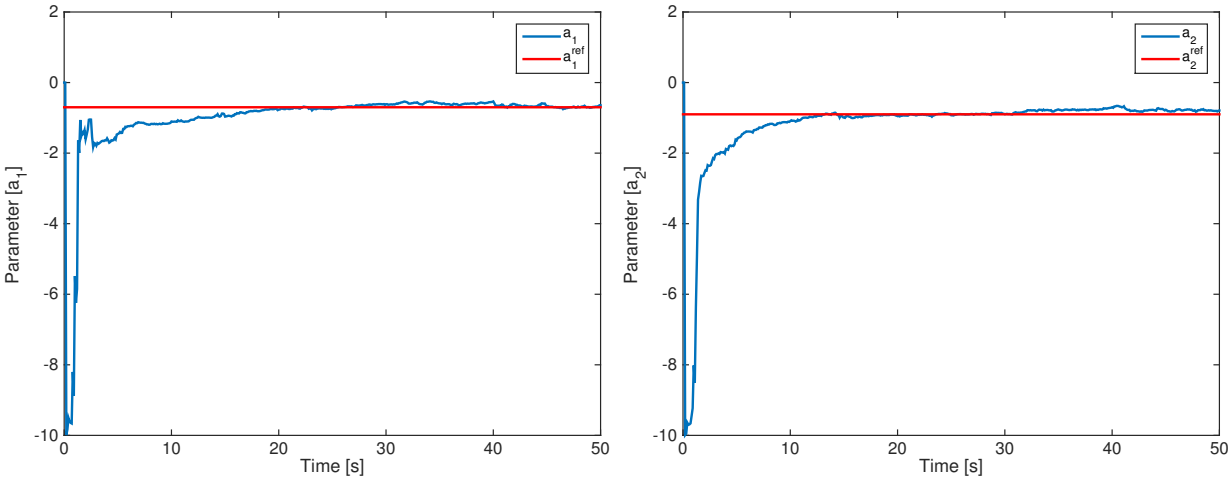

(a) Parameter estimates $a_{k,1}$.

(b) Parameter estimates $a_{k,2}$.

Figure 8.8: Particle filter parameter estimates.

In Figure 8.8 it can not be seen that the estimates converge to the correct value, and the results need to be further investigated.

Error analysis: Reference is made to Section 8.1.4 for explanation of LSE and LSME, which is plotted in Figure 8.9, and Figure 8.10.

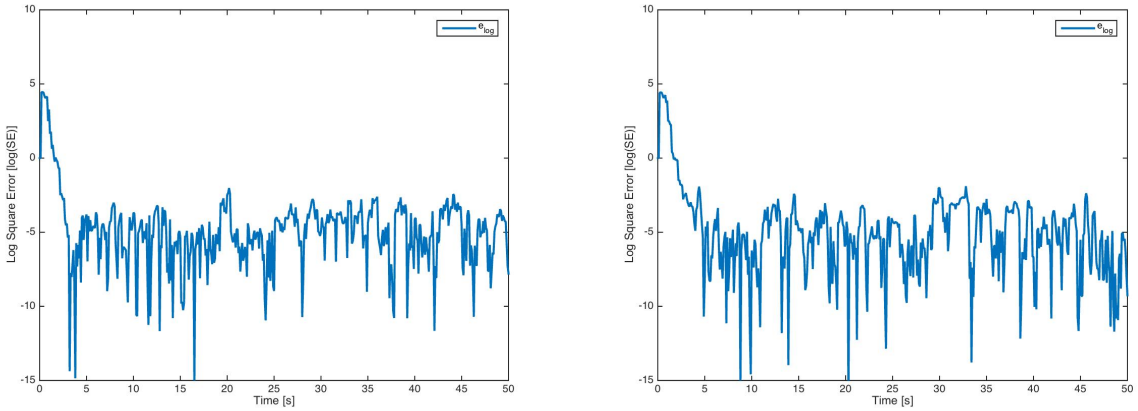

(a) LSE of $a_{k,1}$.

(b) LSE of $a_{k,2}$.

Figure 8.9: Logarithmic squared error of parameter estimates from Particle filter.

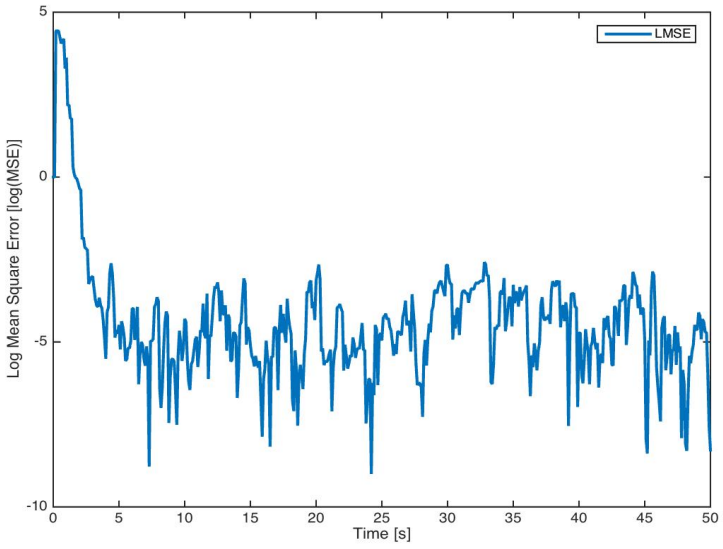

Figure 8.10: Logarithmic mean squared error of parameter estimates from Kalman filter.

It can be observed in Figure 8.9 that both parameters are estimated with the approximately with the same performance, both in LSE and in noise.

From Figure 8.10 it can be seen that the LMSE is oscillating around the value -5, indicating a squared error of 10^{-5}. By this it can be concluded that the estimates in Figure 8.8, converge to the correct value. However, the results are less accurate and more noisy than the Kalman filter estimates.

Variance analysis: The estimated standard deviation from the Particle filter is plotted in Figure 8.11.

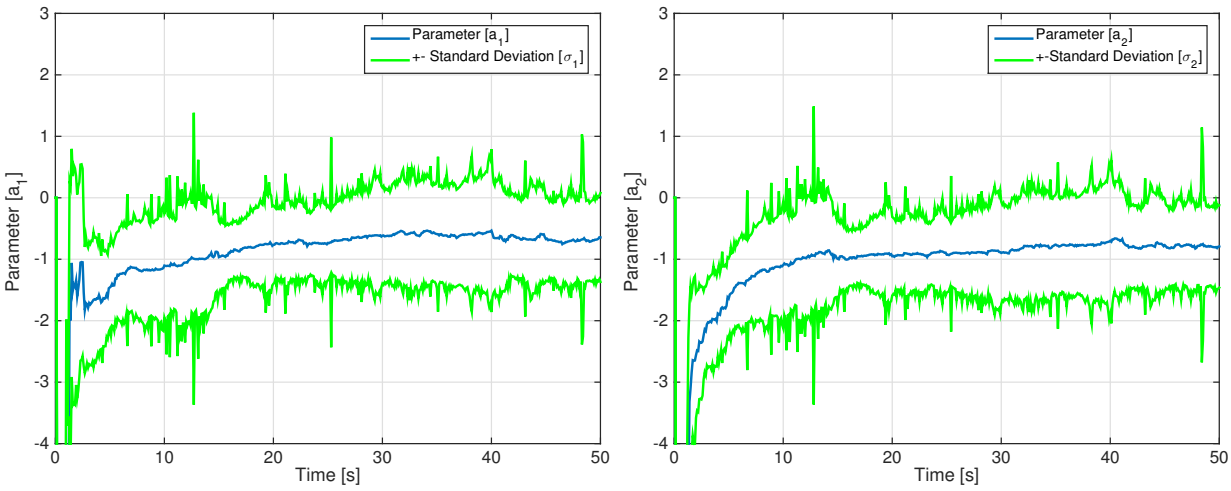

(a) Standard deviation $a_{k,1}$.

(b) Standard deviation $a_{k,2}$.

Figure 8.11: Particle filter standard deviation.

In Figure 8.11, it can be observed that the standard deviations have a value of approximately 0.9, and have a more noisy behavior than the variances estimated by the Kalman filter.

Comparison of Kalman Filter and Particle Filter results

In Figures 8.6 and 8.10, it can be observed that LMSE obtained from the Kalman filter is around $LMSE = -8$, and for the Particle filter oscillating around an approximate value of $LSME = -5$. This implies a squared error of respectively 10^{-8}, and 10^{-5}. There can be many reasons to the difference in the performance. For instance the Kalman filter can better tuned than the Kalman filter.

Comparing Figure 8.7 and Figure 8.11 it can be seen that the Particle filter estimate a higher standard deviation[1], than the Kalman filter. One reason for this can be related to the noise distribution in the Cauchy model, which is discussed in the following paragraph.

As previously elaborated, the Cauchy distribution is more long tailed than the Gaussian distribution. This allows the estimates to cover a greater area of the state space, which could lead to a greater variance. To investigate this the Particle filter has also been implemented with Gaussian noise, where the results are given in Appendix A.5. From these results it can be seen that the standard deviations are smoother and smaller than for

[1]Note that the y-axis in the Kalman filter plots and the Particle filter plots are differently scaled

the those obtained with the Cauchy state noise. This supports the theory that the Cauchy distribution makes the variance more noisy and larger. However, the large variance can also be influenced by bad tuning of the Particle filter with the Cauchy state noise, although the filter is tuned after the author's best ability.

8.1.5 Concluding Remarks of Case Study 1

The results indicates that the Gaussian mathematical model with the use of the Kalman filter has a better performance than the Particle filter for this specific process given in this case study. The possible reasons might be that

- the Cauchy state noise spans a wider set of the state space, such that the variance increases, and
- the tuning of the Kalman filter might be better than the Particle filter.

Although this case should not generalize the Kalman and the Particle filters abilities for spectral estimation, it is chosen to only proceed with the Kalman filter.

8.2 Case Study 2: Single Peaked Ship Response Spectrum

In this case study, it is assumed that the vessel moves simultaneously in heave with waves simulated from the JONSWAP spectrum, see Figure 8.12. The motive of the case study is to analyze the algorithm's performance in recreating a full spectrum.

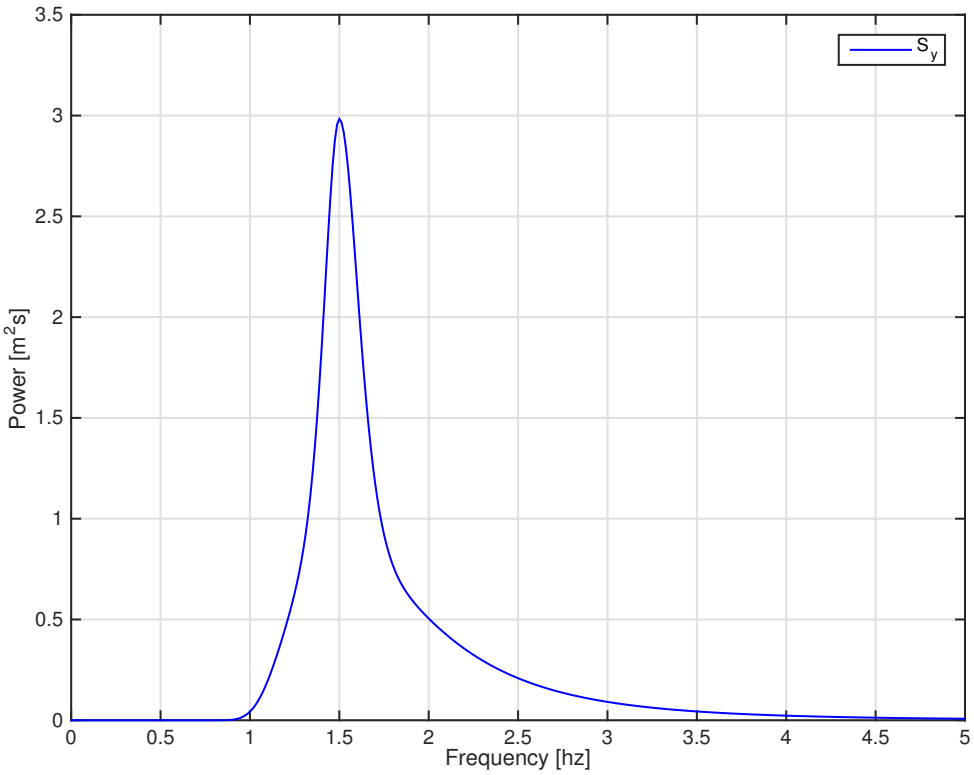

Figure 8.12: The JONSWAP spectrum.

8.2.1 Process Plant

As previously elaborated in Chapter 2, the output y_k can be simulated from wave spectra by realizations. The particular wave spectrum of choice in this case study, is the JONSWAP spectrum with the following parameters:

Parameters	**Value**
Peak frequency f_0	1.5 hz
Significant wave height H_s	6 m

Table 8.2: Process Parameters.

It is assumed that the vessel is moving simultaneously with the waves and with equal magnitude, which simplifies the response amplitude operator to $RAO = 1$. In addition it is assumed that the spreading function is neglected, i.e. the waves are long crested. Furthermore, it is assumed that the incoming waves encounter the bow of the vessel, known as *head sea waves*.

The output is analyzed in the origin, that is $x = 0$ and $y = 0$, such that Equation (2.7) is simplified to

$$\zeta_k = \sum_{q=1}^{N} \sqrt{2S_\zeta(\omega)\Delta\omega}\sin(\omega_q t + \epsilon). \tag{8.5}$$

where S_ζ is the wave spectrum. Since $|RAO| = 1$, it follows that $S_y = S_\zeta$. In addition, it is assumed that there exists some observation noise that contributes to the model residuals $e_{1:k}$. This leads to the following output equation,

$$y_k = \sum_{q=1}^{N} \sqrt{2S_y(\omega)\Delta\omega}\sin(\omega_q t + \epsilon) + e_k, \tag{8.6}$$

where $\epsilon \sim \mathcal{U}(0, 2\pi)$, and $e_k \sim \mathcal{N}(0, 0.1)$. The process is plotted in Figure 8.13, with simulation time of $t = 50s$, and a sample time of $\Delta t = 0.1s$.

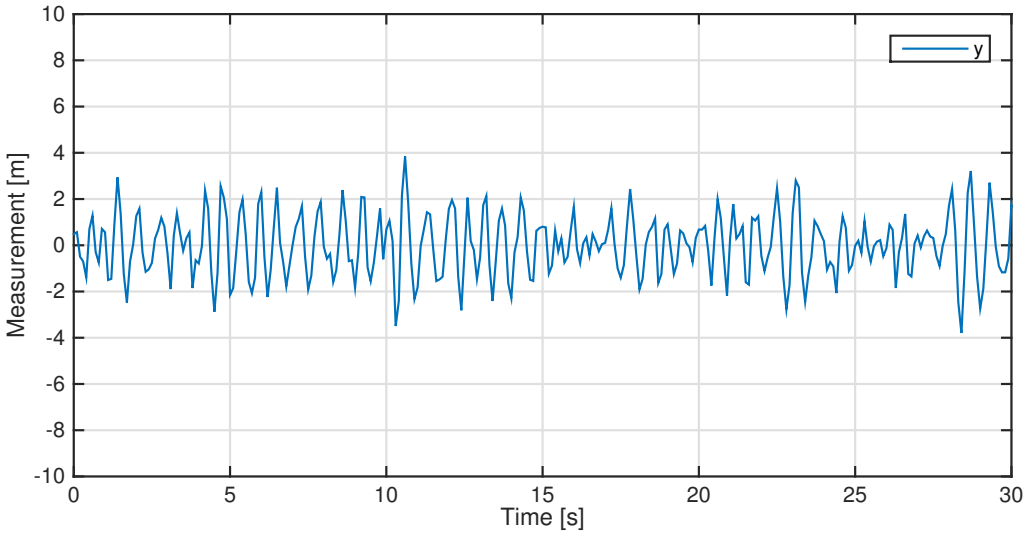

Figure 8.13: Realization from JONSWAP.

8.2.2 Mathematical Modeling

In this case study only the Gaussian mathematical model developed in Chapter 4 is used. From the model evaluation criteria described in Chapter 6, the calculated BIC values from $p = 3 - 45$ are presented in Figure 8.14.

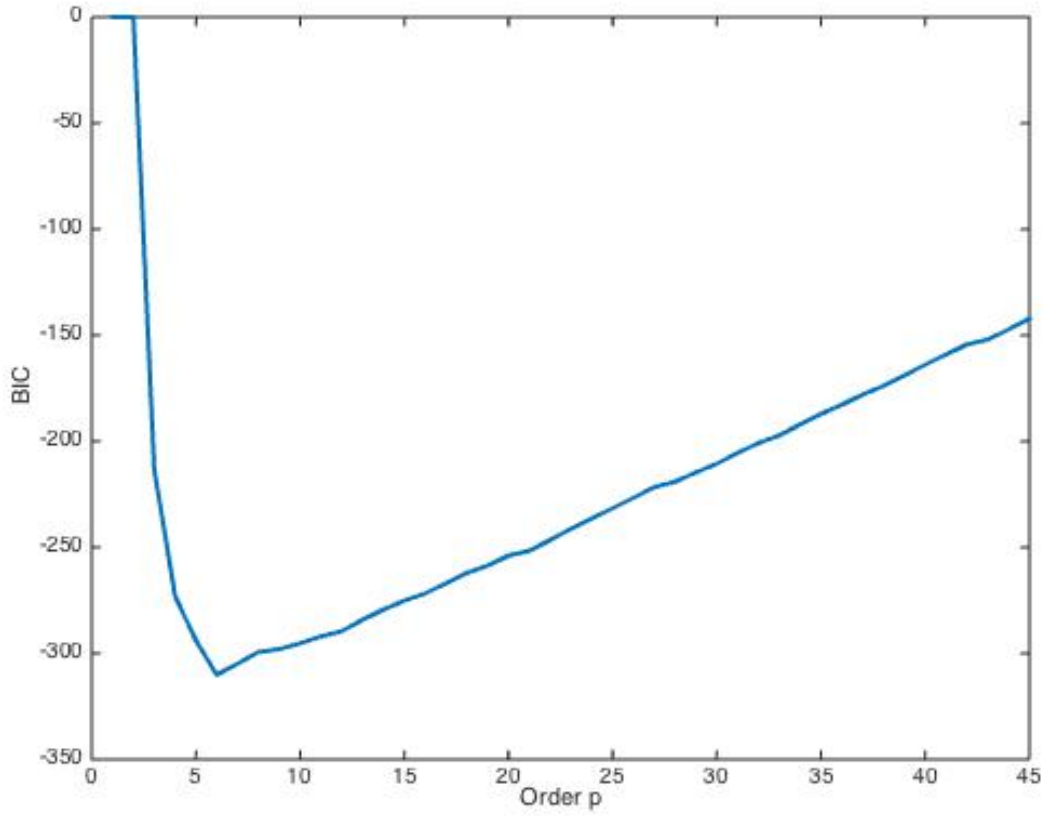

Figure 8.14: BIC value for different model order p.

The minimum BIC value is found at $p = 6$, and is the chosen order for the mathematical model developed.

8.2.3 Estimation Results

The motive of the case study is to test the algorithm's capacity of estimating an entire spectrum. This is related to the SNR ratio mentioned in Section 5.2. Therefore first in this section, a sensitivity analysis of the Kalman filter parameters is presented.

Except the form of the spectrum, there are two quantities that are of particular interest when analyzing the performance: the peak frequency and the area below the curve. The peak frequency indicates at which frequency most of the energy in the spectrum is centered. The area below represent the total energy in the sea state, and is directly related to H_s. Therefore, these two quantities can serve as indicators of the performance of the TVAR algorithm.

Sensitivity Analysis of Tuning Parameters

Large Q-covariance, Small R-covariance: The Kalman filter can be tuned such that the model residuals e_k, become very small or disappears. By reducing R and increasing Q the measurements are considered as more reliable than the model. In the following the Kalman filter is implemented with the parameters given in table Table 8.3.

Conditions	**Value**
State noise Q	10^{-1}
Observation noise R	10^{-5}

Table 8.3: Kalman filter parameters.

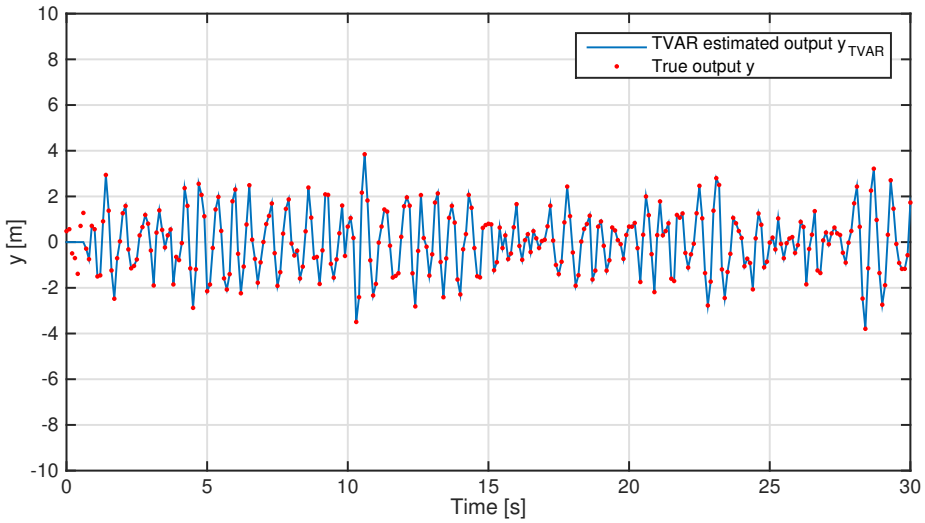

Figure 8.15: Output versus estimated output.

In Figure 8.15, it can be seen that the estimated output y_{TVAR} is able to follow the generated output y_k from the JONSWAP spectrum.

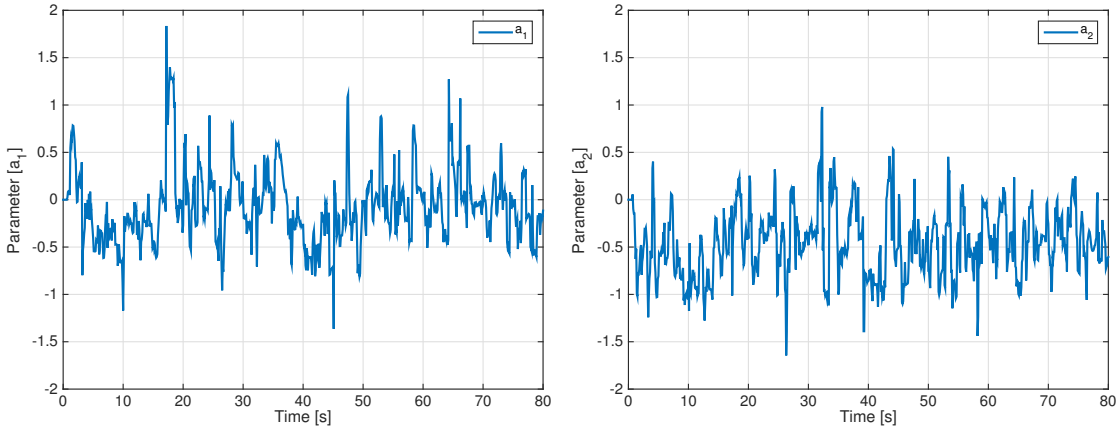

(a) TVAR estimated a_1.

(b) TVAR estimated a_2.

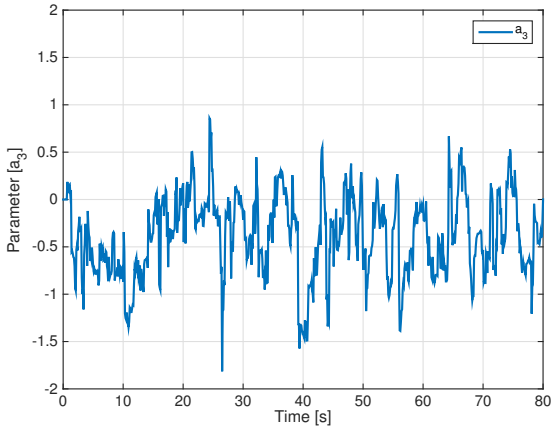

(c) TVAR estimated a_3.

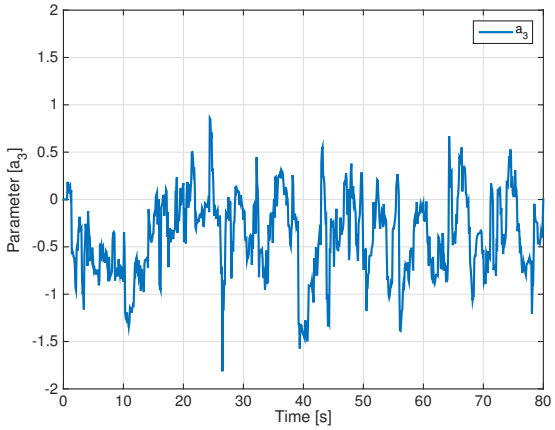

(d) TVAR estimated a_4.

Figure 8.16: TVAR estimated parameters.

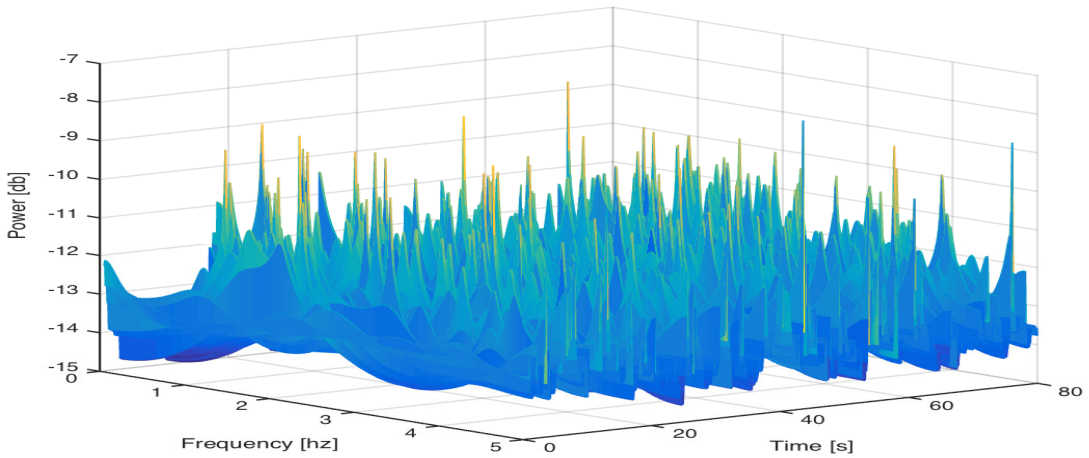

Figure 8.17: Evolutionary power spectrum with tuning parameters given in Table 8.3.

The first four estimated parameters are shown in Figure 8.15. It can be observed that they are noisy and do not converge to constant values. By substituting these parameters

into Equation (7.12), the following spectra is obtained.

Figure 8.17 shows a spectrum which is contaminated by noise. In addition, the power is here given in decibel [db], which is a logarithmic scale. This was necessary to be able to capture the variations in the spectrum. Another observation is that the power is small, with an approximate mean of $10^{-12}db$.

Small Q-covariance, Large R-covariance: To ensure that the parameters vary slowly, a low Q-parameter must be chosen. In addition, the R-value is set to the value of observation variance.

Conditions	**Value**
State noise Q	10^{-5}
Observation noise R	10^{-1}

Table 8.4: Kalman filter parameters.

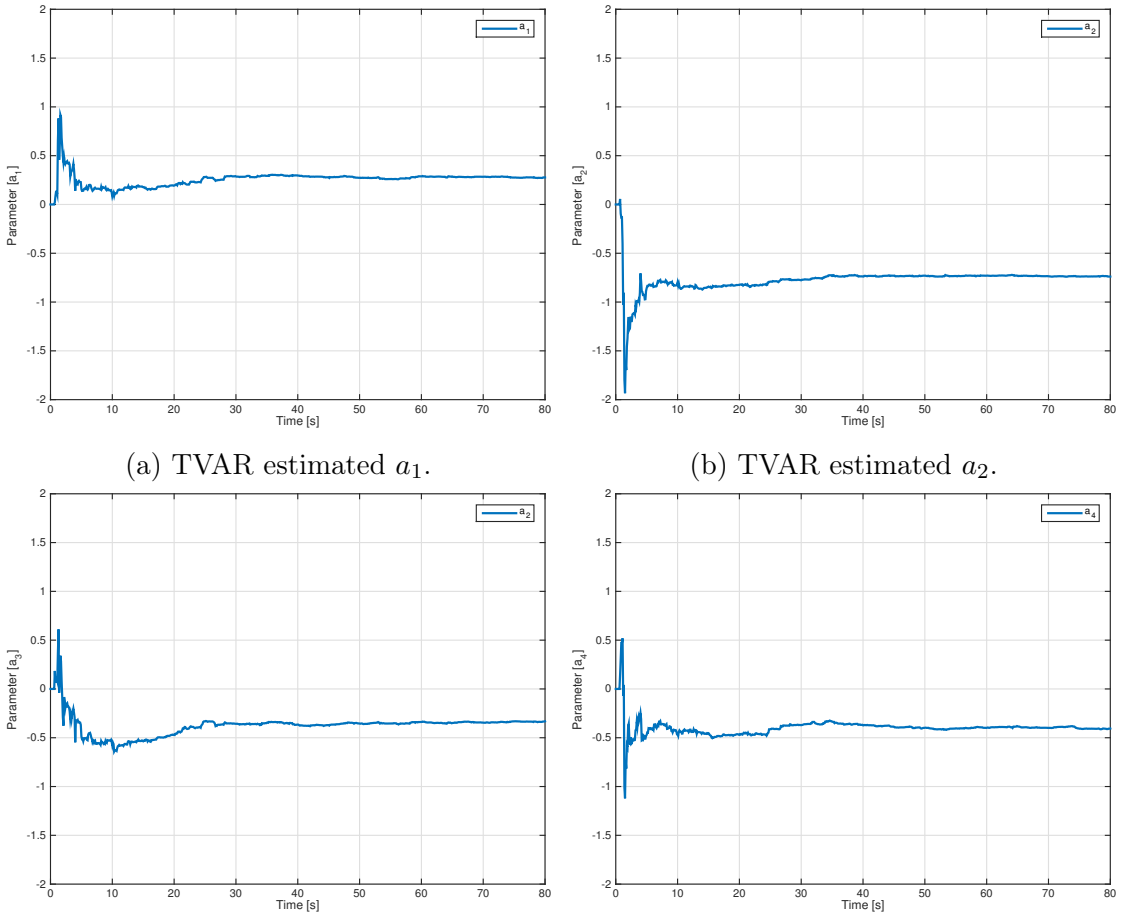

(a) TVAR estimated a_1.

(b) TVAR estimated a_2.

(c) TVAR estimated a_3.

(d) TVAR estimated a_4.

Figure 8.18: TVAR estimated parameters.

In Figure 8.18 the first four estimated parameters are shown. It can be seen that the estimates are smooth and converge to constant values approximately after 20 seconds. By substituting these parameters into Equation (7.12), the spectrum shown in Figure 8.19 is obtained.

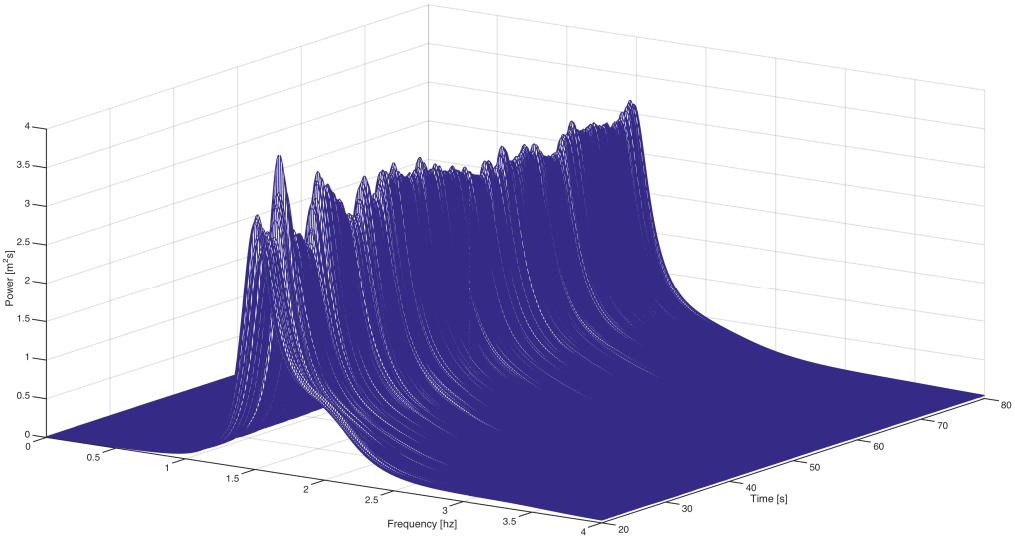

Figure 8.19: Estimated power spectrum with tuning parameters given in Table 8.4.

Figure 8.19 shows the estimated evolutionary power density spectrum. Note that the spectrum is plotted from $t = 20 - 80s$ to avoid transient behavior in the plot. The spectrum shows a smooth behavior, with a minor oscillating behavior of the magnitude.

Comparison of the Tuning Parameter Sets: Although the algorithm, with the parameters given in Table 8.3 is able to follow the output which is shown in Figure 8.15, the algorithm is not able to recreate the spectrum of the process. The reasons for this are explained in the following paragraphs.

By recalling Equation (7.12), it can be seen that the parameters are related to the *poles* of the estimation model. Perturbations in the parameters can therefore make the system unstable[2]. A high Q-parameter, allows the states in the Kalman filter to change much at each time instant to find the optimal solution. This induces noisy behavior of the parameters, and by observing Figure 8.17 it can be seen that this occurs.

[2]In this thesis unstable means in the sense of making the spectrum rise where it should not.

In addition, it can be seen in Equation (7.12) that the algorithm is dependent on model residuals $e_{1:k}$ in terms σ_e^2 to work. If the model residuals go to zero, the variance will also go to zero $\sigma_e \to 0$, resulting in the estimated spectrum goes to zero $S_y(f,t) \to 0$. In other words, the algorithm is dependent on that the noise is filtered out.

In Figure 8.18 the parameters are smoother compared to Figure 8.16. In addition the parameters converge to a relative constant value, resulting in a stable spectrum given in Figure 8.19. Therefore, the constraints given in the Q and R matrices are important for the algorithm's performance.

As mentioned in Section 5.2, the ratio between the Q and R matrices is defined as SNR. The results above show that there are reasons to believe that a low SNR value is decisive to obtain a reasonable result.

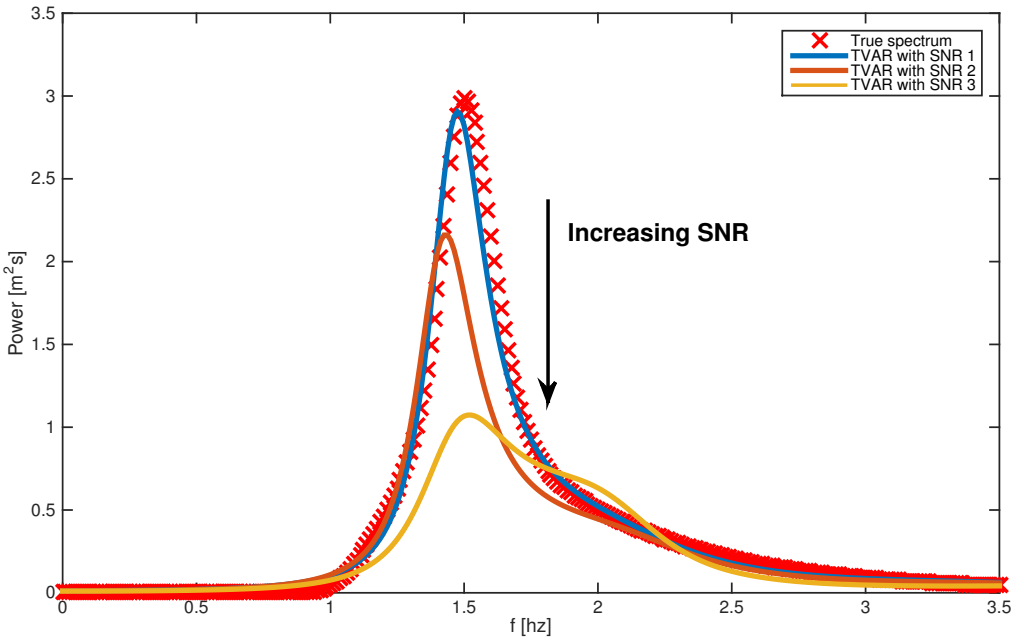

Figure 8.20: Instantaneous spectrum with different tuning parameters.

In Figure 8.20, the TVAR estimated spectrum at specific time instant is plotted for three different SNR values. It seems like the quality of the performance decreases, for increasing SNR value. In other words, the performance is sensitive to the SNR, and a method to find this optimal ratio is yet to be found.

Peak Frequency and Area Analysis

The results with the last tuning parameters are analyzed further in this paragraph. By taking the mean of the steady [3] spectrum in Figure 8.19, the following result is obtained in Figure 8.21.

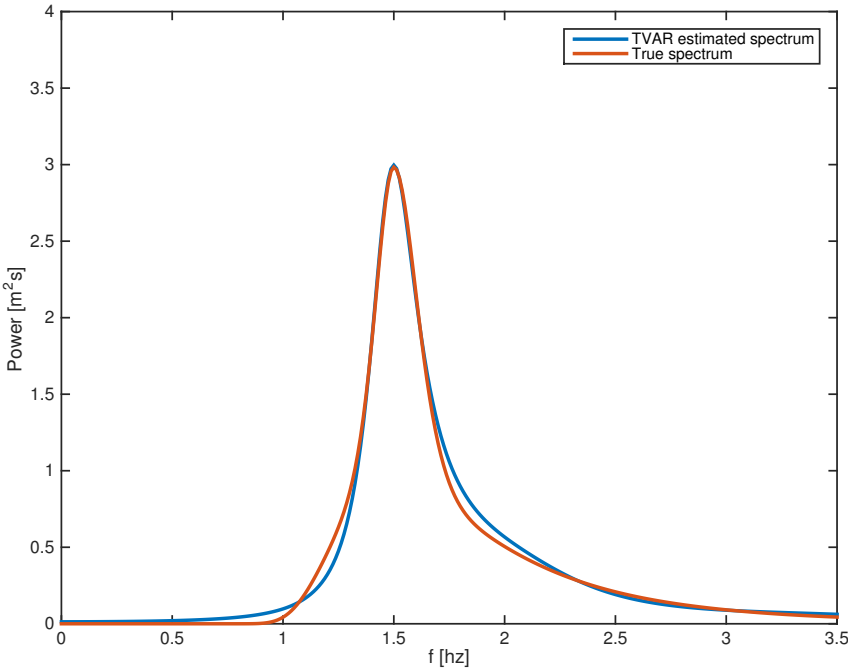

Figure 8.21: Mean of estimated EPDS vs true spectra.

In Figure 8.21, the mean of evolutionary power spectrum is compared with the true spectrum. The TVAR estimated spectrum and the true spectrum are almost identical.

[3] In this regard, 'steady' means that the transient part is neglected.

To analyze whether this is the case at each distinct time instant, N plots are required. Instead of doing this, the area and the peak frequency are investigated.

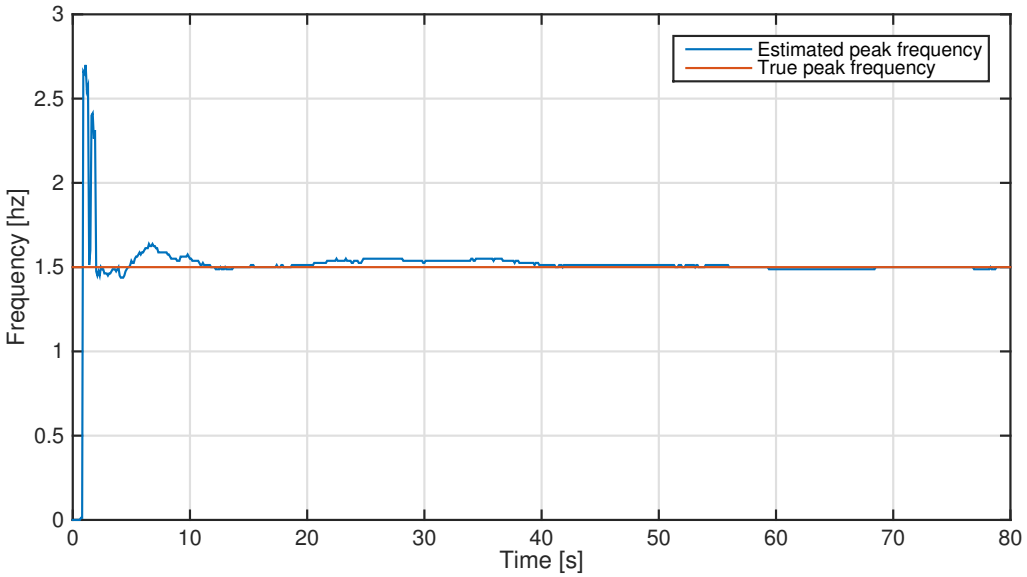

Figure 8.22: Peak frequency.

In Figure 8.22, it can be observed that there exist some transients in the beginning. Furthermore, the peak frequency converges to the correct peak value after approximately 40 seconds.

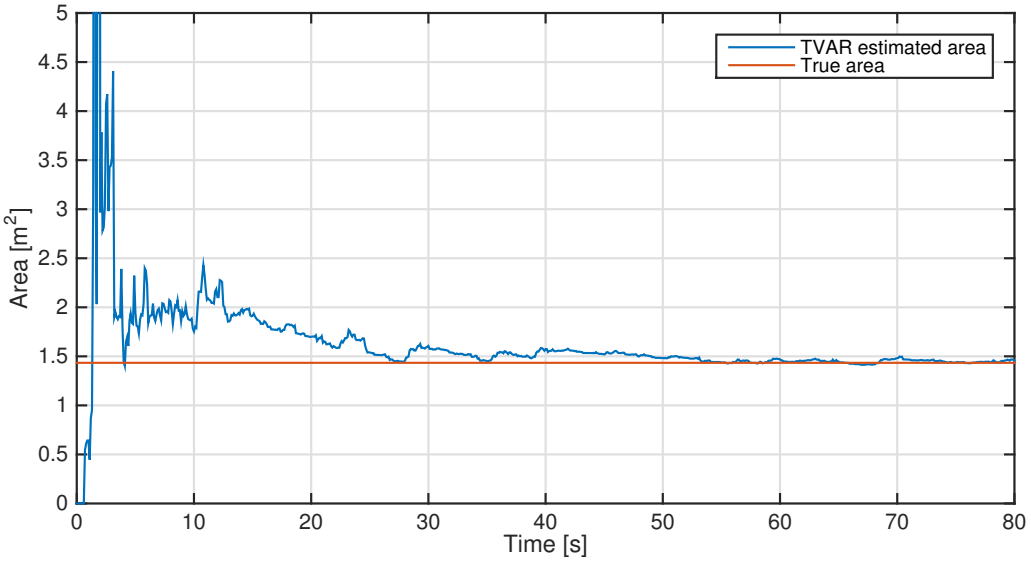

Figure 8.23: Area below the spectrum.

In Figure 8.23, the area below the estimated spectrum is shown. It can be seen that this

quantity is also affected by the transient period. However, after 50 seconds the TVAR algorithm finds the correct area.

8.2.4 Concluding Remarks of Case Study 2

In this case study, the importance of correct tuning parameters of the Kalman filter has been shown.

To be more precise a low SNR value is, according to the results obtained in this case study, important to obtain a stable spectrum. The reasons for this is that a low SNR value

- constraint the states such that they vary slowly,
- and filters out noise with a variance which decides the magnitude of the spectrum.

Furthermore, the optimal SNR value is found manually in this case study, by trial and error. Therefore, an adaptive way to find the ratio is yet to be done.

By having an optimal tuning ratio, the results of this case study show that the algorithm is able to detect both the correct peak frequency and area for this particular realization. In addition the shape of the spectrum is also very similar to the true one.

8.3 Case Study 3: Estimating Double Peaked Spectrum

To increase the complexity, it is assumed in this case study that the vessel follows the wave motion generated from the Torsethaugen spectrum, see Chapter 2 and Figure 8.24. Note that this case follows the same structure as the case study presented in Section 8.2, and therefore only the results are presented. The Torsethaugen spectrum is simulated with the parameters given in Table 8.5.

Parameters	**Value**
Peak frequency ω_0	3 rad/s
Significant wave height H_s	5 m

Table 8.5: Process Parameters

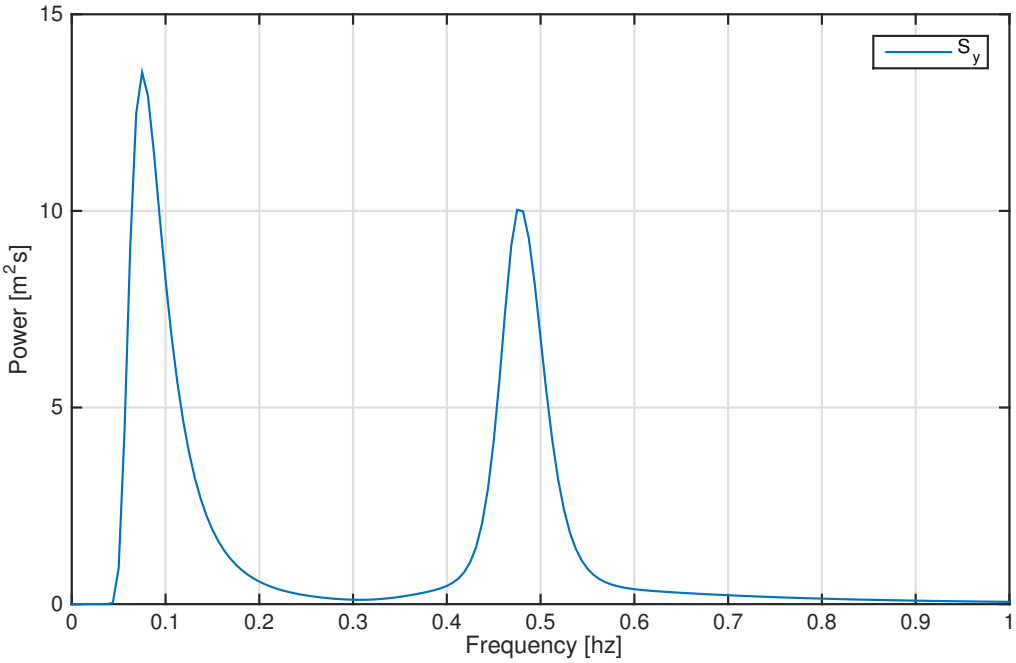

Figure 8.24: Torsethaugen spectrum

8.3.1 Estimation Results

The results are presented in terms of the estimated parameter, the EPDS, a snapshot of the estimated spectrum, the instantaneous peak frequency- and area analysis. The Kalman filter was implemented with the parameters given in Table 8.6.

Conditions	**Value**
State noise Q	0.0000001
Observation noise R	1

Table 8.6: Kalman filter parameters.

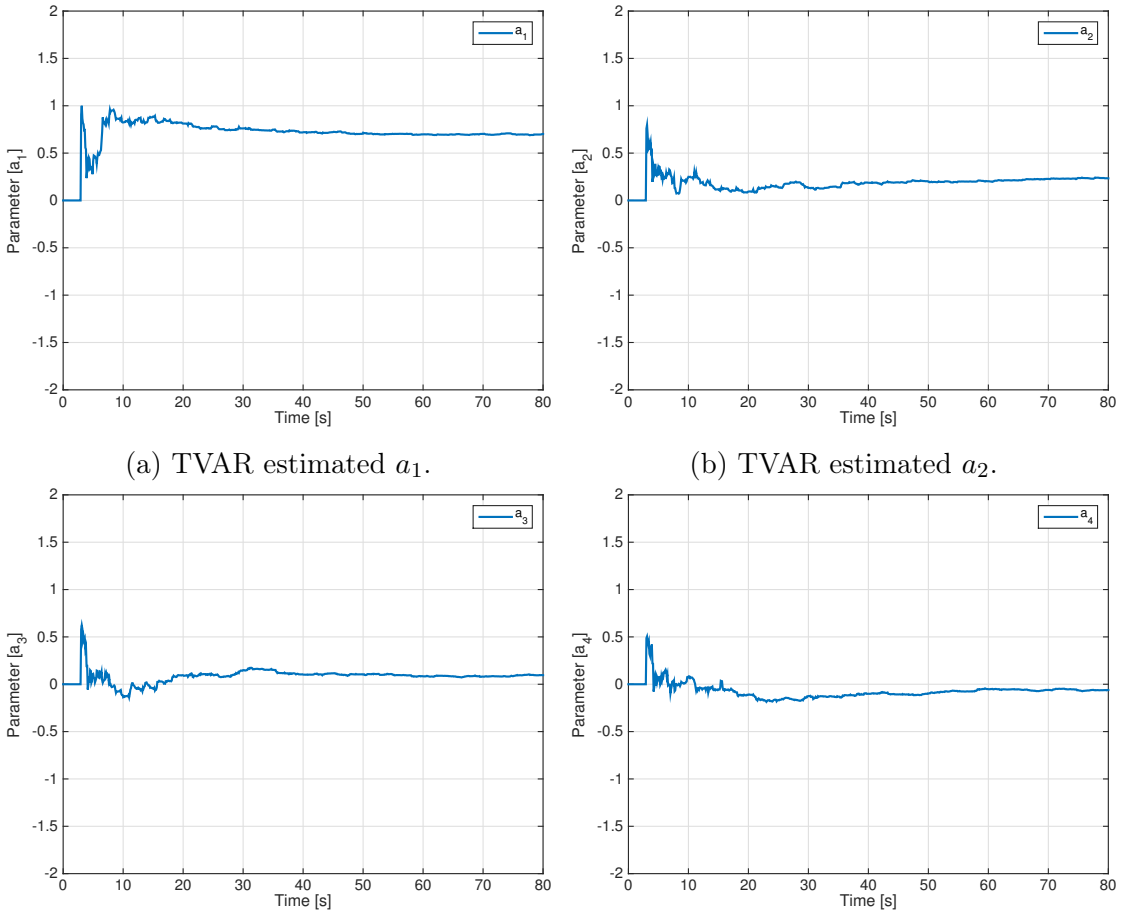

(a) TVAR estimated a_1.

(b) TVAR estimated a_2.

(c) TVAR estimated a_3.

(d) TVAR estimated a_4.

Figure 8.25: TVAR estimated parameters.

The first four estimated parameters are given in Figure 8.25. It can be seen that there exist transient in the parameters in the beginning, but they stabilize to constant values after approximately 40 seconds. Substituting these values into Equation (7.12), the following EPDS is obtained.

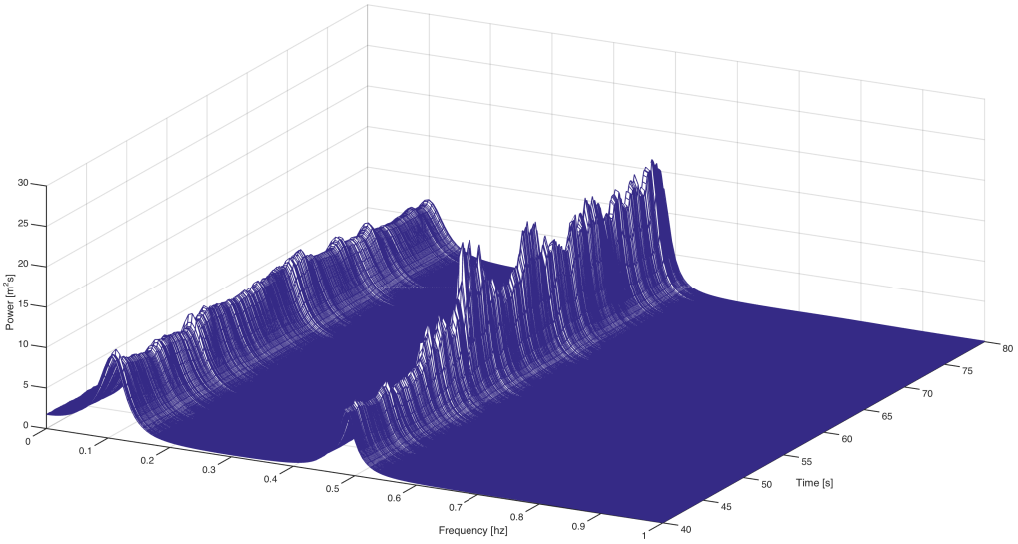

Figure 8.26: Estimated power density spectrum.

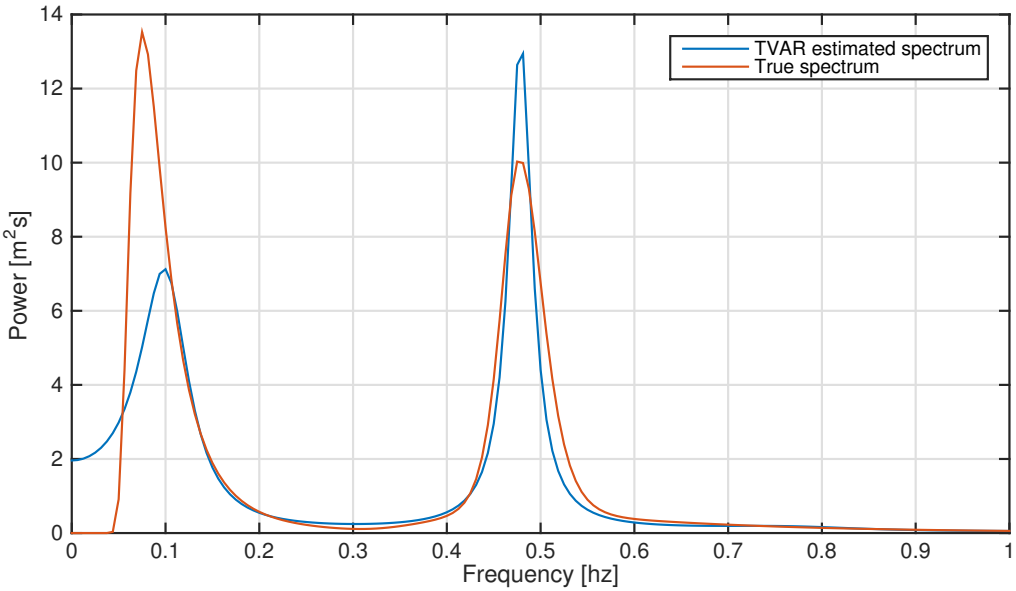

Figure 8.27: Estimated power spectrum vs real spectrum at $t = 60s$.

In Figure 8.26, it can be seen that both peaks are detected. However, it is observed that the second peak contains more magnitude noise than the first peak. Furthermore, in Figure 8.27 the estimated spectrum is shown at $t = 60s$. It can be seen that the estimated shapes differs from the true spectrum.

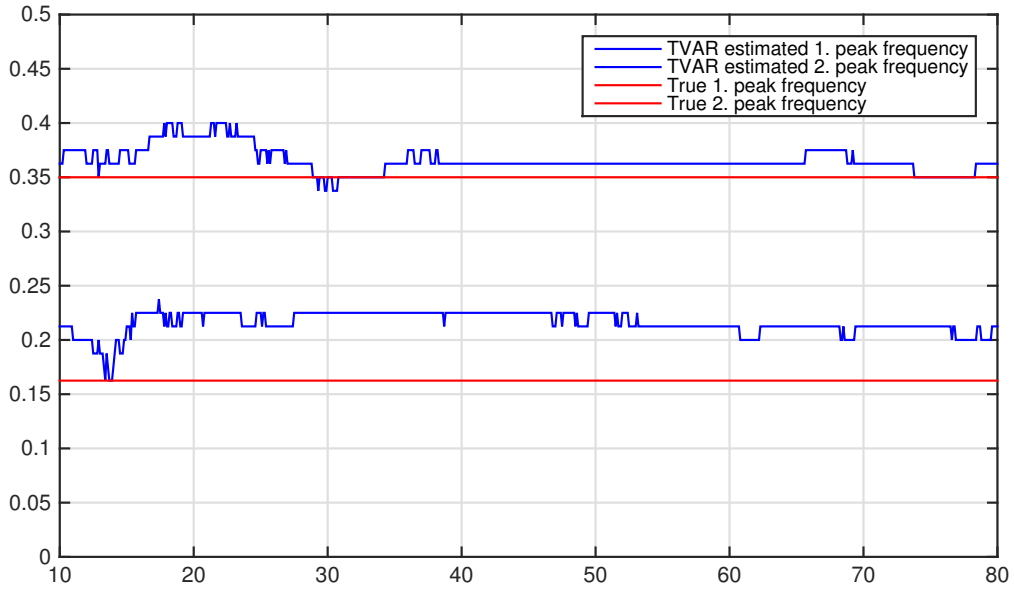

Figure 8.28: Peak frequency.

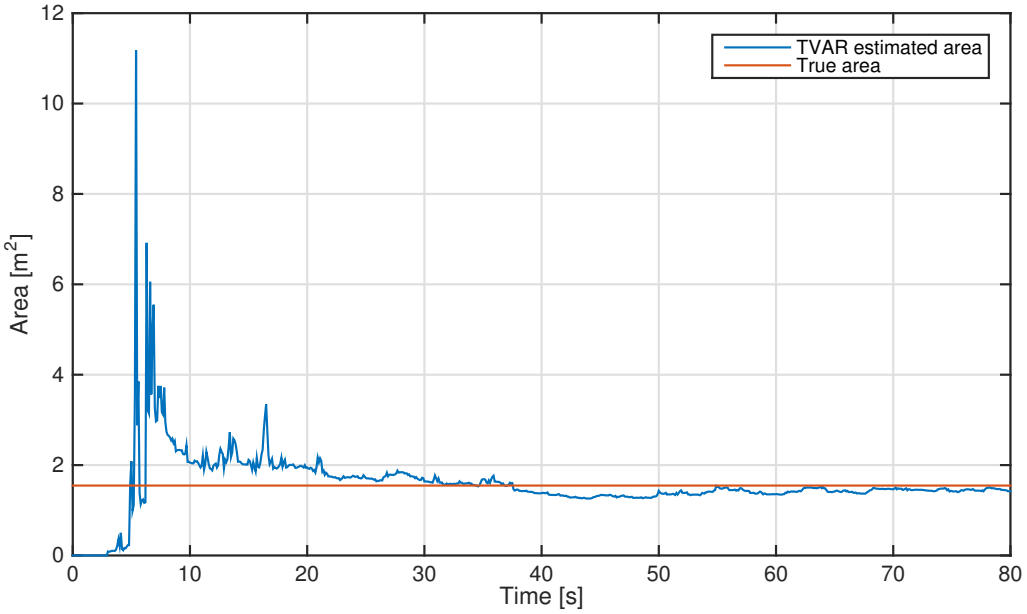

Figure 8.29: Area below the spectrum.

In Figure 8.28 the instantaneous peak frequencies are plotted against the true peak frequencies. It can be seen that the there is a smaller offset in the higher frequency peak than the other.

The estimated area is plotted against the true area in Figure 8.29, and it can be seen that the estimated area is close to the true area.

Discussion

In Figure 8.26, it can be seen that the algorithm is able to detect the two peaks. However, second peak contains more magnitude noise than the first. The reason for this is unclear, but possible related to the tuning of the filter or sub-optimal model order.

In Figure 8.29 it can be seen that the total energy in terms of the area is estimated accurately. However, the distribution in terms of the shape in Figure 8.27 is totally different.

8.3.2 Concluding Remarks of Case Study 3

In this case study it has been shown that the algorithm's performance in estimating a spectrum decreases with increasing complexity of the spectrum.

Chapter 9

Non-Stationary Simulation Studies

In this chapter, non stationary case studies are analyzed, see Figure 9.1. As previously elaborated, non-stationary processes have time varying describing parameters. Due to the lack of time-varying transfer functions, these processes are simulated by changing the describing parameters of the wave spectra during a time series, such as T_p and H_s, see Chapter 3.

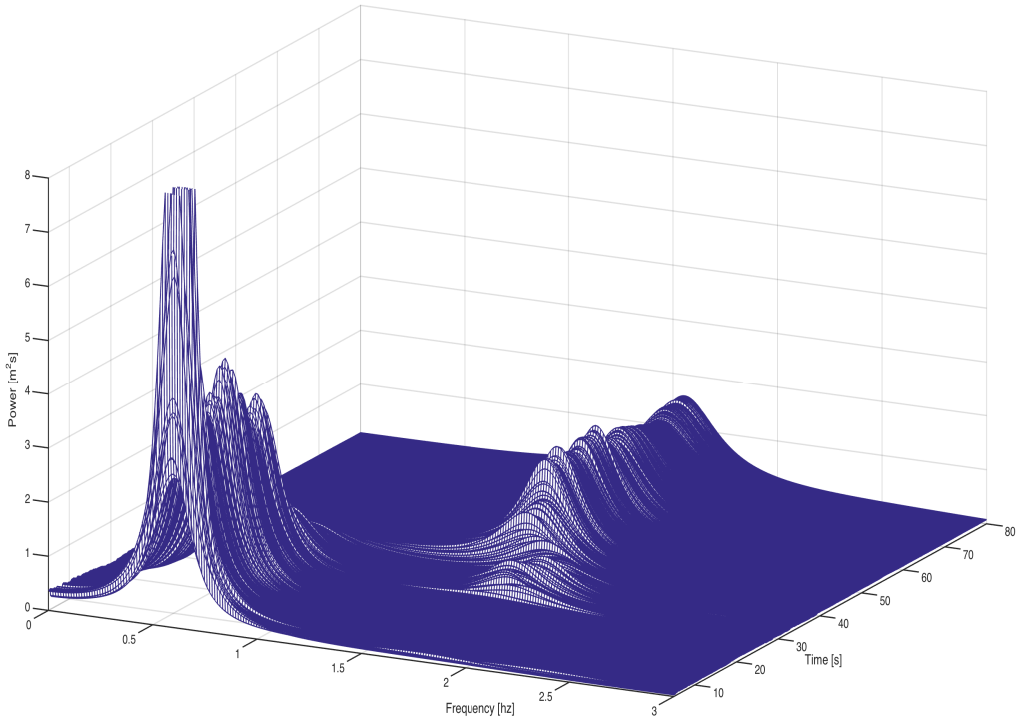

Figure 9.1: Example of Non-Stationary Ship Response Spectrum.

9.1 Case Study 4: Estimating Changing Power and Peak Frequency

In this section it is assumed that the $RAO = 1$, and the ship response output comes from a time varying JONSWAP spectrum, meaning that T_p and H_s changes during the simulation time.

In the first 26.67, seconds, the realizations are drawn from $S_1(\omega)$ and the rest of the time, the realizations are drawn from $S_2(\omega)$, see Figure 9.2, and Figure 9.3. The spectra are implemented with the following parameters given in Table 9.1. Furthermore, the process changes abruptly at $t = 26.67s$ both in frequency and area, and may not reflect the reality. On the other hand, similar characteristics may occur when a vessel transiting in head sea, which suddenly changes heading and receiving waves from the side. By this maneuver the encounter frequency and the power will change. However, this case study is made to test the algorithm's ability to detect changes in a ship response, and is therefore considered as reasonable.

Spectrum	H_s	T_p
$S_1(\omega)$	4 m	0.5 s
$S_2(\omega)$	6 m	1.5 s

Table 9.1: Parameters of the time varying JONSWAP spectrum.

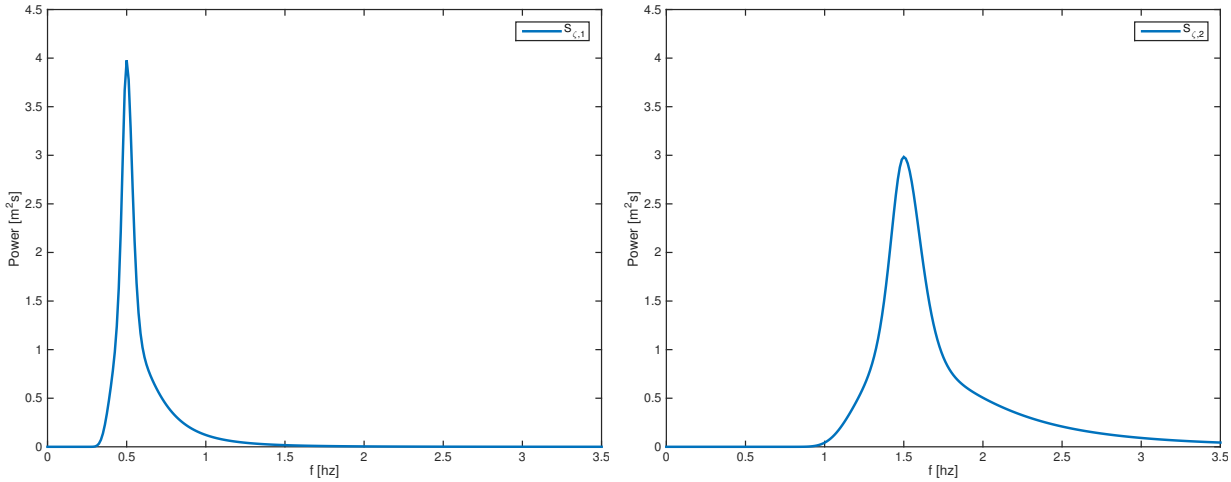

(a) JONSWAP spectrum $S_1(\omega)$. (b) JONSWAP spectrum $S_2(\omega)$.

Figure 9.2: Time varying JONSWAP spectrum.

9.1.1 Process Plant

The time varying JONSWAP spectra shown in Figure 9.2 are realized by the following equation,

$$y_k = \begin{cases} \sum_{q=1}^{N} \sqrt{2S_1(\omega_q)\Delta\omega}\sin(\omega_q t + \epsilon) + e_k & \text{if } k \leq \frac{N}{3} \\ \sum_{q=1}^{N} \sqrt{2S_2(\omega_q)\Delta\omega}\sin(\omega_q t + \epsilon) + e_k & \text{if } k > \frac{N}{3}, \end{cases} \tag{9.1}$$

where $e_k \sim \mathcal{N}(0, 0.1)$. In Figure 9.3, it can be observed that the main frequency of the components increases and the amplitude increases as a result of an increasing T_p and H_s. This corresponds to the parameters given in Table 9.1. (This can also be related to Figure 9.2, since an increase in H_s coincides to an increase in area).

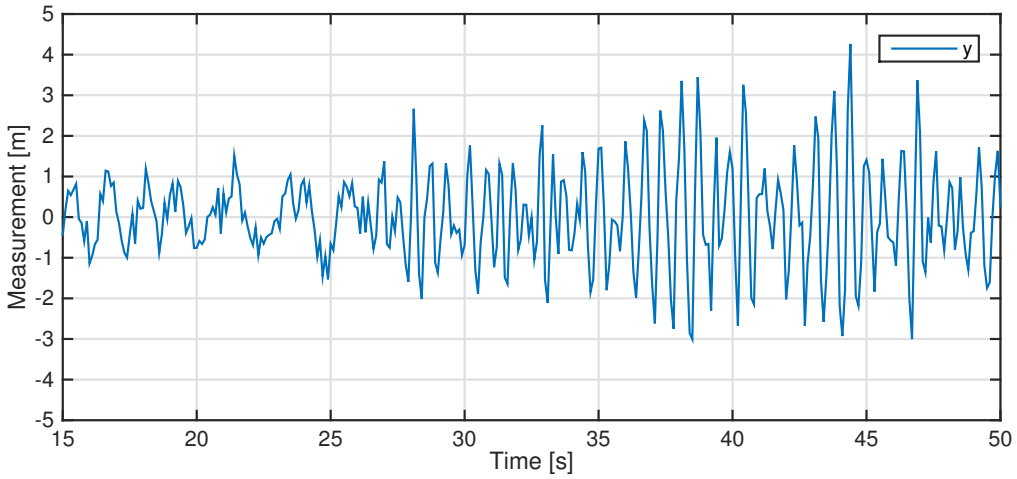

Figure 9.3: Time dependent JONSWAP spectrum that changes parameters

9.1.2 Mathematical Modeling

In Chapter 6, it was mentioned that high model order numbers can give spurious peaks in the estimated spectrum, even though the model order has been recommended by the BIC. In this case, such an event occurs.

The BIC curve is fairly flat between $p = 15 - 45$, but the least BIC number corresponds to $p = 34$, see Figure 9.4. However, this results in the spectrum given in Figure 9.5.

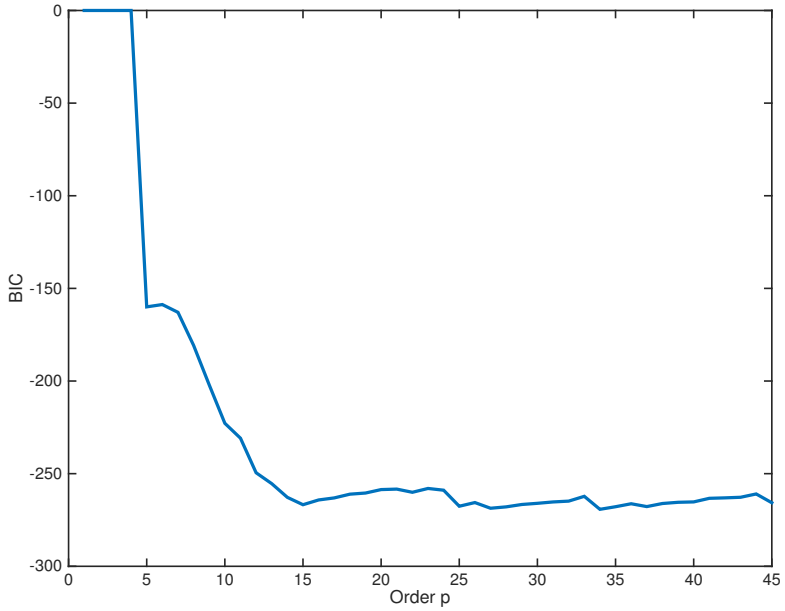

Figure 9.4: BIC values for different model orders.

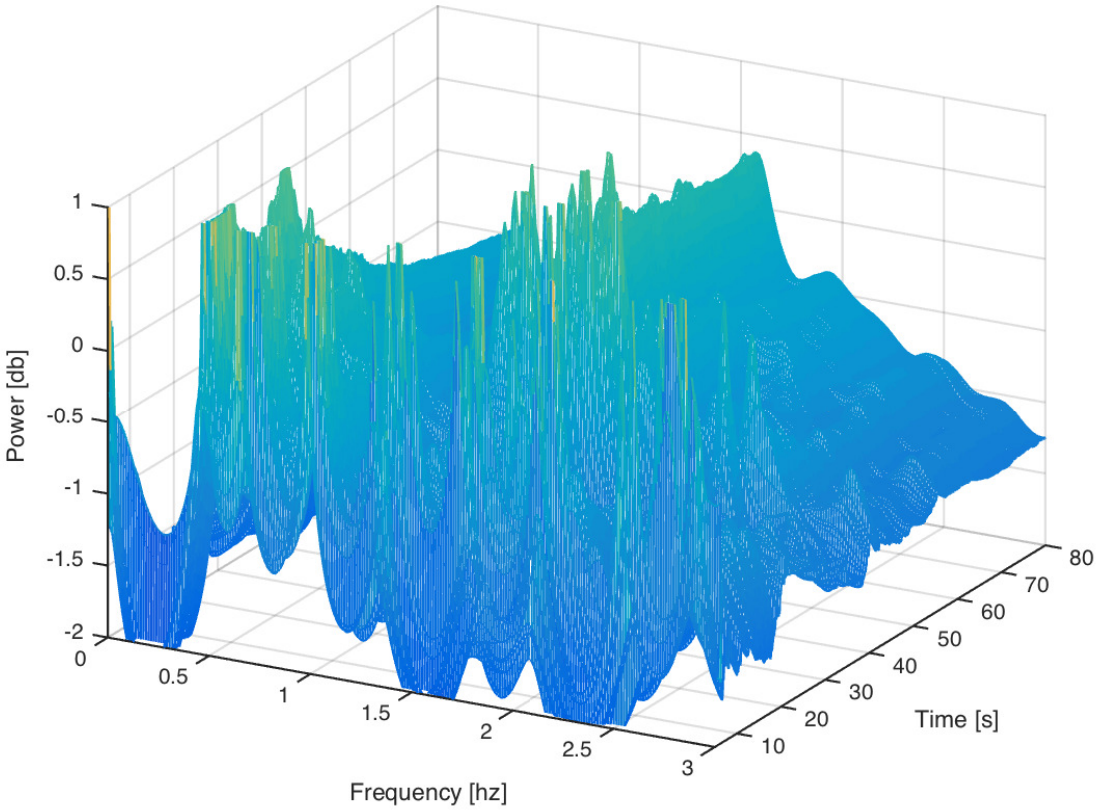

Figure 9.5: TVAR estimated spectrum with non-optimal model order.

From Figure 9.5, it can be observed that the optimal model indicated by the BIC number is not necessarily the correct one. As discussed in Chapter 6, the BIC number does not say anything about the spurious peaks that occur for a high model order number. Therefore, the model evaluation criteria stated in this thesis, should only serve as an indicator.

9.1.3 Estimation Results

By trial and error, the final model order was set to be $p = 8$, and the results obtained with this mathematical model are given in this section. The Kalman filter was implemented with the Q and R values given in Table 9.2.

Conditions	**Value**
State noise Q	10^{-11}
Observation noise R	10^{-1}

Table 9.2: Kalman filter parameters.

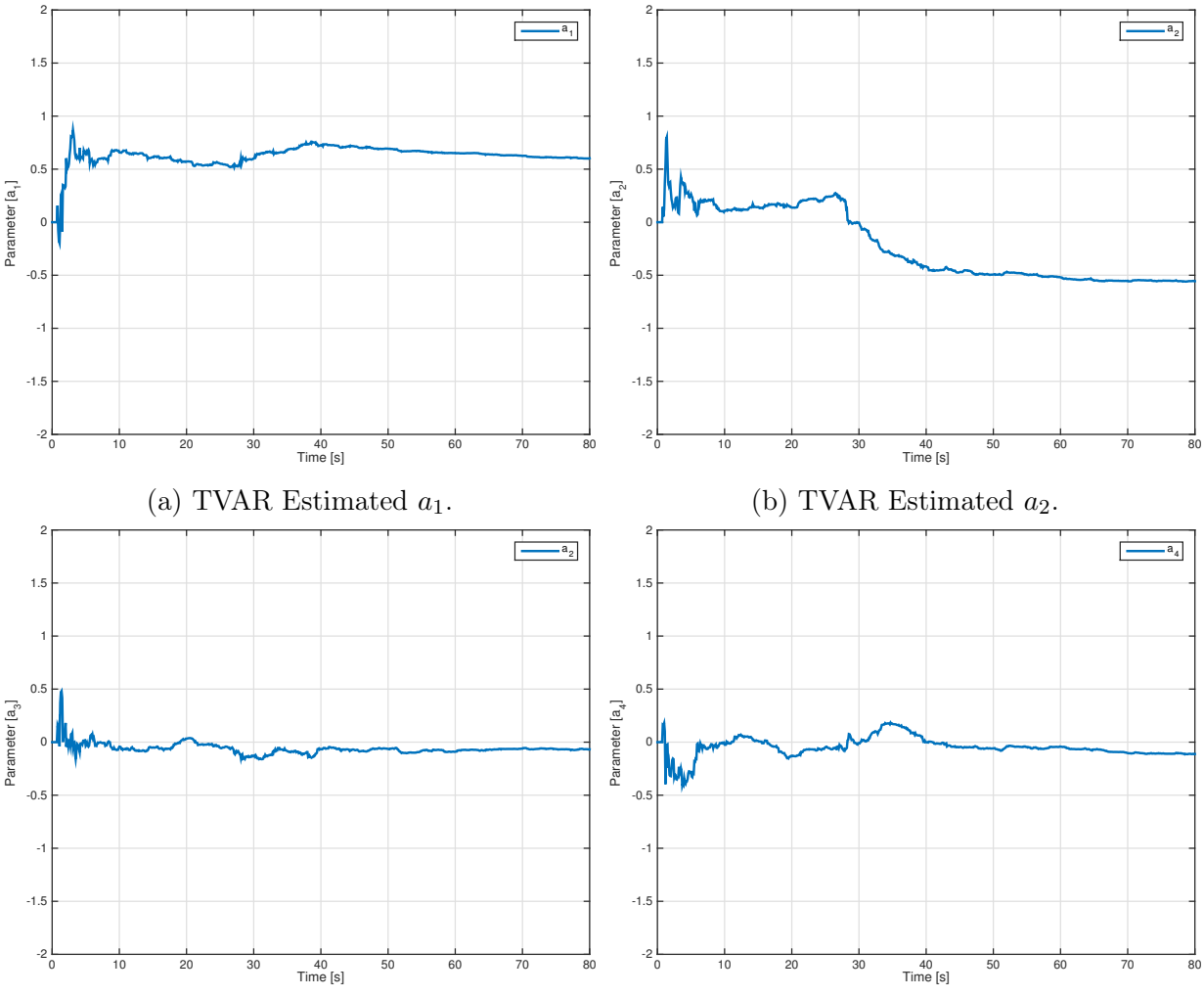

(a) TVAR Estimated a_1.

(b) TVAR Estimated a_2.

(c) TVAR Estimated a_3.

(d) TVAR Estimated a_4.

Figure 9.6: TVAR estimated parameters.

In Figure 9.6, the first 4 parameters are shown. In the plot it can be seen that the parameters change value after $26.67s$. Furthermore, it can be observed that the parameters have more noise before $26.67s$, than after.

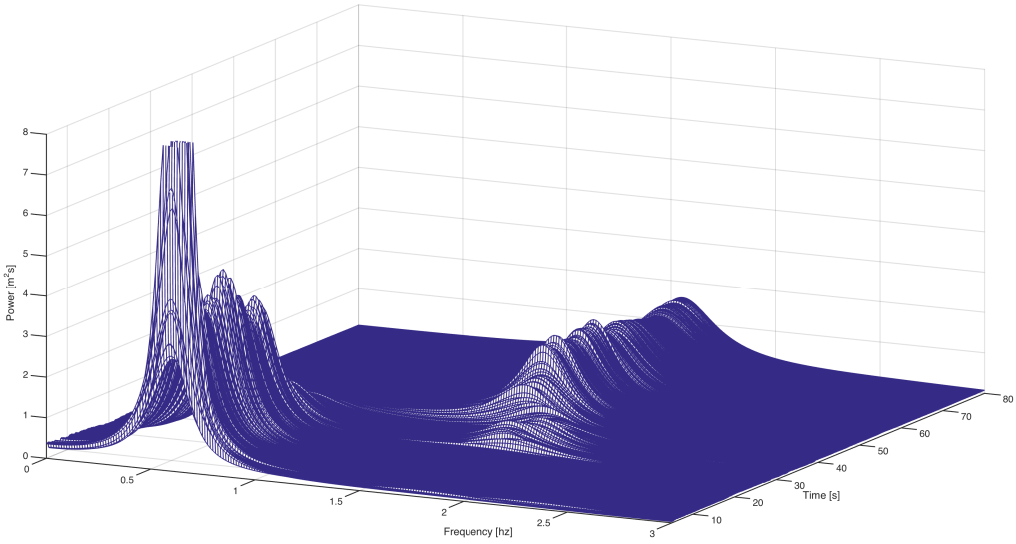

Figure 9.7: TVAR estimated spectrum.

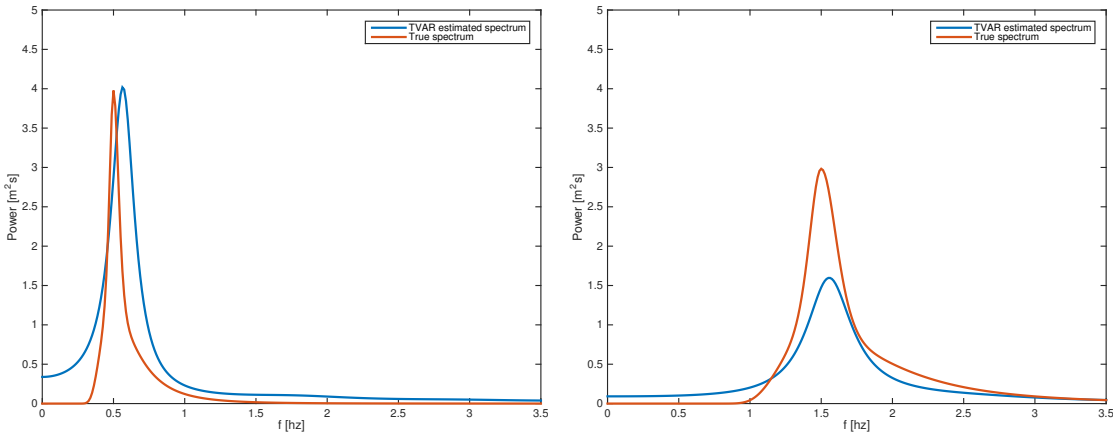

(a) Estimated spectrum at $t = 10s$. (b) Estimated spectrum at $t = 80s$.

Figure 9.8: Snapshot of estimated spectrum.

In Figure 9.7, it can be seen that the spectrum changes during the simulation time, both in terms of peak frequency and area. In addition, it can be observed that there are some higher peaks in the beginning than in the end.

In Figure 9.14a, a snapshot of the estimated spectrum at $t = 10s$ is shown. The estimated spectrum over estimate the power at low frequency. In Figure 9.14b, a snapshot of the estimated spectrum at $t = 80s$ is shown, and it can be observed that the algorithm under estimate the power.

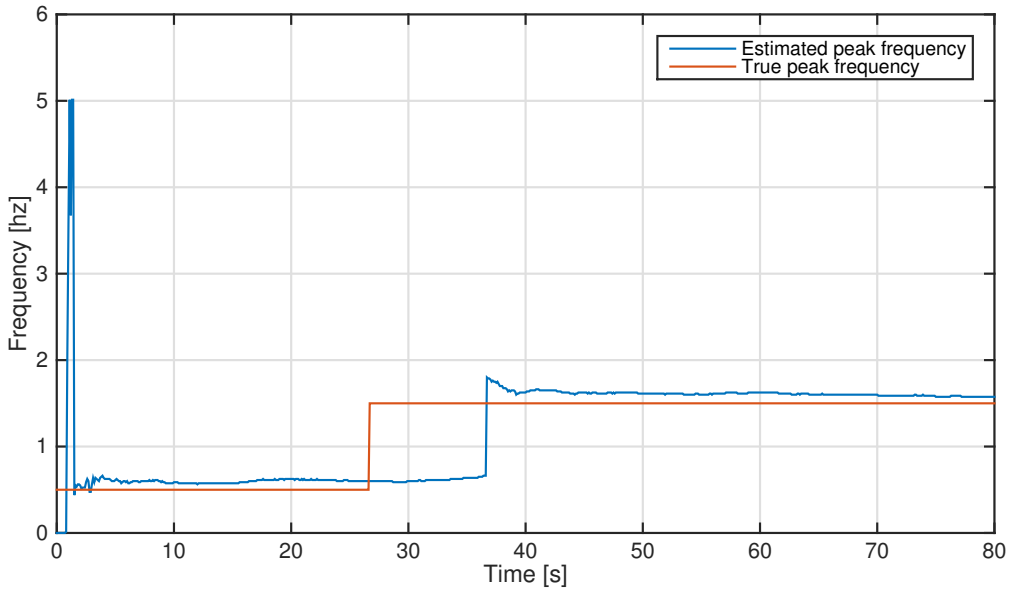

Figure 9.9: Peak frequency estimation

In Figure 9.9 the true versus the estimated peak frequency are shown. From the plot it can be seen that there is a lag between the true spectrum, and the estimated spectrum, when the parameter changes.

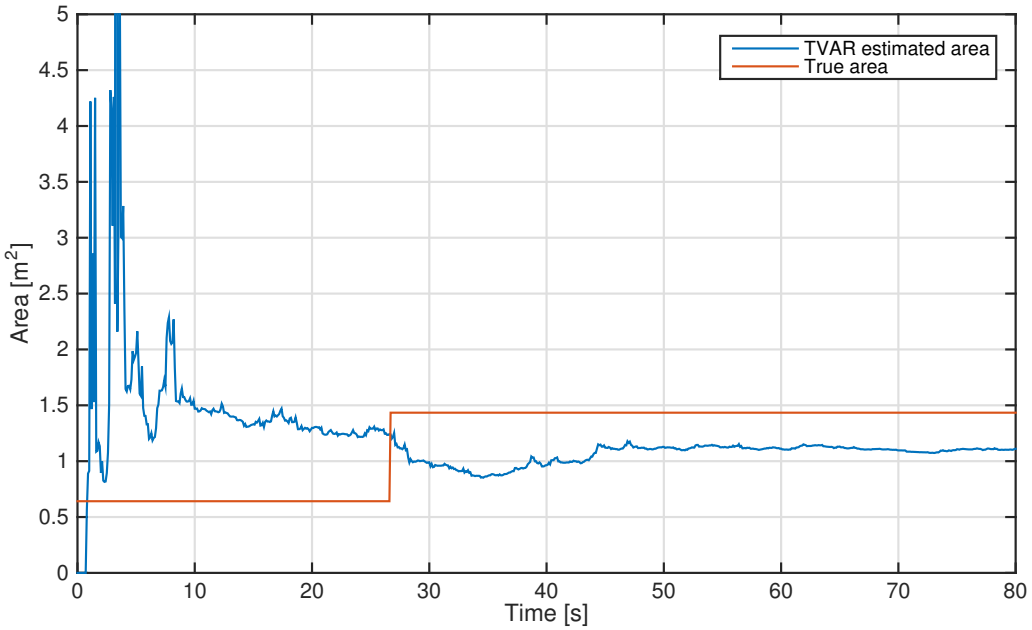

Figure 9.10: Area below spectrum.

In Figure 9.10 it can be seen that the algorithm is not able to detect the change in magnitude.

Discussion: In Figure 9.7, it can be seen that the magnitude oscillates more before the spectrum changes characteristics. The reason can be related to the estimated parameters in Figure 9.3, which are more noisy before the change. Due to the sensitivity the algorithm has to noise in the parameters, the magnitude of the spectrum will also oscillate, see Section 8.2. An explanation of why there is more noise in the beginning is due to the tuning of the estimation filter. Since the dynamics of the process changes when the spectrum change, the SNR ratio should be tuned according to both processes

In Figure 9.14b the algorithm estimates that there exist some energy at low frequency. The reason might be that the white noise, which has a uniform distribution across the frequencies, is not completely filtered out.

Furthermore in Figure 9.9, there is a lag between the estimated and the true peak frequency when the process change. The reason for this can be explained by the algorithm's build up. By observing Equation (4.8), the output (y_k) depends on the previous outputs ($y_{k-1}, y_{k-2}...y_{k-p}$). Therefore, the algorithm might having trouble with changing before all the previous outputs have changed. In addition, the Q-matrix has low values to ensure low noise in the parameters. This causes the parameters to change slowly.

9.1.4 Concluding Remarks of Case 4

In this case study the BIC seems to give a poor indication for the choice of model order. The results show therefore that the BIC should only serve as an indicator for this particular case. An adaptive approach to find the optimal model order could therefore be of interest.

Furthermore, although the algorithm estimated the peak frequency with a small error, the performance of estimating the changing area was not that good. The reason for this can be that

- the tuning of the SNR ratio might be only optimal to one of the two processes,
- or a sub-optimal model order was used.

This case study shows also that an adaptive SNR algorithm could be might be a solution to this problem.

9.2 Case Study 5: Estimating Changing Power

The algorithm's ability to estimate the spectrum magnitude is investigated further in this section, by letting the spectrum power change. Note that this case follows the structure as in Section 9.1, and therefore only the results are presented. The peak frequency is the same, while the significant wave height changes according to Table 9.3, after 40 seconds. The corresponding spectra are plotted in Figure 9.11.

Spectrum	H_s	f_0
$S_1(\omega)$	7 m	1.5 hz
$S_2(\omega)$	8 m	1.5 hz

Table 9.3: Parameters of the spectra.

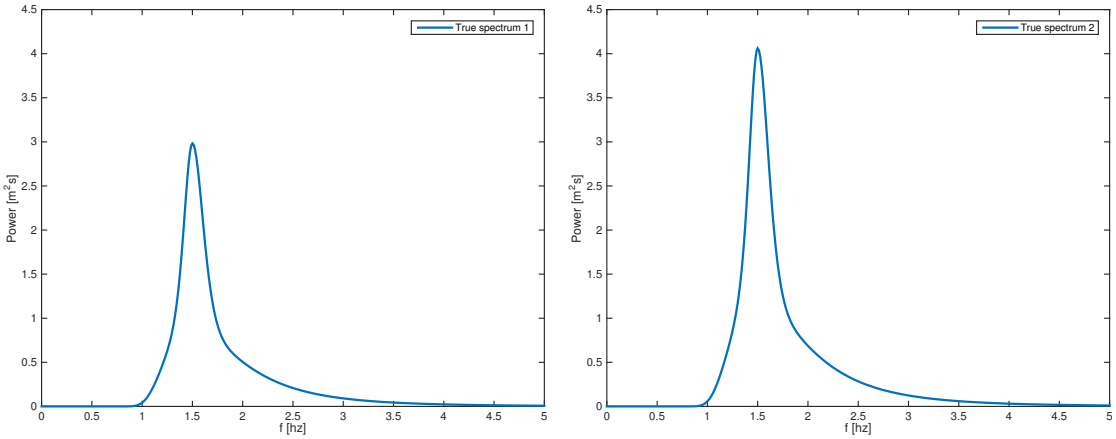

(a) JONSWAP spectrum $S_1(\omega)$.

(b) JONSWAP spectrum $S_2(\omega)$.

Figure 9.11: Time varying JONSWAP spectrum. The ship response realizations is changed from the left plot to the right plot after $t = 40s$.

9.2.1 Estimation Results

The results are presented in terms of the estimated parameters in Figure 9.12, the EPDS in Figure 9.13, the estimated spectrum before and after the power change plotted versus the real spectrum Figure 9.14, and instantaneous area plot in Figure 9.13. The algorithm is implemented with the Kalman filter parameters given in Table 9.4.

Conditions	**Value**
State noise Q	$10^{-11} \cdot I$
Observation noise R	10^{-1}

Table 9.4: Kalman filter parameters.

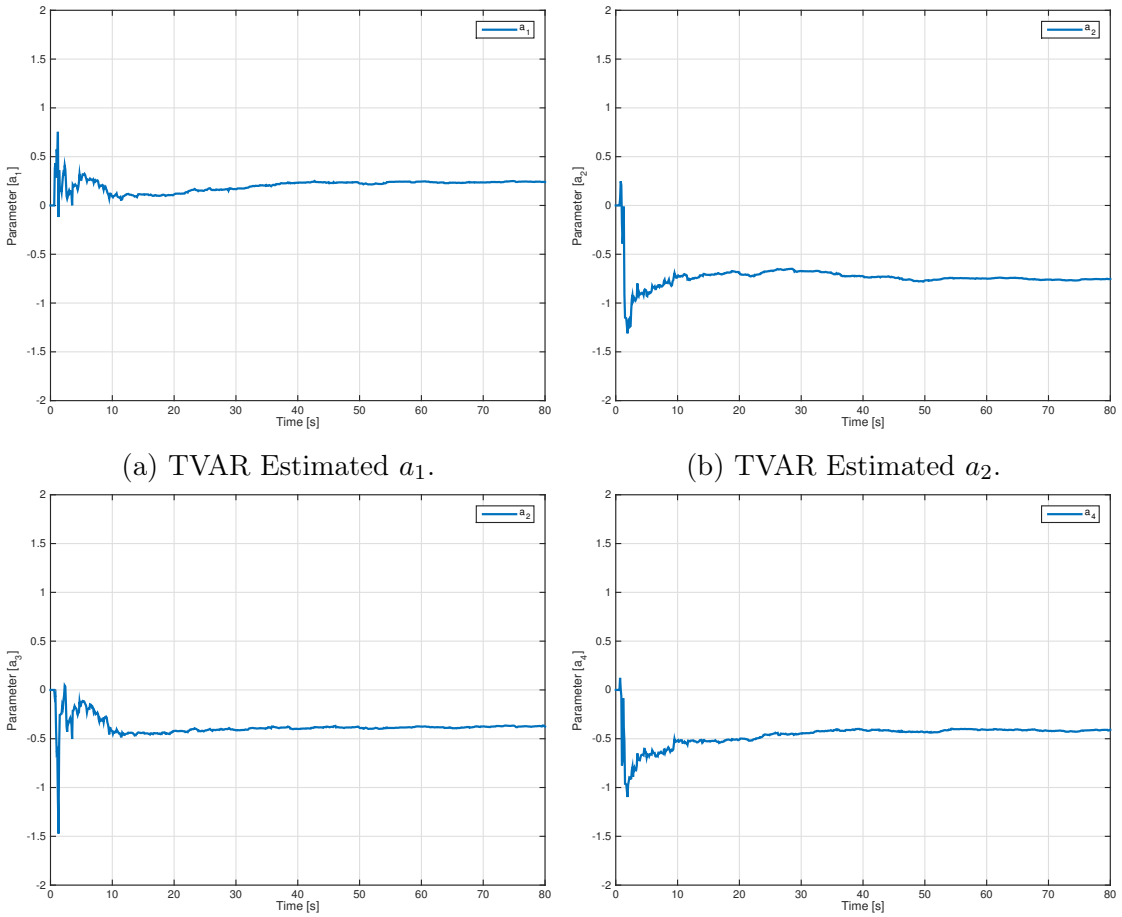

(a) TVAR Estimated a_1.

(b) TVAR Estimated a_2.

(c) TVAR Estimated a_3.

(d) TVAR Estimated a_4.

Figure 9.12: TVAR estimated parameters.

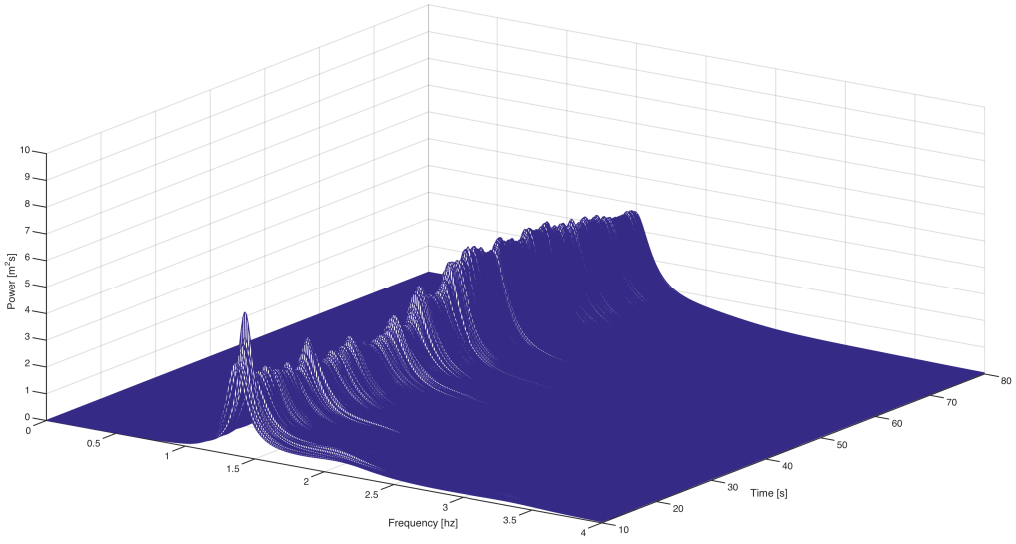

Figure 9.13: Estimated power density spectrum.

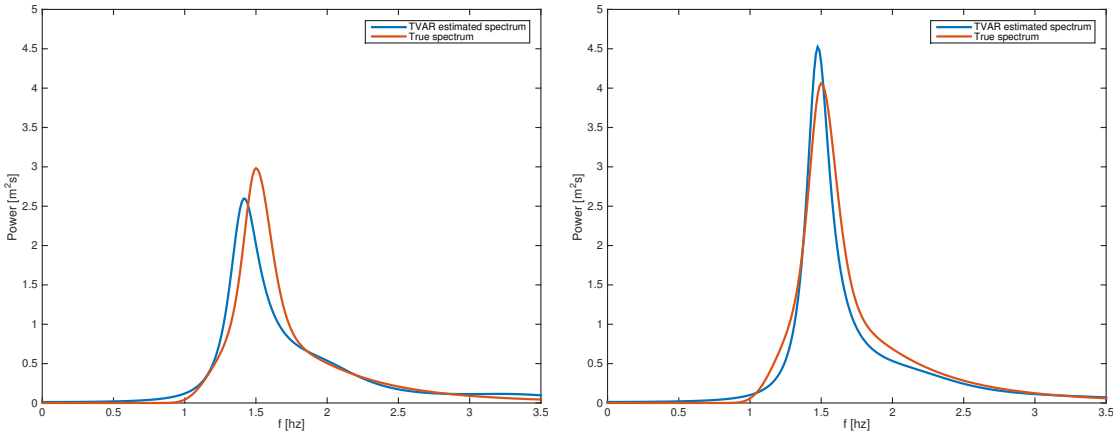

(a) Estimated spectrum at $t = 10s$ (b) Estimated spectrum at $t = 80s$.

Figure 9.14: Snapshot of estimated spectrum.

In Figure 9.13, it can be seen that the algorithm is able to detect the change of parameters after 40 seconds. Furthermore, in Figure 9.14 the estimated spectra at $t = 10s$ and $t = 80s$ are shown, and it can be seen that the estimated spectra are closed to the true spectra.

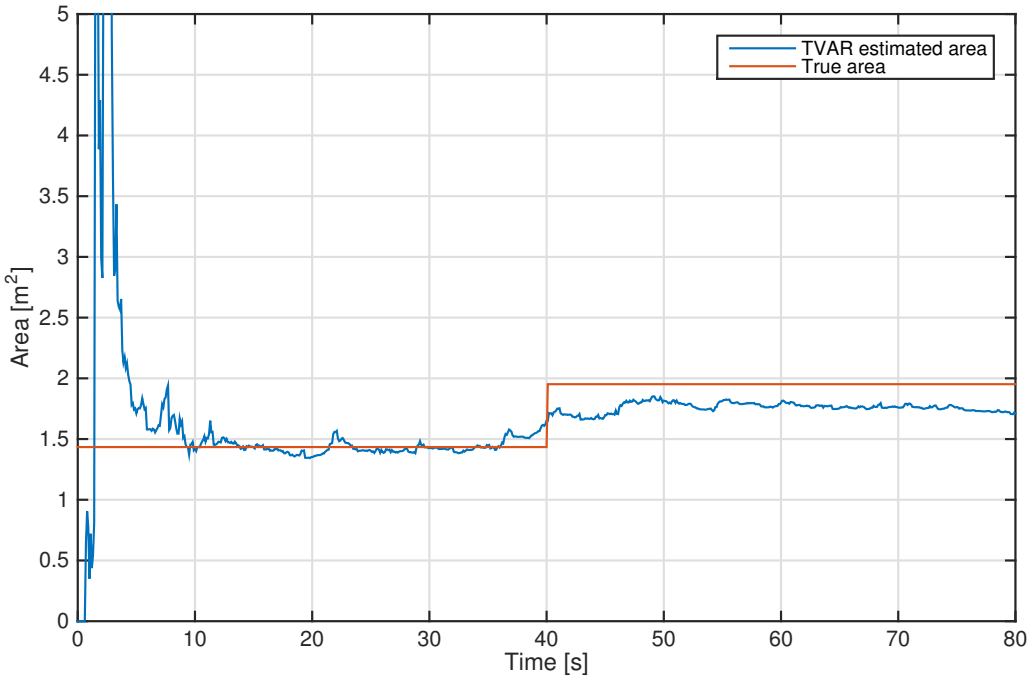

Figure 9.15: Area below the spectrum.

Discussion of Results

It can be observed that in Figure 9.13, the algorithm detect the magnitude change of the spectrum. However, in Figure 9.15 it can be seen that the algorithm is not able to find the correct magnitude. The reason for this might be that the SNR ratio is only optimal for the process before the parameters change.

9.2.2 Concluding Remarks of Case 5

In this case study the algorithm seems to be able to detect the magnitude to change, but not perfectly. The reason can possibly be related to the SNR.

Chapter 10

Ship Response Estimation of Cybership III

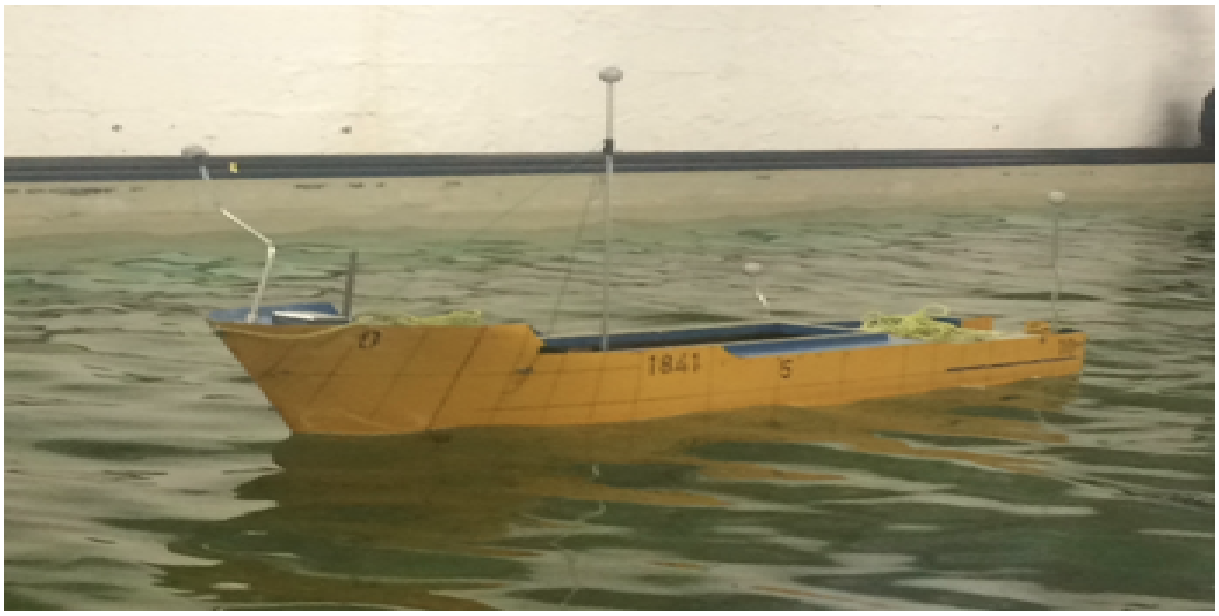

Figure 10.1: Cybership III.

In this case study, the algorithm has been tested on a model scaled test. The test was conducted in the MClab at the department of Marine Technology, NTNU, with the model Cybership III, see Figure 10.1. The characteristics of the model is given in Table 10.1. The model vessel has a station keeping capabilities, and sensors that measure orientation of the vessel. The MClab has a wave generator that can generate long crested irregular waves realized from several spectra, such as the Pierson Moscovitz, JONSWAP and Torsethaugen. The lab also has a sensor that measures the generated sea state.

Parameters	**Model**	**Ship**
Length	1.97 m	59 m
Beam	0.44 m	13.2 m
Draught	0.16.	4.8 m
Mass	89 kg	$2.4 \cdot 10^6$

Table 10.1: Main dimensions of Cybership III (Ruth 2008).

10.1 Process Plant

The generated spectra is the JONSWAP spectra, with $T_p = 1.48s$, and $H_s = 0.05m$. The measured heave movement in the first 10 seconds is given in Figure 10.2.

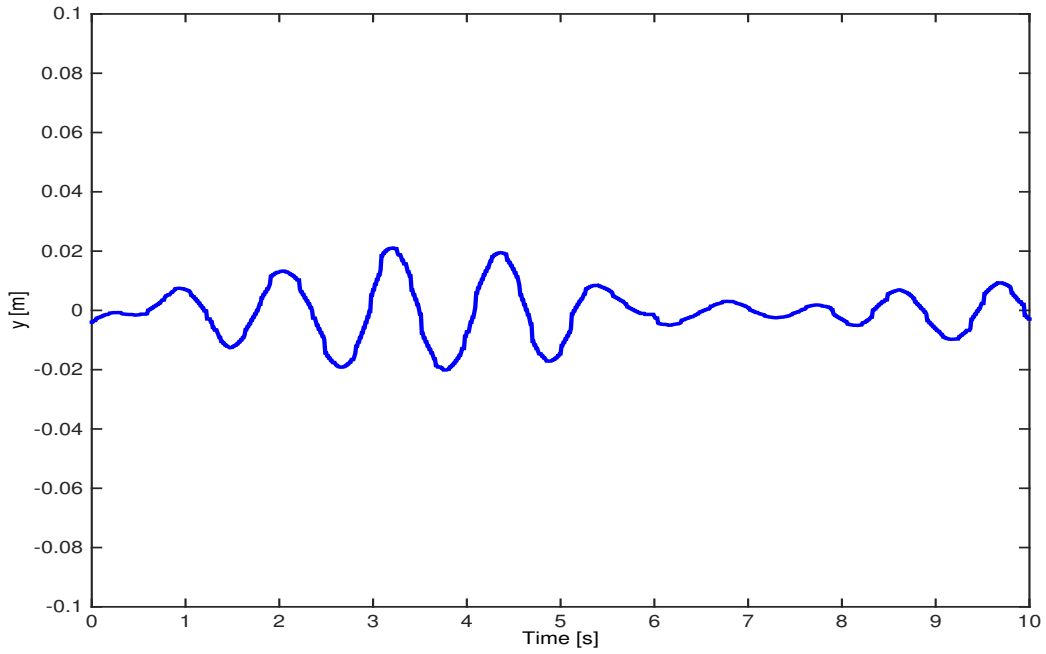

Figure 10.2: Measured response of Cybership III.

10.2 Reference Spectrum

In order to obtain a reference ship response spectrum that can be compared with TVAR estimated spectrum, the JONSWAP spectrum is multiplied with the square of the RAO of Cybership III, see Equation (3.4). The RAO is taken from MC-Sim, which is a simulation platform developed in Matlab/Simulink by the Department of Marine Cybernetics NTNU. This particular RAO is calculated for head sea waves, meaning that the vessel needs to point in the direction of encountering waves. Therefore, this is the control objective of the vessel, and the case is considered as stationary. The wave spectra, the RAO, and the ship response is shown in Figure 10.3.

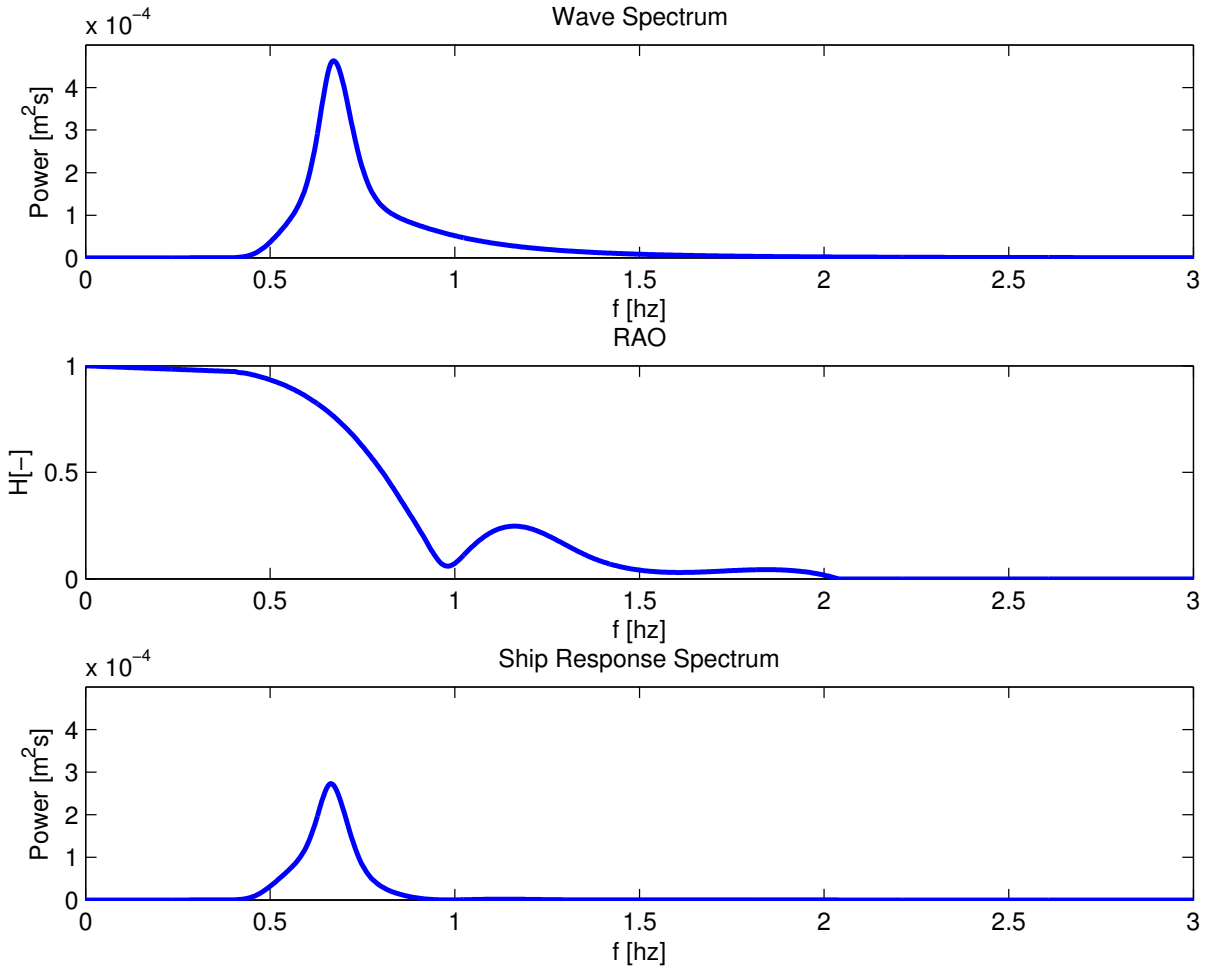

Figure 10.3: Wave spectrum, transfer function and ship response.

10.3 Mathematical Modeling

In Section 9.1 it is shown that the BIC can give misleading indication of optimal model order. Therefore the model order is found by trial and set equal to $p = 22$.

10.4 Estimation Results

In the following the TVAR estimated parameters are shown.

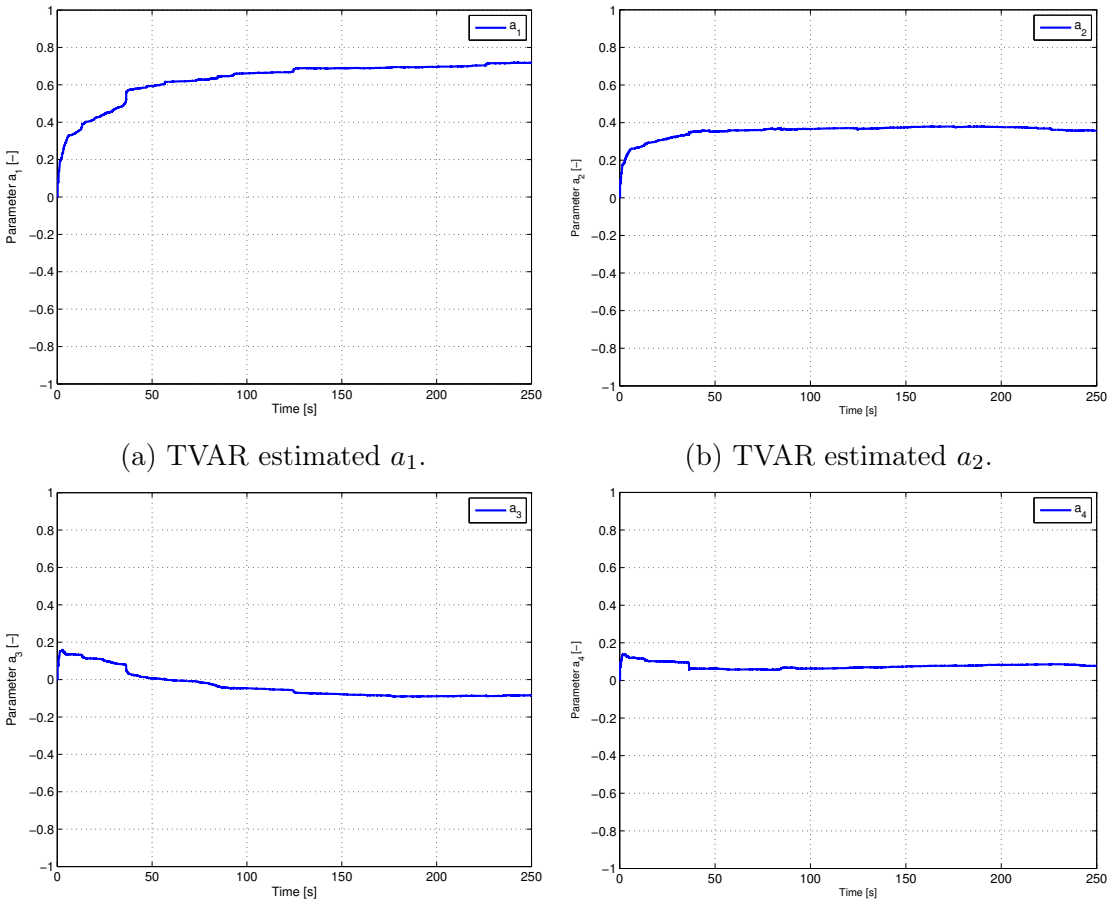

(a) TVAR estimated a_1.

(b) TVAR estimated a_2.

(c) TVAR estimated a_3.

(d) TVAR estimated a_4.

Figure 10.4: TVAR estimated Parameters.

In Figure 10.4 the first four parameters are shown. The parameters are smooth, and seems to converge to constant values.

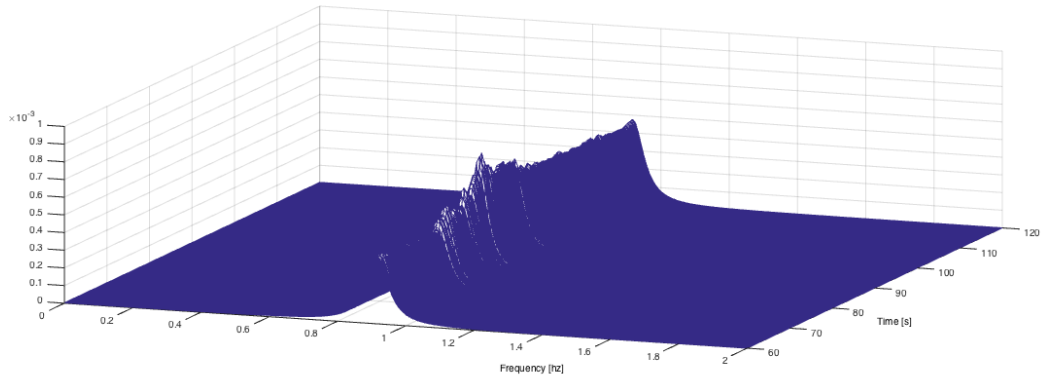

Figure 10.5: TVAR estimated evolutionary power density spectrum of Cybership III in head sea waves.

In Figure 10.5 the estimated power spectral density are shown. The figure shows that the spectrum is smooth, which indicates a stationary process. This makes it able to include a third reference, which is the spectrum estimated from the WAFO toolbox in Matlab. This is non-parametric method that the uses FFT and smoothing functions to estimate the spectrum. Furthermore, by taking the mean of Figure 10.5, the TVAR estimated spectrum can be compared with two references.

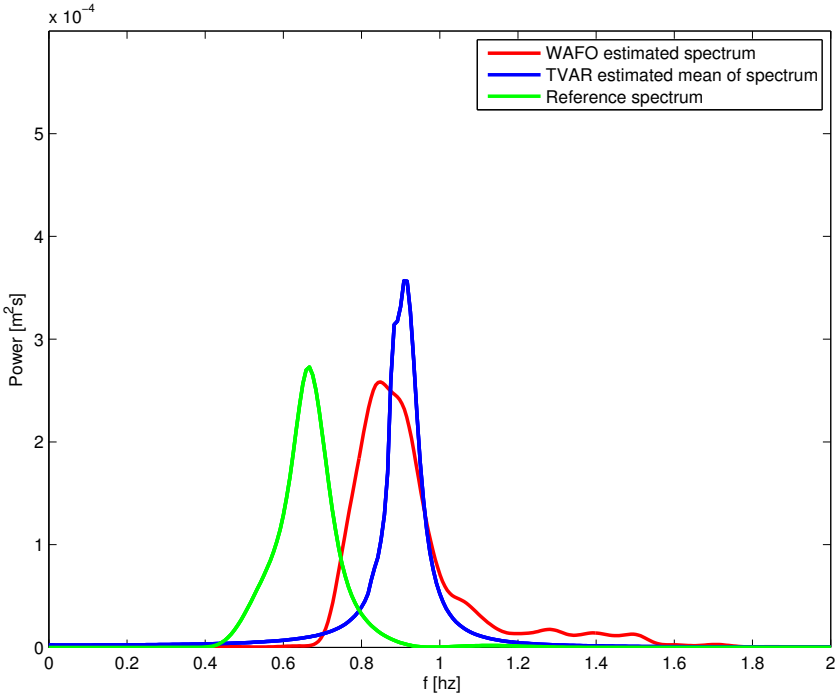

Figure 10.6: Spectrum calculated from transfer function, WAFO calculated spectrum, and TVAR estimated spectrum.

In Figure 10.6, it can be seen that the reference spectrum, differs substantially from the

TVAR and WAFO estimated spectrum. Furthermore, the TVAR estimated spectrum is more narrow, than the two others and has a slightly higher peak frequency.

10.4.1 Discussion

Since both the estimation methods differs quite much in magnitude from the reference spectrum there might be something wrong. From Figure 10.3 and Figure 10.6, it can be seen that the RAO has a cancellation point where the WAFO and TVAR methods have maximums. This indicates that there is an error with the RAO of Cybership III.

Due to these findings a further investigation of the RAO was initiated, and it was found that the battery packages of the vessel has been replaced, without an update of the RAO (Astrid H. Brodtkorb 2015).

Since the RAO is also a function of the load condition, including both the weight and the distribution of the weight in the vessel, the RAO needs to be updated for the new load condition. Therefore, it is incorrect to compare the estimation results with the reference spectrum. Therefore, the WAFO and the TVAR estimated are compared.

It can be observed that the TVAR estimated spectrum is more narrow than the WAFO estimated spectrum. If the WAFO estimated spectrum is equal to the real ship response spectrum, the TVAR estimated spectrum is too narrow. As previously discussed the TVAR algorithm is very sensitive to the SNR ratio, and therefore there are reasons to believe that this is also the case in this study. In addition, the model order can be sub-optimal not recreating the correct spectrum.

Chapter 11

Conclusion

In this thesis it is found that the ship response is non-stationary for changing operational conditions such as vessel speed or course angle. This is addressed by introducing a time varying auto-regressive model, which can be used to form an estimate of the non-stationary ship response spectrum.

The simulation studies indicates that the TVAR algorithm can estimate single peaked spectra with a satisfying accuracy. However, by increasing the complexity by double peaks, the performance of the algorithm decreases. The same holds for the level of non-stationarity. The algorithm was able to track the change in power when this was the only the time-varying describing parameter. When both the peak frequency and the power changed, the performance decreased.

Furthermore, the simulation studies indicates that key factors of the algorithm is shown to be the SNR value. A low SNR value contribute to slowly varying parameters, which contribute to a stable spectrum.

The main limitation with the method is that the optimal SNR value has to be tuned manually. In addition, the model evaluation criteria can sometimes give wrong indications of which model order is the optimal one. Adaptive algorithms in estimating the SNR value and the model order needs to be investigated to be able to reach the potential of the method.

Chapter 12

Recommendations for Further Work

Real ship response data is yet to be tested for the TVAR algorithm. Unfortunately, the RAO of Cybership III was shown to be for a different load condition, and therefore the algorithm could not be tested on real data with a proper reference.

As stated in Section 4.3.2, the Cauchy and the Particle filter should be implemented and tested in case studies where changes occur more abruptly, for instance a ship in an extreme weather conditions. In order to do so, it is suggested to use smoothing algorithms to reduce the noise.

In spectral estimation of ship response, the TVAR method is still an area in need of more research. In particular, it is recommended that adaptive algorithms to can find the optimal SNR ratio should be investigated, and it is suggested to look into smoothing algorithms such as Kalman smoother etc.

When these algorithms are obtained, the algorithm should also be implemented in wave spectra estimation algorithms. This would bring the concept one step closer of having a database receiving data from seas all around the world, and make the ocean more predictable.

Bibliography

Akaike, H. (1974), 'A new look at the statistical model identification', *IEEE Transactions on Automatic Control* **19**(6), 716–723.

Arulampalam, S. M., Maskell, S., Gordon, N. & Clapp, T. (2002), 'A tutorial on particle filters for online nonlinear/non-Gaussian Bayesian tracking', *IEEE Transactions on Signal Processing* **50**(2), 174–188.

Astrid H. Brodtkorb (2015), 'Discussion with PhD. Candidate (NTNU) Astrid H. Brodtkorb'. Dated 25.05.2015.

Balchen, J. G., Fjeld, M. & Solheim, O. A. (2003), *Reguleringsteknikk*, Vol. 5, Tapir, Institutt for teknisk kybernetikk, NTNU.

Brekke, E. F. (2010), Clutter mitigation for target tracking, PhD thesis, PhD thesis, Norwegian University of Science and Technology, Trondheim.

Doucet, A., De Freitas, N. & Gordon, N. (2001), *An introduction to Sequential Monte Carlo Methods*, Springer, New York City.

Faltinsen, O. (1990), *Sealoads on Ships and Offshore Structures*, Campbridge University Press, Campbridge UK.

Fossen, T. I. (2011), *Handbook of marine craft hydrodynamics and motion control*, John Wiley & Sons, Hoboken, NJ, USA.

Gardner, W. (1990), *Introduction to Random Processes: With application to signals and system*, McGraw-Hill Inc, New York.

Gordon, N. J., Salmond, D. J. & Smith, A. F. (1993), Novel approach to nonlinear/non-gaussian bayesian state estimation, *in* 'IEEE Proceedings F (Radar and Signal Processing)', Vol. 140, IET, pp. 107–113.

Gustafsson, F. (2010*a*), 'Particle filter theory and practice with positioning applications', *Aerospace and Electronic Systems Magazine, IEEE* **25**(7), 53–82.

Gustafsson, F. (2010*b*), 'Statistical sensor fusion'.

Hammersley, J. M. & Morton, K. W. (1954), 'Poor man's Monte Carlo', *Journal of the Royal Statistical Society. Series B (Methodological)* pp. 23–38.

Higham, N. J. (2002), *Accuracy and stability of numerical algorithms*, Siam, Philadelphia, USA.

Isard, M. & Blake, A. (1998), 'Condensation—conditional density propagation for visual tracking', *International journal of computer vision* **29**(1), 5–28.

Iseki, T. (2004), Extended bayesian estimation of directional wave spectra, *in* 'ASME 2004 23rd International Conference on Offshore Mechanics and Arctic Engineering', American Society of Mechanical Engineers, pp. 611–616.

Iseki, T. & Terada, D. (2003), 'Study on real-time estimation of the ship motion cross spectra', *Journal of marine science and technology* **7**(4), 157–163.

Kalman, R. (1960), 'A new approach to linear filtering and prediction problems', *Transactions of the ASME-–Journal of Basic Engineering* **Series D**, 35–45.

Kitagawa, G. (1996), 'Monte carlo filter and smoother for non-gaussian nonlinear state space models', *Journal of computational and graphical statistics* **5**(1), 1–25.

Kitagawa, G. & Gersch, W. (1985), 'A smoothness priors time-varying AR coefficient modeling of nonstationary covariance time series', *Automatic Control, IEEE Transactions on* **30**(1), 48–56.

Leira, B. (2005), Stochastic theory of sealoads: probabilistic modelling and estimation (lecture notes), Technical report, UK-2005–72: Department of Marine Technology, NTNU.

Luenberger, D. (1971), 'An introduction to observers', *IEEE Transactions on automatic control* **16**(6), 596–602.

Marple, S. L. (1986), *Digital Spectral Analysis: With Applications*, Prentice-Hall, Inc., Upper Saddle River, NJ, USA.

Myrhaug, D. (2007), 'Kompendium TMR4180 Marin Dynamikk–Uregelmessig sjø', *Trondheim: Department of Marine Technology* .

Nielsen, U. D. (2005), Estimation of Directional Wave Spectra from Measured Ship Responses, PhD thesis, Technical University of Denmark.

Price, W. G. & Bishop, R. E. D. (1974), *Probabilistic theory of ship dynamics*, Halsted Press, New York.

Priestley, M. (1965), 'Evolutionary Spectra and Non-stationary Processes', *Journal of the Royal Statistical Society. Series B (Methodological)* **27**(2).

Proakis, J. G. & Manolakis, D. K. (2006), *Digital Signal Processing (4th Edition)*, Prentice-Hall, Inc., Upper Saddle River, NJ, USA.

Reddy, G. & Rao, R. (2014), 'Non-stationary Signal Analysis using TVAR Model', *International Journal of Signal Processing, Image Processing & Pattern Recognition* **7**(2).

Robotnor Centre for Advanced Robothics (2015), 'Mathematical Modelling'. Viewed 2015-04-08
`http://robotnor.no/expertise/fields-of-competence/mathematical-modeling-for-control/`.

Ruth, E. (2008), Propulsion control and thrust allocation on marine vessels, PhD thesis, PhD thesis, Norwegian University of Science and Technology, Trondheim.

Schwarz, G. et al. (1978), 'Estimating the dimension of a model', *The annals of statistics* **6**(2), 461–464.

Simon, D. (2006), *Optimal state estimation: Kalman, H infinity, and nonlinear approaches*, John Wiley & Sons.

Simon Godsill (2009), 'Sequential Monte Carlo Methods'. Viewed 01.10.2014
`http://mlg.eng.cam.ac.uk/mlss09/mlss_slides/Godsill_1.pdf`.

Sørensen, A. J. (2012), 'Marine Control Systems Propulsion and Motion Control of Ships and Ocean Structures Lecture Notes', *TMR 4240 Marine Control Systems, Department of Marine Technology NTNU* .

Spyers-Ashby, J., Bain, P. & Roberts, S. (1998), 'A comparison of fast fourier transform (FFT) and autoregressive (AR) spectral estimation techniques for the analysis of tremor data', *Journal of Neuroscience Methods* **83**, 35–43.

Stoica, P. & Moses, R. L. (1997), *Introduction to spectral analysis*, Vol. 1, Prentice hall Upper Saddle River.

Tannuri, E. A., Sparanoa, J. V., Simosa, A. N. & Da Cruz, J. J. (2003), 'Estimating directional wave spectrum based on stationary ship motion measurements', *Applied Ocean Research 25* **5**, 243–261.

Ting, C.M Sh-Hussain Salleh, Z. M. Z. & Bahar, A. (2011), 'Spectral estimation of nonstationary EEG using particle filtering with application to event-related desynchronization (ERD)', *IEEE transaction on biomedical engineering* pp. 321–331.

Wei, W. W. (2006), *Time series analysis: univariate and multivariate methods*, Pearson Addison Wesley, New York.

Yazid, E., Liew, M. S. & Parman, S. (2012), 'Time-varying spectrum estimation of offshore structure response based on a time-varying autoregressive model', *Journal of Applied Sciences* **12**, 2383–2389.

Appendix A

Appendix

A.1 Stationary processes

Definition 3 (Stationary processes) *(Wei 2006) The n^{th} order joint distribution is given as*

$$F(x_{t_1}, x_{t_2}, ..., x_{t_n}) = P(x_{t_1} < \beta_1, x_{t_2} < \beta_2, ..., x_n < \beta_n) \tag{A.1}$$

If $F(x_{t_1}, x_{t_2}, ..., x_{t_n}) = F(x_{t_{1+\tau}}, x_{t_{1+\tau}}, ..., x_{t_{n+\tau}})$, the process is strictly stationary.

This means that the cumulative distribution function are not explicitly dependent on time, only on the time shift. This definition also holds for the higher order probability density function $p(x_1, x_2, ..., x_n)$.

A.2 Multivariate Gaussian Distribution

If y_k is a vector the density function becomes multivariate, and can be written as

$$p_v(y_k - C_k x_k) = \frac{1}{(2\pi)^{\frac{q}{2}}|\Sigma_w|^{\frac{1}{2}}} e^{-\frac{1}{2}([y_k - C_k x_k] - \mu_v)^T \Sigma_v^{-1}([y_k - C_k x_k] - \mu_v)} \tag{A.2}$$

where $|\Sigma_e|$ is the determinant of Σ_e, and q is the order of the observation vector y_k. The multivariate co-variance and mean of the observation noise, given as

$$\Sigma_e = \begin{bmatrix} \sigma_{e_{1,1}} & \sigma_{e_{1,2}} & \dots & \sigma_{e_{1,q}} \\ \sigma_{e_{2,1}} & \sigma_{e_{2,2}} & \dots & \sigma_{e_{2,q}} \\ \vdots & \vdots & \ddots & \vdots \\ \sigma_{e_{q,1}} & \sigma_{e_{q,2}} & \dots & \sigma_{e_{q,q}} \end{bmatrix}, \qquad \mu_e = \begin{bmatrix} E[e_1] \\ E[e_2] \\ \vdots \\ E[e_q] \end{bmatrix} = \begin{bmatrix} 0 \\ 0 \\ \vdots \\ 0 \end{bmatrix} \tag{A.3}$$

A.3 Derivation of Bayesian Update Recursion

The Bayes update recursion can be derived from Bayes Law, the Markov property defined in Section 4.3.2, and factorization and marginalization properties of random variables:

Definition 4 (Bayes Law) *The probability of event A, given event B can be written as*

$$\begin{aligned} p(A|B) &= \frac{p(A,B)}{p(B)} \\ &= \frac{p(B|A)p(A)}{p(B)}. \end{aligned} \tag{A.4}$$

Definition 5 (Factorization) *The density is factorisable if it can be divided into terms like the following*

$$p(A_{1:k}) = p(A_k, A_{1:k-1}) = p(A_k|A_{1:k-1})p(A_{1:k-1}). \tag{A.5}$$

Definition 6 (Marginalization) *Consider the joint probability density function $p(x,y)$. Then it follows that*

$$p(A) = \int p(A,B)dB. \tag{A.6}$$

Having these definitions in mind, the measurement update is derived in the following

$$\begin{aligned} p(x_k|y_{1:k}) &= \frac{p(y_{1:k}|x_k)p(x_k)}{p(y_{1:k})} \\ &= \frac{\overbrace{p(y_k, y_{1:k-1}|x_k)}^{Factorization} p(x_k)}{p(y_k, y_{1:k-1})} \\ &= \frac{\overbrace{p(y_k|x_k, y_{1:k-1})}^{Markov\ Property} p(y_{1:k-1}|x_k)p(x_k)}{p(y_k|y_{1:k-1})p(y_{1:k-1})} \\ &= \frac{p(y_k|x_k) \quad \overbrace{p(y_{1:k-1}|x_k)p(x_k)}^{Bayes\ Law}}{p(y_k|y_{1:k-1}) \quad p(y_{1:k-1})} \\ &= \frac{p(y_k|x_k)p(x_k|y_{1:k-1})}{p(y_k|y_{1:k-1})}. \end{aligned} \tag{A.7}$$

The time update can be found by first considering the joint probability distribution

$$\begin{aligned} p(x_{k+1}, x_k|y_{1:k}) &= p(x_{k+1}|x_k, y_{1:k})p(x_k|y_{1:k}) \\ &= p(x_{k+1}|x_k)p(x_k|y_{1:k}) \end{aligned} \tag{A.8}$$

Further, marginalizing this with respect to x_k, the prior density function can be written as

$$p(x_{k+1}|y_{1:k}) = \int p(x_{k+1}|x_k)p(x_k|y_{1:k})dx_k. \tag{A.9}$$

The same procedure can be repeated for time instant $k+1$, and therefore the recursive formula for calculating the posterior is now derived.

A.4 Kalman Filter Derivation

The following derivation is based on Simon Godsill (2009).

A.4.1 Measurement update

The measurement update starts with Bayes law Equation (5.1), where the normalization Equation (5.2) is omitted. This is allowed since this term only serve to normalize the posterior density distribution, meaning that

$$\int p(x_k|y_{1:k})dx_k = 1. \tag{A.10}$$

However, this means that the posterior are proportional to

$$p(x_k|y_{1:k}) \propto p(y_k|x_k)p(x_k|y_{1:k-1}). \tag{A.11}$$

Both the prior and the likelihood function, denoted $p(y_k|x_k)$ are Gaussian, therefore the posterior can be written as

$$\begin{aligned} p(x_k|y_{1:k}) &\propto \mathcal{N}(y_k, C_k x_k, R) \cdot \mathcal{N}(x_k, \mu_{k|k-1}, P_{k|k-1}), \\ &= \mathcal{N}(x_k, \mu_{k|k}, P_{k|k}). \end{aligned} \tag{A.12}$$

Let $\bar{P} = P_{k|k-1}$, $\hat{P} = P_{k|k}$, $\bar{\mu} = \mu_{k|k-1}$, and $\hat{\mu} = \mu_{k|k}$. Writing out the posterior as

$$\mathcal{N}(x_k, \hat{\mu}, \hat{P}) \propto exp\Big(-\frac{1}{2}\Big[x_k^T \hat{P}^{-1} x_k - 2x_k^T \hat{P}^{-1}\hat{\mu} + \hat{\mu}^T \hat{P}^{-1}\hat{\mu}\Big]\Big), \tag{A.13}$$

and writing out the prior, and likelihood function as

$$\begin{aligned} \mathcal{N}(y_k, C_k x_k, R) &\propto exp\Big(-\frac{1}{2}\Big[(y_k - C_k x_k)^T R^{-1}(y_k - C_k x_k)\Big]\Big) \\ \mathcal{N}(x_k, \bar{\mu}, \bar{P}) &\propto exp\Big(-\frac{1}{2}\Big[(x_k - \bar{\mu})^T \bar{P}^{-1}(y_k - \bar{\mu})\Big]\Big) \\ \mathcal{N}(x_k, \hat{\mu}, \hat{P}) &\propto exp\Big(-\frac{1}{2}\Big[(x_k - \hat{\mu})^T \hat{P}^{-1}(y_k - \hat{\mu})\Big]\Big), \end{aligned} \tag{A.14}$$

and put these into Equation (A.12), the following equation is obtained.

$$
\begin{aligned}
p(x_k|y_{1:k}) \propto exp\Big(-\frac{1}{2}\Big[& x_k^T \Big(\underbrace{C_k^T R^{-1} C_k + \bar{P}^{-1}}_{\hat{P}^{-1}} \Big) x_k \\
& - 2x_k^T \Big(\underbrace{C_k^T R^{-1} y_k + \bar{P}^{-1}\bar{\mu}}_{\hat{P}^{-1}\hat{\mu}} \Big) + y_k^T \Big(R^{-1} \Big) y_k \\
& + \bar{\mu}^T \Big(\bar{P} \Big) \bar{\mu} \Big] \Big)
\end{aligned}
\tag{A.15}
$$

By observing Equation (A.13), and noticing that $P_{k|k}$ is between $(x_k ... x_k^T)$, and $\mu_{k|k}$ is behind $(-2x_k P_{k|k}^{-1} ...)$, the updated co-variance and expected value can be found after observing them in Equation (A.15). Thus, updated co-variance and expected value can be written as

$$\hat{P} = (C_k^T R^{-1} C_k + \bar{P}^{-1})^{-1} \tag{A.16}$$

and

$$\hat{\mu} = \hat{P}(C_k^T R^{-1} y_k + \bar{P}^{-1}\bar{\mu}) \tag{A.17}$$

The Kalman gain appears in

$$\hat{P} = \Big(I - K_k C_k \Big) \bar{P} \tag{A.18}$$

and can be found by using the Matrix Inversion Lemma

Lemma 1 (Matrix Inversion Lemma) *Higham (2002)*

$$(A + UCV)^{-1} = A^{-1} - A^{-1} U \Big(C^{-1} + V A^{-1} U \Big)^{-1} V A^{-1} \tag{A.19}$$

Using the lemma on Equation (A.16),

$$
\begin{aligned}
\hat{P} &= (C_k^T R^{-1} C_k + \bar{P}^{-1})^{-1} \\
&= \bar{P} - \bar{P} C_k^T \Big(R + C_k \bar{P} C_k^T \Big) C_k \bar{P} \\
\hat{P} &= \Big[I - \underbrace{\bar{P} C_k^T \Big(R + C_k \bar{P} C_k^T \Big)^{-1}}_{K_k} C_k \Big] \bar{P}
\end{aligned}
\tag{A.20}
$$

Thus the Kalman gain is equal to

$$K_k = \bar{P} C_k^T \underbrace{\Big(R + C_k \bar{P} C_k^T \Big)^{-1}}_{S_k^{-1}} \tag{A.21}$$

Furthermore, is known that

$$\hat{\mu} = \bar{\mu} + K_k(y - C_k\bar{\mu}) \tag{A.22}$$

To prove this, Equation (A.17) is written out

$$\begin{aligned} \hat{\mu} &= \hat{P}(C_k^T R^{-1} y_k + \bar{P}^{-1}\bar{\mu}) \\ &= \hat{P}C_k^T R^{-1} y_k + \hat{P}\bar{P}^{-1}\bar{\mu} \\ &= (I - C_k K)\mu + \hat{P}C_k^T R^{-1} y_k \end{aligned} \tag{A.23}$$

Comparing with Equation (A.22), it needs to be shown that $K_k = \hat{P}C_k^T R^{-1}$.

$$
\begin{aligned}
\hat{P}C_k^T R^{-1} &= \Big[I - \bar{P}C_k^T\Big(R + C_k\bar{P}C_k^T)^{-1}C\Big]\bar{P}C_k^T R^{-1} \\
&= \Big[\bar{P}C^T - \bar{P}C^T\Big(R + C_k\bar{P}C_k^T\Big)^{-1}C_k\bar{P}C_k^T\Big]R^{-1} \\
&= \bar{P}C_k^T\Big[I - \Big(R + C_k\bar{P}C_k^T\Big)^{-1}C_k\bar{P}C_k^T\Big]R^{-1} \\
&= \bar{P}C_k^T\Big[S_k^{-1}S_k - \underbrace{\Big(R + C_k\bar{P}C^T\Big)^{-1}}_{S_k^{-1}}C_k\bar{P}C_k^T\Big]R^{-1} \\
&= \bar{P}C_k^T S_k^{-1}\Big[\underbrace{\Big(R + C_k\bar{P}C_k^T\Big)}_{S_k} - C_k\bar{P}C_k^T\Big]R^{-1} \\
&= \bar{P}C_k^T S_k^{-1}
\end{aligned}
\tag{A.24}
$$

Therefore, it follows that Equation (A.17) can be written as Equation (A.22).

A.4.2 Time Update

For the time update, consider Equation (5.3),

$$
\begin{aligned}
p(x_{k+1}|y_{1:k}) &= \int \mathcal{N}(x_{k+1}, \bar{\mu}, \bar{P})\mathcal{N}(x_k, \hat{\mu}, \hat{P})dx_k \\
&= \mathcal{N}(x_{k+1}, \bar{\mu}, \bar{P})\underbrace{\int \mathcal{N}(x_{k|k}, \hat{\mu}, P_{k|k})dx_k}_{1} \\
&= \mathcal{N}(x_{k+1}, \bar{\mu}, \bar{P})
\end{aligned}
\tag{A.25}
$$

The expected value can be found by

$$
\begin{aligned}
\bar{\mu} &= E[x_{k+1}] \\
&= E[\Phi x_k] + \underbrace{E[\Gamma v_k]}_{0} \\
&= \Phi\hat{\mu}
\end{aligned}
\tag{A.26}
$$

The co-variance matrix can be found by

$$
\begin{aligned}
P_{k+1|k} &= E[(x_{k+1} - \bar{\mu})(x_{k+1} - \bar{\mu})^T] \\
&= E[(\Phi x_k + \Gamma v_k - \Phi\bar{\mu})(\Phi x_k + \Gamma v_k - \Phi\bar{\mu})^T] \\
&= E[(\Phi(x_k - \hat{\mu}) + \Gamma v_k)(\Phi(x_k - \hat{\mu}) + \Gamma v_k)^T] \\
&= E[(\Phi(x_k - \hat{\mu})(x_k - \hat{\mu})^T\Phi^T + \Gamma v_k v_k^T\Gamma^T) \\
&= E[(\Phi(x_k - \hat{\mu})(x_k - \hat{\mu})^T\Phi^T) + E(\Gamma v_k v_k^T\Gamma^T) \\
&= \Phi \underbrace{E[((x_k - \hat{\mu})(x_k - \hat{\mu})^T)}_{P_{k|k}}\phi^T + \underbrace{E(\Gamma v_k v_k^T\Gamma^T)}_{Q} \\
&= \Phi\hat{P}\Phi^T + \Gamma Q\Gamma^T
\end{aligned}
\tag{A.27}
$$

A.5 Particle Filter with Gaussian State Noise

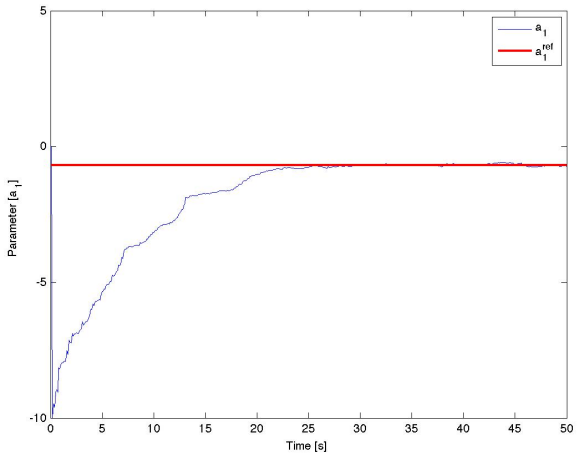

(a) Case 1: Parameter estimates $a_{k,1}$

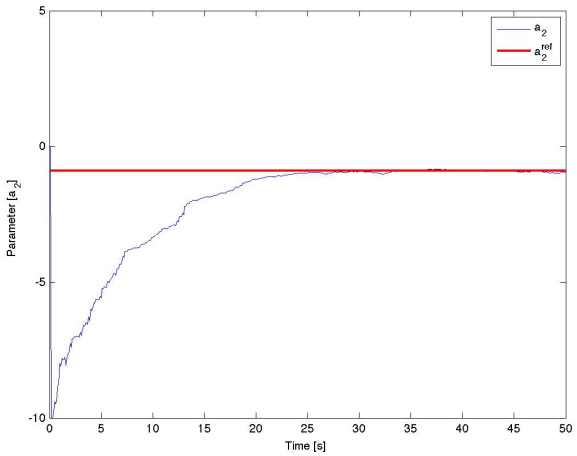

(b) Case 1: Parameter estimates $a_{k,2}$

Figure A.1: Case 1: Particle Filter Parameter Estimates

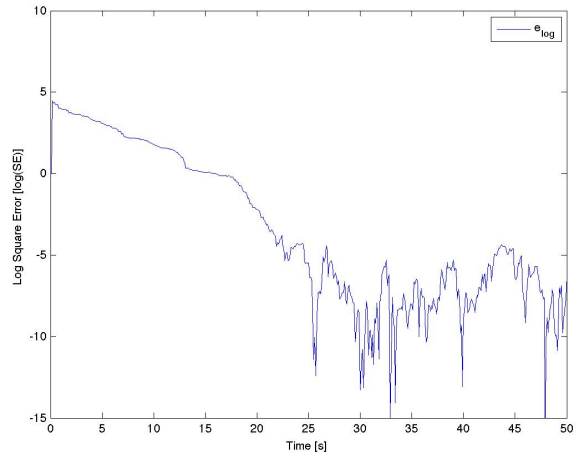

(a) Case 1: Log Square Error

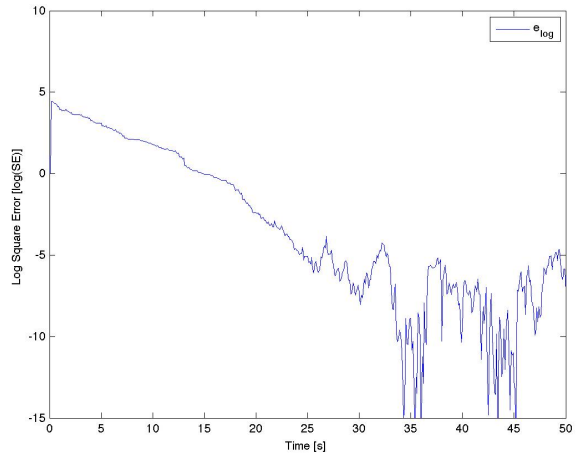

(b) Case 1: Log Square Error

Figure A.2: Case 1: Log Square Error

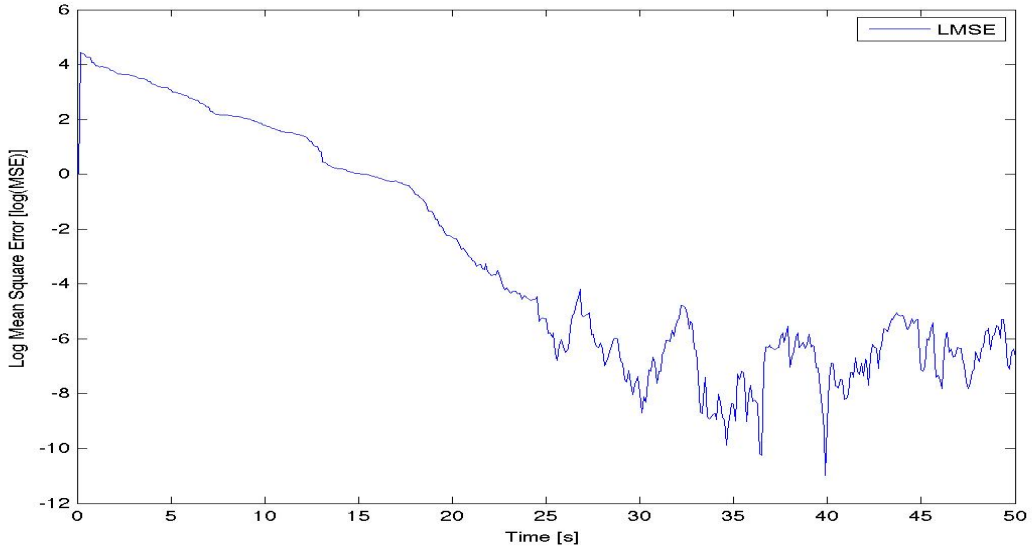

Figure A.3: Case 1: Particle filter log mean square error with Gaussian state noise

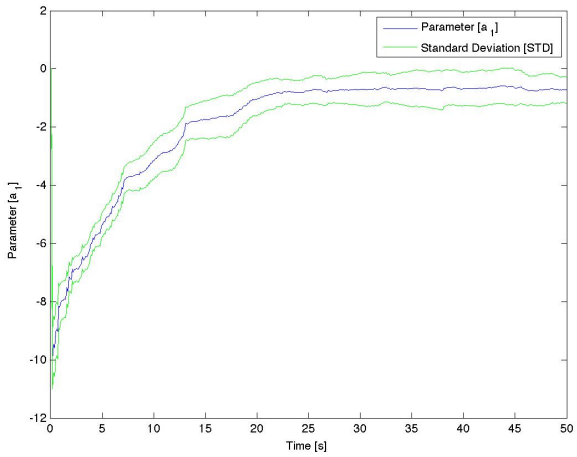

(a) Case 1: Standard deviation $a_{k,1}$

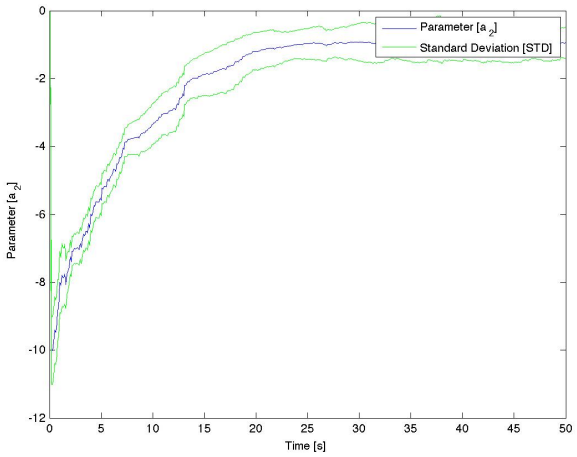

(b) Case 1: Standard deviation $a_{k,2}$

Figure A.4: Case 1: Standard deviation from Particle filter with Gaussian state noise

A.6 Importance Weights Update Law

The following derivation is given in Arulampalam et al. (2002).

Let the importance sampling function and the posterior density function for the whole trajectory $x_{1:k}$ be factorisable such that,

$$q(x_{0:k}|y_{1:k}) = q(x_k|x_{0:k-1}, y_{1:k})q(x_{0:k-1}|y_{1:k}) \tag{A.28}$$

and

$$p(x_{0:k}|y_{1:k}) = p(x_{0:k}|x_{k-1})p(x_{0:k-1}|y_{0:k-1}). \tag{A.29}$$

Then consider Bayes law given in Equation (5.1)

$$\begin{aligned} p(x_{0:k}|y_{1:k}) &= \frac{p(y_k|x_{0:k})p(x_{0:k}|y_{1:k-1})}{p(y_k|y_{1:k-1})} \\ &= \frac{\overbrace{p(y_k|x_k)p(x_{0:k}|x_{k-1})}^{Factorization}\, p(x_{0:k-1}|y_{0:k-1})}{p(y_k|y_{1:k-1})} \\ &\propto p(y_k|x_k)p(x_{0:k}|x_{k-1})p(x_{0:k-1}|y_{0:k-1}) \end{aligned} \tag{A.30}$$

Putting (A.28) and (A.30) into (5.21), the following is obtained

$$\begin{aligned} \hat{w}_k^i &\propto \frac{p(y_k|x_k)p(x_k|x_{k-1})}{q(x_k|x_{0:k-1})} \frac{\overbrace{p(x_{0:k-1}|y_{1:k-1})}}{\underbrace{q(x_{0:k-1}|y_{1:k-1})}_{w_{k-1}}} \\ &= \hat{w}_{k-1}^i \frac{p(y_k|x_k)p(x_k|x_{k-1})}{q(x_k, y_{1:k})} \end{aligned} \tag{A.31}$$